

# Invariant operator approach for the analysis of simulation bundles

Jan Tobias Tesch

Born 7th February 1995 in Troisdorf, Germany

15th October 2018

Master's Thesis Mathematics

Advisor: Prof. Dr. Jochen Garcke

Second Advisor: Prof. Dr. Carsten Burstedde

Advisor at Fraunhofer SCAI: Dr. Rodrigo Iza-Teran

INSTITUTE FOR NUMERICAL SIMULATION

FRAUNHOFER INSTITUTE FOR ALGORITHMS AND SCIENTIFIC COMPUTING SCAI

MATHEMATISCH-NATURWISSENSCHAFTLICHE FAKULTÄT DER  
RHEINISCHEN FRIEDRICH-WILHELMS-UNIVERSITÄT BONN



## Contents

<b>1</b>	<b>Introduction</b>	<b>1</b>
<b>2</b>	<b>Simulation data</b>	<b>5</b>
2.1	Numerical simulations in industry . . . . .	5
2.2	Simulation data as functions . . . . .	6
<b>3</b>	<b>Invariant operator approach</b>	<b>8</b>
3.1	Construction of the continuous operators . . . . .	11
3.1.1	Basics of Differential Geometry . . . . .	11
3.1.2	Affine-invariant metric . . . . .	17
3.1.3	Fokker-Planck operator . . . . .	26
3.2	Numerical Evaluation of the Operators . . . . .	30
3.2.1	Laplace-Beltrami operator . . . . .	31
3.2.2	Fokker-Planck operator . . . . .	36
3.3	Invariance of operators . . . . .	37
3.3.1	Invariant operator in the representation of groups . . . . .	37
3.3.2	Invariance of the Laplace-Beltrami operator . . . . .	40
3.3.3	Invariance of the Fokker-Planck operator . . . . .	46
3.4	Separation of effects . . . . .	47
3.4.1	Numerical observations . . . . .	49
3.4.2	Theoretical framework . . . . .	50
3.5	Decay of the spectral coefficients . . . . .	57
3.5.1	Numerical observations . . . . .	58
3.5.2	Theoretical framework . . . . .	60
3.6	Summary . . . . .	66
<b>4</b>	<b>Taylor approach</b>	<b>68</b>
4.1	Theoretical framework . . . . .	68
4.2	Undoing transformations . . . . .	72
4.3	Summary . . . . .	75
<b>5</b>	<b>Conclusion</b>	<b>78</b>
	<b>References</b>	<b>79</b>



## 1 Introduction

Nowadays, in the digital age, an important step in the development of industrial products is the implementation and exploration of numerical simulations. Consider, for instance, the car industry. Before a new car goes into production, its behaviour in car crashes is analysed. Numerical simulations of the crash offer many advantages over real crashes. Executing them is faster and cheaper than actually producing and crashing each prototype. This enables the engineer to simulate the crash behaviour for many different configurations of the car. While, due to technological progress, more and more simulations can be executed, the analysis and evaluation of them becomes more and more challenging. In this thesis, we will consider the example of crash simulations to investigate two approaches which may assist the engineer in this task. Both approaches can be applied analogously for the analysis of many other types of numerical simulations in industry and research. We will examine the approaches analysing the deformation of a specific part of the car during the crash.

In contrast to many other approaches from the field of knowledge discovery and machine learning, the presented approaches do not consider the simulations as *points* on a manifold embedded in a high dimensional Euclidean space, but represent the simulation data as *functions* on a reference embedding of the considered object, in our case, the car part.

The car part is modelled as a (two-dimensional) surface  $M$  in  $\mathbb{R}^3$ . It is discretized using a triangular surface mesh consisting of  $N$  nodes, see Figure 1.1. The output of a simulation are the coordinates of the nodes at each timestep and sometimes further data as the stress acting on each node at each timestep. In general, the data is interpreted as samples of square integrable functions in  $L^2(M)$ .

In the first part of Chapter 2, I will present the considered simulation data in more detail. In the second part of the chapter, we will contemplate in more detail how the data can be interpreted as elements of  $L^2(M)$ .

The focus of this thesis is Chapter 3, where we will analyse the invariant operator approach, proposed by Iza-Teran in [Iza17]. Iza-Teran suggests representing the simulation data (viewed as functions in  $L^2(M)$ ) in the spectral domain of operators that act on  $L^2(M)$  and possess certain invariances. For this purpose, he uses in [Iza17] and [IG17] the Laplace-Beltrami operator and a Fokker-Planck operator. First observations and considerations in [Iza17] and [IG17] suggest multiple benefits of the invariant operator approach:

1. It can be used to reduce the dimensionality of the data, either to represent it directly in a low dimensional space as  $\mathbb{R}^3$ , where the engineer can easily identify similar points

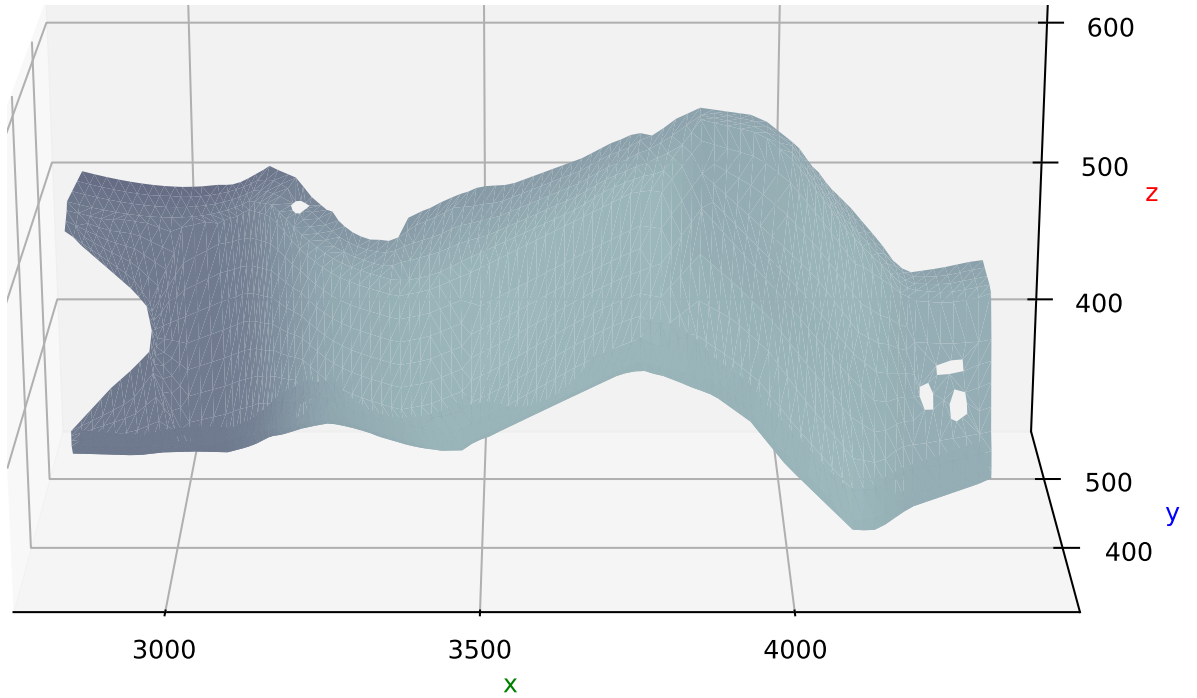


Figure 1.1: Model and discretization of the considered car part, given by its embedding in the initial state of a crash simulation.

and outliers, or as preprocessing to reduce the complexity of further analysis methods. As the data from all simulations is transformed to the spectral domain of the same operator, the complexity is linear in the number of simulations as opposed to many other approaches. Given a new simulation, it can readily be transformed to the same spectral domain while for other approaches the embedding of new simulations is often cumbersome.

2. Iza-Teran observes that different spectral coefficients correspond to different basic transformations. This is in the sense that varying a selected coefficient for the coordinate functions of an embedding, the embedding is translated, rotated or transformed differently. He refers to this as *separation of effects*. Iza-Teran observes a connection between the invariances of the operator and the observed basic transformations. The Laplace-Beltrami operator, for instance, is in a sense invariant under isometries. Isometric transformations are transformations that preserve intrinsic distances. Examples are translations and rotations, but also the crumpling of a sheet of paper. The transformations observed for variations in the spectral domain of the Laplace-Beltrami operator seem to be isometric. In [Iza17], Iza-Teran conjectures the existence of a representation of the group of isometries in the space of eigenfunctions of the Laplace-Beltrami

---

operator.

Writing a complex transformation as composition of several basic transformations yields the opportunity to analyse the influence of parameter changes on the different basic transformations separately. Given, for example, that the car part breaks, the engineer might be able to focus specifically on the transformation leading to the break. On the other hand, ignoring certain projection coefficients would yield a representation which is invariant under the corresponding transformations.

3. Finally, Iza-Teran proposes constructing embeddings in between two timesteps  $t$  and  $t + 1$  of a simulation by linearly interpolating between the spectral coefficients of the embeddings at time  $t$  and time  $t + 1$ . He proposes proceeding analogously to obtain simulation data for parameter combinations in between parameter combinations for which one already executed the simulations. This would be a benefit since running a numerical simulation is still time-consuming.

Concerning the last point, we note that interpolating linearly between all spectral coefficients is equivalent to a straight away linear interpolation between the embeddings or other function data in the standard (Euclidean) basis. Iza-Teran's observations in this regard are therefore independent of the basis and thus no benefit of the representation of the data in the spectral domain of invariant operators.

In this thesis, we will examine the influence of the invariances of the used operators on the dimensionality reduction and the observed basic transformations in the separation of effects. To do so, we will formalize in what sense the Laplace-Beltrami operator and the Fokker-Planck operator are invariant. I will depict several problems concerning Iza-Teran's conjecture of the existence of a representation of the group of isometries in the spectral domain of the Laplace-Beltrami operator. For that purpose, I will give a very brief introduction to the representation of groups and distinguish the invariance of the Laplace-Beltrami operator under isometries from the invariance of operators in the representation of groups. Further, I implemented a Laplace-Beltrami operator using an equi-affine invariant metric. This operator is in the same sense invariant under isometries with respect to the equi-affine invariant metric as the standard Laplace-Beltrami operator is invariant under isometries with respect to the Euclidean metric. We will compare the basic transformations in the separation of effects for both Laplace-Beltrami operators and the Fokker-Planck operator.

Concerning the dimensionality reduction, we will prove an optimality statement for the representation of smooth functions in the spectral domain of the Laplace-Beltrami operator. It

explains the observations of the strong decay of the spectral coefficients for all three operators. I will depict gaps in the proof of the decay estimate for the spectral coefficients of the Fokker-Planck operator presented by Iza-Teran in [Iza17].

In Chapter 4, I will present the Taylor approach. In the beginning of my work with the crash data and the invariant operator approach, the assumption that all embeddings of a simulation bundle are transformations of a reference embedding raised the question whether one can characterize those transformations in a more direct way than the invariant operator approach does. The idea of the Taylor approach is to do a Taylor expansion for those transformations.

A detailed investigation of the Taylor approach was out of scope of this work. This is why I will only present the basic idea, show an exemplary application for the analysis of the crash data and state possible further applications, leaving several questions unanswered. To my knowledge, a similar approach has not been used in the context of simulation bundles or related fields like shape recognition from computer vision.

While in this thesis we will consider the analysis of car crash simulations, both approaches can be applied to different types of simulations. The crash simulations produce data on (two-dimensional) surfaces in  $\mathbb{R}^3$ , but the approaches can analogously be applied to simulations that produce for example (one-dimensional) curves in  $\mathbb{R}^2$  or  $\mathbb{R}^3$ , modelling a scalar quantity of interest for the engineer over time or, in a different context, the spatial position of a particle in time. Only the definition of the equi-affine invariant metric and the corresponding Laplace-Beltrami operator presented in this thesis are restricted to the case of surfaces in  $\mathbb{R}^3$ .

At this point, I would like to acknowledge Professor Dr. Jochen Garcke and Dr. Rodrigo Iza-Teran for their support and advice. In particular, I would like to thank Professor Dr. Jochen Garcke for the opportunity to write this thesis at the Fraunhofer SCAI. Special thanks go to my girlfriend Rebekka for her motivating words during difficult phases of my work on this thesis and her intensive proofreading.

## 2 Simulation data

In this chapter, we will take a closer look at our simulation data. The first part will give a brief idea how the simulations are generated and what data they produce. Further, it will introduce a car crash simulation bundle which we will use in several numerical examples in Chapters 3 and 4. The second part will explain in more detail how we interpret the data as functions on a reference embedding of the simulated object. It will explain informally how we can restrict ourselves to the representation of a smaller set of functions than  $L^2(M)$ .

### 2.1 Numerical simulations in industry

Numerical simulations of industrial products allow faster and cheaper development of optimized products. In the car industry, for instance, it was previously necessary to crash dozens of cars during the design of a single model, while, nowadays, most of those crashes are simulated on the computer. Only a few are performed physically to verify the results in the end of the design process [Boa15].

The simulations investigated in this thesis are numerical solutions of nonlinear differential equations. The differential equations model physical processes taking into account parameter changes concerning for example material properties or the geometry of the considered object. Finding analytical solutions of those equations is in general impossible. The first step of the numerical solution process is to discretize the object and to define a timestep. Next, a parameter configuration for the specific simulation is chosen. Then, several methods as, for example, the finite element method are used to solve the differential equations. The simulation resulting from this process contains the coordinates of the nodes of the discretized object at all timesteps. Sometimes it contains additionally data as stress, velocity, acceleration or temperature at the nodes.

The number of nodes in the discretization of the entire car in a crash simulation is nowadays in the order of 3-4 millions, indicating the size of the problem. Nevertheless, using high performance computers, hundreds of variants can be simulated and need to be evaluated by the engineers.

*Simulation bundles* are many similar simulations for different parameter configurations. Parameters are for example material properties, geometries and load cases.

Further information on the simulation and the evaluation process can be found in [Iza17].

### Example

In Chapters 3 and 4, we will consider in several examples a simulation bundle produced by Iza-Teran at the Fraunhofer Institute SCAI. The simulated object is a Chevrolet C2500 pick-up truck, a model with around 60,000 nodes from the National Crash Analysis Center<sup>1</sup>. Using the finite element program LS-DYNA<sup>2</sup>, Iza-Teran produced 116 simulations of a vehicle frontal crash. For the different simulations, the thicknesses of nine car parts is varied randomly up to  $\pm 30\%$ . Each simulation contains 17 timesteps.

We focus in this thesis on a specific part of the car, depicted in Figure 1.1. It is discretized with 1714 nodes. The variation of the thicknesses for the different simulations results in different deformations of the part.

## 2.2 Simulation data as functions

In this section, we will illustrate at the above example how the data from a simulation bundle can be interpreted as functions on a reference embedding of the simulated object. Here, I will only present the rough idea. Several concepts, like regular surfaces, integration on those and isometric maps will be defined later.

Let  $M$  be a reference embedding of the car part in  $\mathbb{R}^3$ , for example the car part at timestep zero of a reference simulation, see Figure 1.1. It is modelled as a (two-dimensional, regular) surface in  $\mathbb{R}^3$  and discretized with a triangular surface mesh consisting of  $N$  nodes. The simulation data are the coordinates of the nodes at each timestep. We interpret the  $x$ -,  $y$ - and  $z$ -coordinates as samples of square integrable functions in  $L^2(M)$ . Analogously, data as stress or temperature at the nodes can be interpreted as samples of functions in  $L^2(M)$ .

Restricting ourselves to coordinate functions, we do not need to consider the whole space  $L^2(M)$ . Assuming that the embeddings of the car part at the different timesteps of the simulations are smooth, isometric transformations of the reference embedding, the set of possible coordinate functions is given by

$$\{g \in L^2(M) \mid g = f_x \text{ for a } C^\infty\text{-isometry } f : M \rightarrow f(M) \subset \mathbb{R}^3\}.$$

More generally, if the only requirement on the transformations is that all embeddings are smooth transformations of the reference embedding and no (physically impossible) crossings

<sup>1</sup>Now 'Center for Collision Safety and Analysis, CCSA', <https://www.ccsa.gmu.edu/> (2018).

<sup>2</sup><http://www.lstc.com/products/ls-dyna> (2018)

of the car part occur, the set of possible coordinate functions is given by

$$\{g \in L^2(M) \mid g = f_x \text{ for } f \in \text{Emb}(M, \mathbb{R}^3)\},$$

where  $\text{Emb}(M, \mathbb{R}^3)$  is the space of injective  $C^\infty$ -functions (*i.e.* embeddings) from  $M$  to  $\mathbb{R}^3$ .

Characterizing the set of possible coordinate functions helps to develop useful representations of the coordinate data. In Chapter 3, we will see that the invariant operator approach yields a representation for all functions from  $L^2(M)$ . This is one reason why the benefit of the separation of effects that Iza-Teran observes in [Iza17] and [IG17] is questionable.

### 3 Invariant operator approach

In Chapter 2, we saw how the data from a simulation bundle can be interpreted as elements of the function space  $L^2(M)$ , where  $M$  is a reference embedding of the simulated object. Initially, we have a representation of the data functions in the spatial domain, *i.e.* we are given the function values at points  $x \in M$ . The invariant operator approach transforms the functions in the spectral domain of an operator with certain invariances. In [Iza17] and [IG17], Iza-Teran uses for this the Laplace-Beltrami operator and a Fokker-Planck operator.

The proceeding for the Laplace-Beltrami operator is the following. The operator is defined on  $C^\infty(M)$  and extended to the Sobolev space  $H^{2,2}(M)$ . It exists an orthonormal basis of  $L^2(M)$  consisting of eigenfunctions  $\{\psi_i\}$ ,  $i \in \mathbb{N}$ , of the extended operator. A function  $f \in L^2(M)$  can be written as

$$f = \sum_{i=1}^{\infty} \alpha^i \psi_i$$

with  $\alpha^i = \langle f, \psi_i \rangle_{L^2(M)}$ . Instead of considering the function  $f$  in the spatial domain, we can consider its spectral representation given by the vector  $\alpha = (\alpha^1, \alpha^2, \dots)$ . In general, the complete vector  $\alpha$  is needed to represent a function  $f$ . However, Iza-Teran observes in [Iza17] and [IG17] a strong decay of the spectral coefficients  $\alpha^i$  for smooth functions. This suggests neglecting high coefficients, reducing the dimensionality of the representation.

Apart from observations concerning the decay of the spectral coefficients, Iza-Teran observes that different spectral coefficients seem to correspond to different basic transformations.

In Chapter 2, we saw that, under the assumption that all embeddings of the car part in the simulation bundle are smooth transformations of the reference embedding and no (physically impossible) crossings of the car part occur, their coordinate functions are elements of the subset

$$\{g \in L^2(M) \mid g = f_x \text{ for } f \in Emb(M, \mathbb{R}^3)\}$$

of  $L^2(M)$ .

In the invariant operator approach, we represent an element  $f \in Emb(M, \mathbb{R}^3)$  in the spectral domain of, for instance, the Laplace-Beltrami operator as

$$\begin{pmatrix} f_x \\ f_y \\ f_z \end{pmatrix} = \sum_{i=1}^{\infty} \alpha^i \psi_i, \quad \text{where } \alpha^i = \begin{pmatrix} \langle f_x, \psi_i \rangle_{L^2(M)} \\ \langle f_y, \psi_i \rangle_{L^2(M)} \\ \langle f_z, \psi_i \rangle_{L^2(M)} \end{pmatrix}.$$

Iza-Teran observes that a variation of the first spectral coefficient  $\alpha^1$  seems to correspond to a translation of the embedding. A variation of the second spectral coefficient  $\alpha^2$  appears to be a rotation (see Figure 3.1). In [Iza17], the transformations obtained by the variation of single spectral coefficients are referred to as *independent transformation modes*.

Iza-Teran conjectures in [Iza17] that the observed separation of effects upon variation of the coefficients  $\alpha^i$  can mathematically be expressed as movements along orbits of  $Emb(M, \mathbb{R}^3)$ . Inspired by Bauer et al.'s works on shape spaces, see for instance [MM06], he defines a *simulation space* as

$$Emb(M, \mathbb{R}^3)/G(M),$$

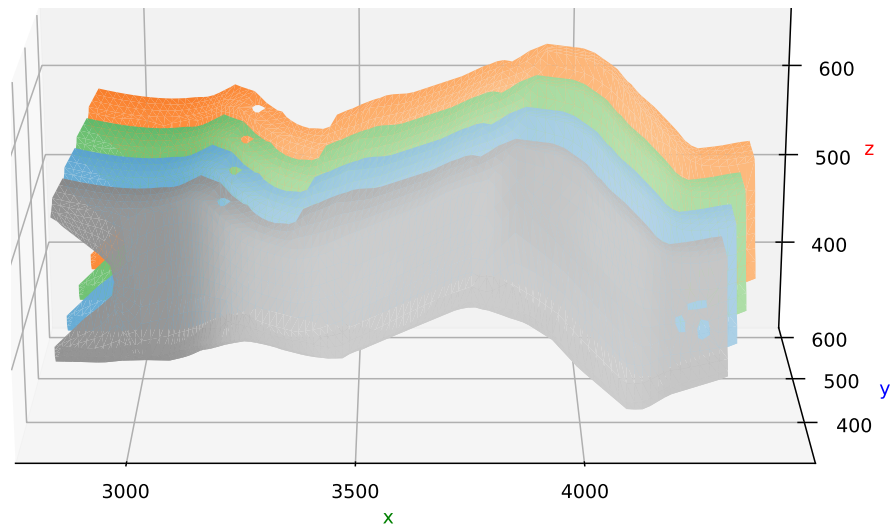
where  $G(M)$  is a group of isometric transformations acting on elements from  $Emb(M, \mathbb{R}^3)$  by composition from the right. However, this setting does not seem to be appropriate as mathematical framework for the observed separation of effects: As the elements of  $G(M)$  act on  $Emb(M, \mathbb{R}^3)$  by composition from the *right*,  $G(M)$  can only contain maps from  $M$  to  $M$ . We can think of those maps as reparametrizations of  $M$ . Concerning the separation of effects, Iza-Teran observed that a variation of the spectral coefficients of a given embedding  $f \in Emb(M, \mathbb{R}^3)$  appears to correspond to an isometric transformation  $h : f(M) \rightarrow h(f(M)) \subset \mathbb{R}^3$  of the embedding  $f(M)$ . Note, that  $h$  acts on the element  $f$  of  $Emb(M, \mathbb{R}^3)$  by composition from the *left*. Note further, that the set of such isometric transformations depends on the embedding  $f \in Emb(M, \mathbb{R}^3)$  and is in general not a group.

Another conjecture in [Iza17] and [IG17] is that there exists a link between the observed "independent deformation modes" and the invariances of the used operator. The Laplace-Beltrami operator, for example, is in some sense invariant under isometric transformations and Iza-Teran observed that the transformations upon variation of the spectral coefficients are predominantly isometric. Iza-Teran presumes a link to Representation Theory, where is known that the eigenspaces of invariant operators can represent groups.

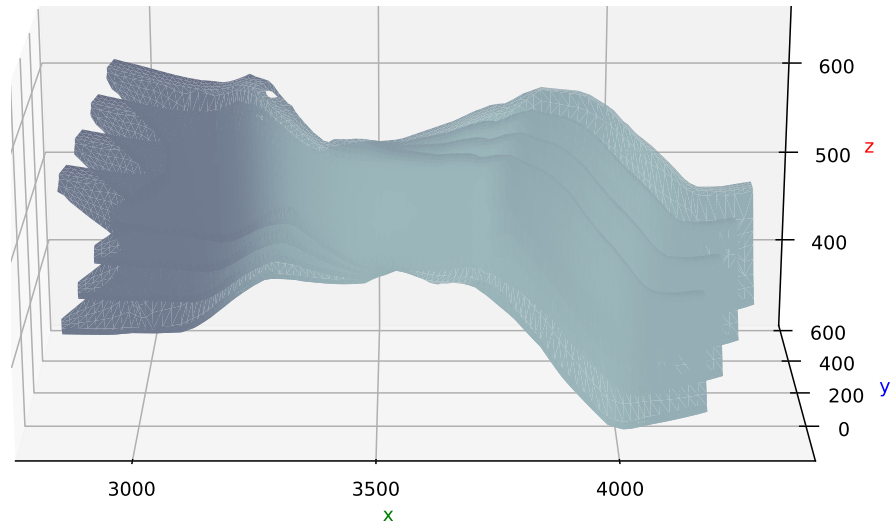
In this chapter, we will examine Iza-Teran's conjectures. Especially, we will analyse the influence of the invariances of the used operator on the observed transformations in the separation of effects. In order to investigate this influence, I implemented a Laplace-Beltrami operator using an equi-affine invariant metric, which we will compare to the operators used by Iza-Teran.

The structure of this chapter is the following. First, we will define the operators which will later be used. To do so, I will give an introduction to the basics of differential geometry, present the equi-affine invariant metric and parts of Singer's and Coifman's work [SC08] on

non-linear independent component analysis which inspired Iza-Teran to define the Fokker-Planck operator. To examine the conjecture of a link between the invariances of the operator and the observed basic transformations, it will follow a section concretizing in what sense the used operators are invariant. Moreover, this section will contain a short insight into invariant operators in the representation of groups and will show problems concerning the hypothesis that the observed separation of effects can be explained by a link to Representation Theory. The chapter will close with numerical observations and explanations concerning the separation of effects and dimensionality reduction properties of the approach.



(a) Variation of the first spectral coefficient seems to correspond to a translation.



(b) Variation of the second spectral coefficient seems to correspond to a rotation.

Figure 3.1: Example of transformations obtained by variation of selected spectral coefficients for the coordinate functions of an embedding of the car part.

## 3.1 Construction of the continuous operators

### 3.1.1 Basics of Differential Geometry

In this section, I will present some basics of differential geometry. I will stick to the case of 2-submanifolds of  $\mathbb{R}^3$ , so-called regular surfaces. Personally, I tend to imagine general manifolds as regular surfaces and their theory is all we need for our application. To generalize the following definitions and statements, only marginal adjustments are needed.

Based on Chapters 3 to 5 of [Bär10] and on [Gri09], we will see how differentiation and integration on regular surfaces are defined, define the notion of Riemannian metric and close with the definition of the Laplace-Beltrami operator. I will present mainly definitions and aim to give an idea of their meaning, leaving out the proofs. Those can be found in [Bär10]. For a more detailed introduction to differential geometry, see for example [Mic08].

Let us start with the definition of the underlying structure. A regular surface is a subset of  $\mathbb{R}^3$  that locally resembles  $\mathbb{R}^2$ .

**Definition 3.1.1** (Regular surface). *A subset  $M \subset \mathbb{R}^3$  is a regular surface if for every point  $p \in M$  exists an open neighbourhood  $V$  of  $p$  in  $\mathbb{R}^3$ , an open set  $U \subset \mathbb{R}^2$  and a smooth (i.e. infinitely often differentiable) map  $\phi : U \rightarrow \mathbb{R}^3$  such that*

1.  $\phi(U) = M \cap V$  and  $\phi : U \rightarrow M \cap V$  is bijective with smooth inverse and
2. the Jacobian matrix  $D\phi(u)$  has rank 2 in every point  $u \in U$ .

$\phi$ , or as well the triple  $(U, \phi, V)$ , is called a local parametrization of  $M$  around  $p$ . The components  $u_1$  and  $u_2$  of  $u$  are called local coordinates of a point  $\phi(u) \in M$  (with respect to the parametrization  $\phi$ ).

To ensure well-definedness of many of the following definitions, we restrict them to smooth functions on regular surfaces.

**Definition 3.1.2** (Smooth functions on regular surfaces). *Let  $M \subset \mathbb{R}^3$  be a regular surface,  $p \in M$  and  $f : M \rightarrow \mathbb{R}^n$ . If the following equivalent conditions are fulfilled,  $f$  is called smooth close to  $p$ :*

1. *It exists an open neighbourhood  $V$  of  $p$  in  $\mathbb{R}^3$  and an extension  $\tilde{f}$  of  $f|_{M \cap V}$  to  $V$  that is smooth (i.e. infinitely often differentiable in the usual sense for functions from an open set  $\Omega \subset \mathbb{R}^n$  to  $\mathbb{R}^m$ ) around  $p$ .*
2. *It exists a local parametrization  $(U, \phi, V)$  with  $p \in V$  such that  $f \circ \phi : U \rightarrow \mathbb{R}^n$  is smooth around  $\phi^{-1}(p)$ .*

3. The function  $f \circ \phi : U \rightarrow \mathbb{R}^n$  is for each local parametrization  $(U, \phi, V)$  with  $p \in V$  smooth around  $\phi^{-1}(p)$ .

Note that the first definition can only be used to define smooth functions on submanifolds while the second and third definition can be used for manifolds in general.

Differentiating a function  $f : \mathbb{R}^d \rightarrow \mathbb{R}$  in a point  $x$  in the direction of a vector  $v \in \mathbb{R}^d$  indicates how the function changes if we move a small amount in direction  $v$ .

A function  $f : M \rightarrow \mathbb{R}$  is only defined on  $M$ . Therefore, differentiation of a function  $f : M \rightarrow \mathbb{R}$  is only defined for directions  $v \in \mathbb{R}^d$  that *stay in*  $M$ . Those directions are characterized by the tangent space of  $M$ .

**Definition 3.1.3** (Tangent space). *Let  $M \subset \mathbb{R}^3$  be a regular surface. The tangent space of  $M$  in a point  $p \in M$  is defined by*

$$T_p M = \left\{ v \in \mathbb{R}^3 \mid \text{It exist } \varepsilon > 0, \gamma : (-\varepsilon, \varepsilon) \rightarrow M \text{ with } \gamma(0) = p, \dot{\gamma}(0) = v \right\}.$$

The tangent space of a regular surface is in every point  $p \in M$  2-dimensional. Given a local parametrization  $(U, \phi, V)$  of  $M$  around  $p$  and  $u \in U$  with  $\phi(u) = p$ , the vectors  $\frac{\partial \phi}{\partial u_i}(u)$ ,  $i = 1, 2$ , form a basis of  $T_p M$ . They describe how a movement in the coordinate directions in the parameter space  $U \in \mathbb{R}^2$  is translated into a movement on the manifold. They are linearly independent by the second requirement in Definition 3.1.1 of a regular surface.

To define the differential  $d_p f$  of a smooth function  $f$  on  $M$  at a point  $p \in M$  in the direction of some vector  $v$  from the tangent space  $T_p M$ , we choose a curve  $\gamma : (-\varepsilon, \varepsilon) \rightarrow M$  in the manifold with  $\gamma(0) = p$ ,  $\dot{\gamma}(0) = v$  for some  $\varepsilon > 0$  as it exists by definition of  $T_p M$ . We consider  $f$  along this curve and use the usual notion of differentiability for functions from an interval  $I \subset \mathbb{R}$  to  $\mathbb{R}$  on the function composition  $f \circ \gamma : (-\varepsilon, \varepsilon) \rightarrow \mathbb{R}$  at the point  $t = 0$ . We set

$$d_p f(v) = \frac{d}{dt}(f \circ \gamma)|_{t=0}. \quad (3.1.1)$$

In the case  $M = \mathbb{R}^2 \times \{0\}$ , an application of the chain rule reveals that this is equivalent to the usual definition of differentiation in  $\mathbb{R}^2$ .

The next step is to define the gradient of  $f$ . Remember that for a smooth function  $f : \mathbb{R}^d \rightarrow \mathbb{R}$ , the gradient can be defined by the requirement that the scalar product of the gradient with a direction  $v \in \mathbb{R}^d$  corresponds to differentiation of  $f$  in direction  $v$ . To transfer this to functions on manifolds, we need scalar products on the tangential spaces  $T_p M$ .

**Definition 3.1.4** (Riemannian metric). *Let  $M \subset \mathbb{R}^3$  be a regular surface. A Riemannian metric assigns to each point  $p \in M$  an inner product  $g_p$  on the tangent space  $T_p M$  such that for any local parametrization  $(U, \phi, V)$  of  $M$  and  $i, j \in \{1, 2\}$  the functions*

$$G_{ij} : U \rightarrow \mathbb{R},$$

$$G_{ij}(u) = g_{\phi(u)} \left( \frac{\partial \phi}{\partial u_i}(u), \frac{\partial \phi}{\partial u_j}(u) \right)$$

*are smooth. The tuple  $(M, g)$  is called Riemannian manifold.*

An example for a Riemannian metric is the induced (Euclidean) metric from the embedding space  $\mathbb{R}^3$

$$g_p(v, w) = \langle v, w \rangle_{\mathbb{R}^3} \text{ for all } v, w \in T_p M \subset \mathbb{R}^3. \quad (3.1.2)$$

The Riemannian metric can be used to generalize notions as lengths, angles, areas and further geometric quantities to the regular surface  $M$ . The metric  $g$  replaces the Euclidean inner product in the definition of those quantities in the Euclidean space.

**Definition 3.1.5** (Length and angle of tangent vectors). *Let  $M$  be a regular surface and  $g$  a Riemannian metric on  $M$ . Let  $p \in M$  and  $v, w$  be vectors from the tangent space  $T_p M$ . We define the length of  $v$  as*

$$\|v\|_p = \sqrt{g_p(v, v)}.$$

*We define the angle  $\theta$  between  $v$  and  $w$  by*

$$\cos \theta = \frac{g_p(v, w)}{\|v\|_p \|w\|_p}.$$

**Definition 3.1.6** (Length of a curve). *Let  $a < b \in \mathbb{R}$ ,  $c : [a, b] \rightarrow M$  be a curve on a Riemannian manifold  $(M, g)$ . We define the length of  $c$  as*

$$\ell(c) = \int_a^b \sqrt{g_{c(t)}(\dot{c}(t), \dot{c}(t))} dt.$$

To define integration for functions on  $(M, g)$ , we integrate piecewise in local parameters  $(U, \phi, V)$  and multiply a deformation factor that incorporates how the area of a small cube in  $U \subset \mathbb{R}^2$  changes when  $\phi$  maps it to  $M \subset \mathbb{R}^3$ . Locally,  $\phi$  can be approximated by the linear map  $\phi(u + v) \approx \phi(u) + D\phi(u)v$ . Hence, the square

$$[u + r_1 e_1, u + r_2 e_2] \subset U,$$

where  $r_1, r_2 \in [0, r]$  with  $r > 0$  small and  $e_i$  the standard basis of  $\mathbb{R}^2$ , maps approximately to the parallelogram

$$\phi(u) + [r_1 \partial_{u_1} \phi(u), r_2 \partial_{u_2} \phi(u)],$$

where  $r_1, r_2 \in [0, r]$ . Using the notions of length and angle given by the metric  $g$ , the volume of that parallelogram can be seen to be  $\sqrt{\det G(u)}$ , where  $G(u)$  is the matrix from Definition 3.1.4 of the Riemannian metric.

**Definition 3.1.7** (Integration). *Let  $M$  be a regular surface,  $g$  a Riemannian metric on  $M$ . Let  $(U, \phi, V)$  be a local parametrization of  $M$  and  $f : M \rightarrow \mathbb{R}$  with  $f|_{M \setminus V} = 0$ .  $f$  is called integrable if the function*

$$\begin{aligned} U &\rightarrow \mathbb{R} \\ u &\mapsto f(\phi(u)) \sqrt{\det(G(u))} \end{aligned}$$

with  $G$  as above is integrable. We define

$$\int_M f dA = \int_U f(\phi(u)) \sqrt{\det G(u)} du.$$

A function  $h : M \rightarrow \mathbb{R}$  is called integrable if it can be written as a finite sum

$$h = h_1 + \dots + h_k$$

such that for each  $h_i : M \rightarrow \mathbb{R}$  exists a local parametrization  $(U_i, \phi_i, V_i)$  of  $M$  such that  $h_i|_{M \setminus V_i} = 0$  and  $h_i$  is integrable according to the definition above. We define

$$\int_M h dA = \sum_{i=1}^k \int_M h_i dA.$$

Back to differentiation. Using the Riesz representation theorem on the functional

$$df_p : T_p M \rightarrow \mathbb{R},$$

sending a tangential vector  $v$  at a point  $p \in M$  on the derivative of  $f$  at point  $p$  in direction  $v$ , we can make the following definition.

**Definition 3.1.8** (Gradient of a function on a manifold). *Let  $M \subset \mathbb{R}^3$  be a regular surface,  $g$  a Riemannian metric on  $M$ . The gradient of a smooth function  $f : M \rightarrow \mathbb{R}$  at a point  $p \in M$  is defined as the unique vector  $\nabla f(p) \in T_p M$  such that*

$$g_p(\nabla f(p), v) = df_p(v) \text{ for all } v \in T_p M.$$

Like the gradient for a function from  $\mathbb{R}^d$  to  $\mathbb{R}$ , the gradient for a function from a Riemannian manifold  $(M, g)$  to  $\mathbb{R}$  points in the direction of the steepest increase within  $M$  with respect to the metric  $g$ .

The gradient assigns to each point  $p \in M$  smoothly a vector  $\nabla f(p)$  in the tangent space  $T_p M$ . Thereby it is an example for a smooth vector field.

**Definition 3.1.9** (Vector field). *A vector field  $W$  on  $M$  assigns to each point  $p \in M$  a vector  $W(p) \in T_p(M)$ . Given a local parametrization  $(U, \phi, V)$  of  $M$ , the vector field on  $M \cap V$  can be written as*

$$W(p) = \sum_{i=1}^2 W^i(p) \frac{\partial \phi}{\partial u_i}(\phi^{-1}(p)).$$

*It is called smooth, if the coefficient functions  $W^i(p) : M \cap V \rightarrow \mathbb{R}$  are smooth. This is equivalent to Definition 3.1.2 of smooth functions on manifolds.*

Next, we need to define differentiation of a smooth vector field  $W$ . We want to proceed as for scalar functions and define differentiation along curves on the surface. However, doing so, the derivative  $\dot{W}$  is no longer a vector field since  $\dot{W}$  is in general not tangential to the surface. To enforce that the derivative of a vector field is again a vector field, we project it on the tangential space. This defines the covariant derivative.

**Definition 3.1.10** (Covariant derivative). *Let  $M \subset \mathbb{R}^3$  be a regular surface with Riemannian metric  $g$ ,  $W$  a smooth vector field on  $M$ ,  $p \in M$  and  $v \in T_p M$ . Let  $c : (-\varepsilon, \varepsilon) \rightarrow M$  with  $c(0) = p$ ,  $\dot{c}(0) = v$ . The covariant derivative  $\nabla_v W \in T_p M$  of  $W$  in  $p$  in direction of  $v$  is defined as*

$$\nabla_v W = \frac{\nabla}{dt}(W \circ c)(0) = \Pi_p \left( \frac{d}{dt} W \circ c|_{t=0} \right),$$

where  $\Pi_p$  is the (w.r.t.  $g$ ) orthogonal projection on the tangent space  $T_p M$ .

Finally, we can define the divergence of a smooth vector field. While the gradient assigns a vector field to a scalar function, the divergence assigns a scalar function to a vector field. We notice that the covariant derivative of a smooth vector field  $W$  defines for each  $p \in M$  an

endomorphism of  $T_pM$

$$\nabla \cdot W : T_pM \rightarrow T_pM, v \mapsto \nabla_v W.$$

**Definition 3.1.11** (Divergence). *The trace of the endomorphism  $\nabla \cdot W$  is called divergence of  $W$  in  $p$ .*

To get an idea of the meaning of the divergence, let us take a look at the divergence theorem.

**Theorem 3.1.12** (Divergence theorem). *Let  $M_{reg} \subset \mathbb{R}^3$  be a regular surface and  $g$  a Riemannian metric on  $M_{reg}$ . Let  $W$  be a smooth vector field on  $M_{reg}$  with compact support. Let  $M \subset M_{reg}$  be a surface with boundary. Let  $\nu$  be the outer unit normal field of  $M$  with respect to  $M_{reg}$  and  $g$ . It holds*

$$\int_M \operatorname{div} W dA = \int_{\delta M} g(W, \nu) ds.$$

For the definitions of a surface with boundary, the outer unit normal field, the integral on the boundary and for a proof of the theorem, I refer to [Bär10]. The theorem yields the following interpretation of the divergence: The vector field  $W$  describes a flux on the regular surface  $M_{reg}$ . The divergence of  $W$  in a point  $p \in M_{reg}$  specifies whether  $p$  is a source or a sink of the flux. To see this, we take as surface with boundary the closure of a small ball  $B$  in  $M_{reg}$  with radius  $r$  and centre  $p$ . The integral on the right hand side specifies how much of the flux leaves the ball  $B$  while the left hand side averages the divergence over the whole ball. The limiting process  $r \rightarrow 0$  yields the above interpretation.

Finally, we can define the Laplace-Beltrami operator as the composition of the divergence and the gradient.

**Definition 3.1.13** (Laplace-Beltrami operator). *Let  $M \subset \mathbb{R}^3$  be a regular surface with Riemannian metric  $g$ . We define the Laplace-Beltrami operator  $\Delta : C^\infty(M) \rightarrow C^\infty(M)$  as*

$$\Delta f = \operatorname{div} \nabla f.$$

Like the definition of  $\operatorname{div}$  and  $\nabla$ , the definition of  $\Delta$  depends on the Riemannian metric  $g$ .

For a compact Riemannian manifold  $(M, g)$ , Helffer shows in [Hel10] that the negative Laplace-Beltrami operator  $-\Delta$  has a selfadjoint, positive semi definite extension with compact resolvent to the Sobolev space  $H^{2,2}(M)$ . Further, he shows that this implies the existence of an orthonormal basis of  $L^2(M)$  consisting of eigenvectors  $\{\psi_i\}$ ,  $i \in \mathbb{N}$ , of  $-\Delta$  with corresponding eigenvalues  $0 \leq \lambda_1 \leq \lambda_2 \leq \dots$ ,  $\lambda_i \rightarrow \infty$ .

### 3.1.2 Affine-invariant metric

In the last section, we saw the definition of the Laplace-Beltrami operator for a general Riemannian metric  $g$ . In [Iza17] and [IG17], Iza-Teran uses the induced Euclidean metric

$$g_p(v, w) = \langle v, w \rangle_{\mathbb{R}^3} \text{ for all } v, w \in T_p M \subset \mathbb{R}^3.$$

In this thesis, we will consider additionally a Laplace-Beltrami operator using an equi-affine invariant metric.

An equi-affine transformation is a transformation of the form  $\psi : \mathbb{R}^3 \rightarrow \mathbb{R}^3$ ,  $\psi(x) = Ax + b$ , where  $A \in \mathbb{R}^{3 \times 3}$  is a quadratic matrix with  $\det A = 1$  and  $b \in \mathbb{R}^3$  is a translation vector. An equi-affine transformation is volume-preserving. To see this, let  $B \subset \mathbb{R}^3$  be a measurable set and  $AB = \{Ax + b \mid x \in B\}$ . Using the transformation formula, we obtain

$$\text{vol}(AB) = \int_{AB} 1 dx = \int_B |\det(A)| dx = \int_B 1 dx = \text{vol}(B).$$

Consider the matrix  $A = \text{diag}(2, 1/2, 1)$  and the vector  $e_1 = (1, 0, 0)^T$ . It holds  $\det A = 1$  and

$$\|e_1\|_{\mathbb{R}^3} = 1 \neq 2 = \|Ae_1\|_{\mathbb{R}^3}.$$

This shows that the Euclidean metric is not invariant under equi-affine transformations.

In the following, I will present a metric which is invariant under such transformations. Using this metric in the definition of the Laplace-Beltrami operator yields an operator which is in the same sense invariant under isometries with respect to the equi-affine invariant metric as the Laplace-Beltrami operator used by Iza-Teran is invariant under isometries with respect to the Euclidean metric, see Section 3.3.

The equi-affine invariant metric was introduced by Blaschke in [Bla23]. Raviv et al. use the metric in several works for the construction of a Laplace-Beltrami operator, see, for instance, [Ra10] and [Ra14]. They use properties of the spectrum of the operator for shape recognition. Utilising the equi-affine invariant metric, their classification of shapes is invariant under equi-affine transformations.

In this thesis, I will follow Raviv et al.'s presentation of the metric in [Ra10] and [Ra14]. At several points, I will add explanations and details. In particular, I will show a connection between the Gaussian curvature in a point and the determinant of the bilinear form used in the construction of the metric. This connection is important for the definition of the metric

on surfaces consisting not only of elliptic points.

The first step to define an equi-affine invariant metric on a regular surface  $M$  is to define pointwise an equi-affine invariant symmetric bilinear form on the tangent spaces  $T_p M$  for  $p \in M$ .

Let  $(U, \phi, V)$  be a local parametrization of  $M$  around  $p$  and  $u \in U$  such that  $\phi(u) = p$ . To define a bilinear form  $b : T_p M \times T_p M \rightarrow \mathbb{R}$ , it suffices to define  $b$  for the basis vectors  $\frac{\partial \phi}{\partial u_1}(u)$  and  $\frac{\partial \phi}{\partial u_2}(u)$  of  $T_p M$ .

Later on, we want to use  $b$  to define a Riemannian metric. Remembering Definition 3.1.5 of the length of a vector, we think of  $b(\frac{\partial \phi}{\partial u_i}(u), \frac{\partial \phi}{\partial u_i}(u))$  as the (squared) length of the tangent vector  $\frac{\partial \phi}{\partial u_i}(u)$ . To define an equi-affine invariant notion of length, we can not use the Euclidean notion of length, but need to employ some property that is preserved under equi-affine transformations. Remembering that equi-affine transformations are volume-preserving, we define

$$B_{ij} = b\left(\frac{\partial \phi}{\partial u_i}(u), \frac{\partial \phi}{\partial u_j}(u)\right) = \det\left(\frac{\partial \phi}{\partial u_1}(u), \frac{\partial \phi}{\partial u_2}(u), \frac{\partial^2 \phi}{\partial u_i \partial u_j}(u)\right), \quad i, j \in \{1, 2\}.$$

From the transformation formula, we know that the volume of a parallelepiped  $P = [a_1 u, a_2 v, a_3 w]$ ,  $a_1, a_2, a_3 \in [0, 1]$ , formed by the vectors  $u, v$  and  $w \in \mathbb{R}^3$  is given by

$$\int_P 1 dx = \int_{[0,1]^3} |\det((u|v|w))| dx.$$

The expression

$$\det\left(\frac{\partial \phi}{\partial u_1}(u), \frac{\partial \phi}{\partial u_2}(u), \frac{\partial^2 \phi}{\partial u_i \partial u_j}(u)\right)$$

gives the *signed* volume of the parallelepiped formed by the vectors  $\frac{\partial \phi}{\partial u_1}(u)$ ,  $\frac{\partial \phi}{\partial u_2}(u)$  and  $\frac{\partial^2 \phi}{\partial u_i \partial u_j}(u)$ , see Figure 3.2.

Like the volume, the signed volume is preserved under equi-affine transformations since

$$\det((Au|Av|Aw)) = \det(A \cdot (u|v|w)) = \det(A) \cdot \det((u|v|w)) = \det((u|v|w)).$$

The symmetric matrix  $B \in \mathbb{R}^{2 \times 2}$  characterizes the bilinear form  $b$ .

The bilinear form  $b$  is equi-affine invariant but it depends on the parametrization  $\phi$ . To see and to remove this dependence, let  $(\tilde{U}, \tilde{\phi}, \tilde{V})$  be another parametrization of  $M$  around  $p$  and  $\tilde{u}$  such that  $\tilde{\phi}(\tilde{u}) = p$ . Let  $\tilde{B}$  and  $\tilde{b}$  be the matrix and the bilinear form defined analogously to

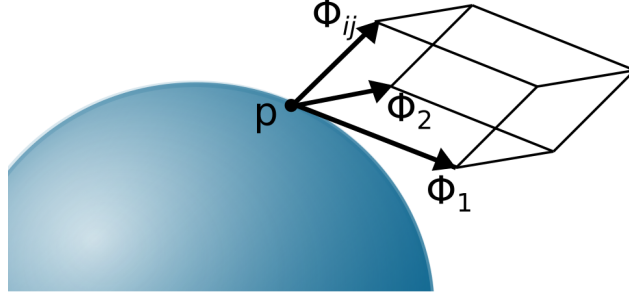


Figure 3.2: To define the bilinear form, use the (signed) volume of the parallelepiped formed by  $\phi_1 = \frac{\partial \phi}{\partial u_1}(u)$ ,  $\phi_2 = \frac{\partial \phi}{\partial u_2}(u)$  and  $\phi_{ij} = \frac{\partial^2 \phi}{\partial u_i \partial u_j}(u)$ , where  $u \in U$  with  $\phi(u) = p$ .

$B$  and  $b$  but using  $\tilde{\phi}$  instead of  $\phi$ . In a neighbourhood  $A \subset U$  of  $u$  we can write the original parametrization  $\phi$  as function composition  $\tilde{\phi} \circ \psi : A \rightarrow V$  for a smooth function  $\psi : A \rightarrow \tilde{U}$  with  $\psi(u) = \tilde{u}$ . Using the chain rule, we obtain

$$\frac{\partial \phi}{\partial u_i}(u) = \frac{\partial(\tilde{\phi} \circ \psi)}{\partial u_i}(u) = \frac{\partial \tilde{\phi}}{\partial \tilde{u}_1}(\psi(u)) \frac{\partial \psi_1}{\partial u_i}(u) + \frac{\partial \tilde{\phi}}{\partial \tilde{u}_2}(\psi(u)) \frac{\partial \psi_2}{\partial u_i}(u).$$

Using  $\psi(u) = \tilde{u}$  and defining

$$\xi_i = \frac{\partial \psi_1}{\partial u_i}(u) \text{ and } \eta_i = \frac{\partial \psi_2}{\partial u_i}(u),$$

we write

$$\frac{\partial \phi}{\partial u_i}(u) = \xi_i \frac{\partial \tilde{\phi}}{\partial \tilde{u}_1}(\tilde{u}) + \eta_i \frac{\partial \tilde{\phi}}{\partial \tilde{u}_2}(\tilde{u}).$$

Further, we get

$$\begin{aligned} \frac{\partial^2 \phi}{\partial u_i \partial u_j}(u) &= \xi_{ij} \frac{\partial^2 \tilde{\phi}}{\partial \tilde{u}_1^2}(\tilde{u}) + \eta_{ij} \frac{\partial^2 \tilde{\phi}}{\partial \tilde{u}_2^2}(\tilde{u}) + \\ &\xi_i \xi_j \frac{\partial^2 \tilde{\phi}}{\partial \tilde{u}_1^2}(\tilde{u}) + (\xi_i \eta_j + \eta_i \xi_j) \frac{\partial^2 \tilde{\phi}}{\partial \tilde{u}_1 \partial \tilde{u}_2}(\tilde{u}) + \eta_i \eta_j \frac{\partial^2 \tilde{\phi}}{\partial \tilde{u}_2^2}(\tilde{u}), \end{aligned}$$

where

$$\xi_{ij} = \frac{\partial^2 \psi_1}{\partial u_i \partial u_j}(u) \text{ and } \eta_{ij} = \frac{\partial^2 \psi_2}{\partial u_i \partial u_j}(u).$$

Using the above formulas to express the bilinear form  $b$  in terms of  $\tilde{\phi}$  yields

$$\begin{aligned} b\left(\frac{\partial\phi}{\partial u_i}(u), \frac{\partial\phi}{\partial u_j}(u)\right) &= \det\left(\frac{\partial\phi}{\partial u_1}(u), \frac{\partial\phi}{\partial u_2}(u), \frac{\partial^2\phi}{\partial u_i\partial u_j}(u)\right) \\ &= \det\left(\xi_1\frac{\partial\tilde{\phi}}{\partial\tilde{u}_1}(\tilde{u}) + \eta_1\frac{\partial\tilde{\phi}}{\partial\tilde{u}_2}(\tilde{u}), \xi_2\frac{\partial\tilde{\phi}}{\partial\tilde{u}_1}(\tilde{u}) + \eta_2\frac{\partial\tilde{\phi}}{\partial\tilde{u}_2}(\tilde{u}), \right. \\ &\quad \xi_{ij}\frac{\partial\tilde{\phi}}{\partial\tilde{u}_1}(\tilde{u}) + \eta_{ij}\frac{\partial\tilde{\phi}}{\partial\tilde{u}_2}(\tilde{u}) + \xi_i\xi_j\frac{\partial^2\tilde{\phi}}{\partial\tilde{u}_1^2}(\tilde{u}) + (\xi_i\eta_j + \xi_j\eta_i)\frac{\partial^2\tilde{\phi}}{\partial\tilde{u}_1\partial\tilde{u}_2}(\tilde{u}) + \\ &\quad \left. \eta_i\eta_j\frac{\partial^2\tilde{\phi}}{\partial\tilde{u}_2^2}(\tilde{u})\right). \end{aligned}$$

Using that the determinant is linear in its columns, that  $\det(v_1, v_2, v_3) = -\det(v_2, v_1, v_3)$  and that  $\det(v_1, v_2, v_3) = 0$  if  $v_i$  and  $v_j$ ,  $i \neq j \in \{1, 2, 3\}$  are linearly dependant, we get

$$\begin{aligned} b\left(\frac{\partial\phi}{\partial u_i}(u), \frac{\partial\phi}{\partial u_j}(u)\right) &= (\xi_1\eta_2 - \xi_2\eta_1) \cdot \det\left(\frac{\partial\tilde{\phi}}{\partial\tilde{u}_1}(\tilde{u}), \frac{\partial\tilde{\phi}}{\partial\tilde{u}_2}(\tilde{u}), \right. \\ &\quad \left. \xi_i\xi_j\frac{\partial^2\tilde{\phi}}{\partial\tilde{u}_1^2}(\tilde{u}) + (\xi_i\eta_j + \xi_j\eta_i)\frac{\partial^2\tilde{\phi}}{\partial\tilde{u}_1\partial\tilde{u}_2}(\tilde{u}) + \eta_i\eta_j\frac{\partial^2\tilde{\phi}}{\partial\tilde{u}_2^2}(\tilde{u})\right). \end{aligned} \quad (3.1.3)$$

On the other hand, the above formulas, the bilinearity of  $\tilde{b}$  and the linearity of the determinant in its columns yield

$$\begin{aligned} \tilde{b}\left(\frac{\partial\phi}{\partial u_i}(u), \frac{\partial\phi}{\partial u_j}(u)\right) &= \det\left(\frac{\partial\tilde{\phi}}{\partial\tilde{u}_1}(\tilde{u}), \frac{\partial\tilde{\phi}}{\partial\tilde{u}_2}(\tilde{u}), \right. \\ &\quad \left. \xi_i\xi_j\frac{\partial^2\tilde{\phi}}{\partial\tilde{u}_1^2}(\tilde{u}) + (\xi_i\eta_j + \xi_j\eta_i)\frac{\partial^2\tilde{\phi}}{\partial\tilde{u}_1\partial\tilde{u}_2}(\tilde{u}) + \eta_i\eta_j\frac{\partial^2\tilde{\phi}}{\partial\tilde{u}_2^2}(\tilde{u})\right) \end{aligned} \quad (3.1.4)$$

We conclude that the bilinear forms  $b$  and  $\tilde{b}$  differ by the factor  $(\xi_i\eta_j - \xi_j\eta_i) = \det D\psi(u)$ .

Using the Jacobian

$$D\psi(u) = \begin{pmatrix} \xi_1 & \xi_2 \\ \eta_1 & \eta_2 \end{pmatrix}$$

of  $\psi$  in  $u$ , Equation 3.1.3 can be written as

$$B_{ij} = (\xi_1\eta_2 - \xi_2\eta_1) \left( D\psi(u)^T \tilde{B} D\psi(u) \right).$$

Using  $\det D\psi(u) = \det D\psi(u)^T = (\xi_1\eta_2 - \xi_2\eta_1)$ , we obtain

$$\det B = (\xi_1\eta_2 - \xi_2\eta_1)^4 \det \tilde{B}. \quad (3.1.5)$$

Finally, we can define an equi-affine invariant symmetric bilinear form  $h$  as

$$h\left(\frac{\partial\phi}{\partial u_i}(u), \frac{\partial\phi}{\partial u_j}(u)\right) = \det B^{-\frac{1}{4}} B_{ij}, \quad i, j \in \{1, 2\}. \quad (3.1.6)$$

For the moment, we assume  $\det B > 0$ , we will later come back to this.

The definition of  $h$  does not depend on the parametrization  $\phi$ , *i.e.*

$$\tilde{h}\left(\frac{\partial\tilde{\phi}}{\partial \tilde{u}_i}(\tilde{u}), \frac{\partial\tilde{\phi}}{\partial \tilde{u}_j}(\tilde{u})\right) = \det \tilde{B}^{-\frac{1}{4}} \tilde{B}_{ij}, \quad i, j \in \{1, 2\}$$

defines the same bilinear form on  $T_p M$ . This can be seen using Equations 3.1.3, 3.1.4 and 3.1.5 to obtain

$$\begin{aligned} \tilde{h}\left(\frac{\partial\phi}{\partial u_i}(u), \frac{\partial\phi}{\partial u_j}(u)\right) &= \det \tilde{B}^{-\frac{1}{4}} \cdot \tilde{b}\left(\frac{\partial\phi}{\partial u_i}(u), \frac{\partial\phi}{\partial u_j}(u)\right) \\ &= (\xi_1\eta_2 - \xi_2\eta_1) \cdot \det B^{-\frac{1}{4}} \cdot (\xi_1\eta_2 - \xi_2\eta_1)^{-1} \cdot b\left(\frac{\partial\phi}{\partial u_i}(u), \frac{\partial\phi}{\partial u_j}(u)\right) \\ &= h\left(\frac{\partial\phi}{\partial u_i}(u), \frac{\partial\phi}{\partial u_j}(u)\right). \end{aligned}$$

To characterize in which cases our assumption  $\det B > 0$  is fulfilled and to construct a Riemannian metric from the bilinear form  $h$ , we need the term of Gaussian curvature. Before we define Gaussian curvature, we need some further notions of differential geometry. The following is based on [Bär10]. We consider regular surfaces equipped with the induced Euclidean metric.

**Definition 3.1.14** (Normal field). *Let  $M \subset \mathbb{R}^3$  be a regular surface. A normal field on  $M$  is a map*

$$N : M \rightarrow \mathbb{R}^3$$

*such that for every  $p \in M$ , the vector  $N(p)$  is orthogonal on the tangent plane of  $M$  in  $p$ ,  $N(p) \perp T_p M$ . A normal field on  $M$  is called unit normal field if it fulfils  $\|N(p)\| = 1$  for all  $p \in M$ .*

Given the definition of normal fields and definition 3.1.2 of smooth maps on  $M$ , we can define orientable surfaces.

**Definition 3.1.15** (Orientable surface). *A regular surface  $M \subset \mathbb{R}^3$  is called orientable if there exists a smooth unit normal field on  $M$ .*

Let me illustrate this concept with two simple examples. Choosing  $N(x) = x$ , we see that the unit sphere is an orientable surface. The Möbius strip on the other hand is an example of a non-orientable surface. An orientable surface has exactly two smooth unit normal fields,  $N$  and  $-N$ .

To characterize how an orientable regular surface with smooth unit normal field  $N$  curves, we examine how  $N$  changes when we move along the surface. Given a point  $p \in M$  and  $v \in T_pM$ , let  $\gamma : (-\varepsilon, \varepsilon) \rightarrow M$  be such that  $\gamma(0) = p, \dot{\gamma}(0) = v$ . We defined the differential of  $N$  at  $p$  in direction  $v$  as

$$d_pN(v) = \frac{d}{dt}(N \circ \gamma)|_{t=0}.$$

As  $N \circ \gamma$  defines a curve on the unit sphere  $S^2 \subset \mathbb{R}^3$  and  $N(\gamma(0)) = N(p)$ , we have  $d_pN(v) \in T_{N(p)}S^2$ . Further, it holds  $T_{N(p)}S^2 = N(p)^\perp = T_pM$ . Therefore, the differential  $d_pN : T_pM \rightarrow T_pM$  is an endomorphism.

It can be shown that the map  $d_pN : T_pM \rightarrow T_pM$  is self-adjoint with respect to the Euclidean inner product of  $\mathbb{R}^3$  restricted to  $T_pM$ . We know from the spectral theorem that we can find an orthonormal basis  $X_1, X_2$  of  $T_pM$  consisting of eigenvectors of  $d_pN$ ,

$$d_pN(X_i) = \kappa_i X_i, \quad i = 1, 2,$$

where  $\kappa_1, \kappa_2 \in \mathbb{R}$ .

**Definition 3.1.16** (Principal curvature). *The eigenvalues  $\kappa_1$  and  $\kappa_2$  are called principal curvatures of the regular surface  $M$  with orientation  $N$  in point  $p$ . The corresponding eigenvectors  $X_1$  and  $X_2$  are called directions of principal curvature.*

One can imagine the principal curvatures as a measure of the minimal and the maximal curvature of the orientable regular surface  $M$  in the direction of the smooth unit normal field  $N$ . Choosing as orientation of  $M$  the unit normal field  $-N$  the principal curvatures switch their signs.

**Definition 3.1.17** (Gaussian curvature). *Let  $M \subset \mathbb{R}^3$  be a regular surface with orientation  $N$ ,  $p \in M$ . Let  $\kappa_1$  and  $\kappa_2$  be the principal curvatures of  $M$  in  $p$ . We define the Gaussian curvature of  $M$  in  $p$  as*

$$K(p) = \kappa_1 \kappa_2.$$

We call the point  $p$

1. *elliptic*, if  $K(p) > 0$ ,

2. *hyperbolic*, if  $K(p) < 0$ ,

3. *parabolic*, if  $K(p) = 0$ .

In an elliptic point, the surface bends in the same direction, independent of the direction in that one moves. In a hyperbolic point, it bends in different directions, while in a parabolic point exists a direction in that it does not bend at all. See Figure 3.3 for examples.

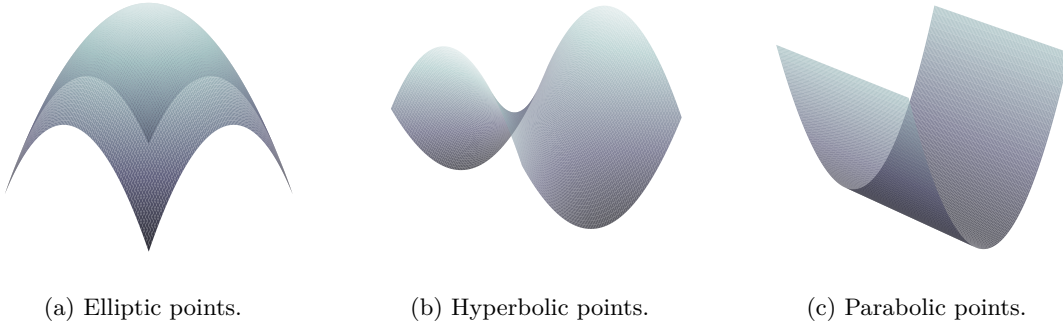


Figure 3.3: Example for regular surfaces with different Gaussian curvatures.

Back to the definition of an equi-affine invariant metric. Given a parametrization  $(U, \phi, V)$  of  $M$  around a point  $p \in M$ , we defined an equi-affine invariant bilinear form  $b$  on  $T_p M$ . This bilinear form depended on the parametrization  $\phi$ . We saw that we can remove the dependence by defining another bilinear form  $h$  as

$$h \left( \frac{\partial \phi}{\partial u_i}(u), \frac{\partial \phi}{\partial u_j}(u) \right) = \det B^{-\frac{1}{4}} B_{ij}, \quad i, j \in \{1, 2\}$$

where  $B \in \mathbb{R}^{2 \times 2}$  is the matrix with entries

$$B_{ij} = \det \left( \frac{\partial \phi}{\partial u_1}(u), \frac{\partial \phi}{\partial u_2}(u), \frac{\partial^2 \phi}{\partial u_i \partial u_j}(u) \right), \quad i, j \in \{1, 2\}.$$

In the definition of  $h$ , we assumed  $\det B > 0$ . This assumption is fulfilled if and only if the Gaussian curvature of  $M$  in  $p$  is greater than 0, *i.e.*  $p$  is an elliptic point. To see this, we use

$$\left\langle \frac{\partial^2 \phi}{\partial u_i \partial u_j}(u), N(p) \right\rangle_{\mathbb{R}^3} = - \left\langle \frac{\partial \phi}{\partial u_i}(u), d_p N \left( \frac{\partial \phi}{\partial u_j}(u) \right) \right\rangle_{\mathbb{R}^3}, \quad (3.1.7)$$

where  $N$  is an orientation of  $M$ . A proof of this equation can for example be found on page 121 of [Bär10].

Omitting the function argument  $u$  for simplicity, by definition of  $B$  holds

$$\det B = \det \left( \frac{\partial \phi}{\partial u_1}, \frac{\partial \phi}{\partial u_2}, \frac{\partial^2 \phi}{\partial u_1^2} \right) \det \left( \frac{\partial \phi}{\partial u_1}, \frac{\partial \phi}{\partial u_2}, \frac{\partial^2 \phi}{\partial u_2^2} \right) - \det \left( \frac{\partial \phi}{\partial u_1}, \frac{\partial \phi}{\partial u_2}, \frac{\partial^2 \phi}{\partial u_1 \partial u_2} \right)^2.$$

We write  $\frac{\partial^2 \phi}{\partial u_i \partial u_j}$  as linear combination of  $\frac{\partial \phi}{\partial u_1}$ ,  $\frac{\partial \phi}{\partial u_2}$  and  $N(p)$ , use the linearity of the determinant in its columns and the fact that  $\det(v, w, v) = 0$  to obtain from the above equation

$$\det B = \det \left( \frac{\partial \phi}{\partial u_1}, \frac{\partial \phi}{\partial u_2}, N(p) \right)^2 \left( \left\langle \frac{\partial^2 \phi}{\partial u_1^2}, N(p) \right\rangle_{\mathbb{R}^3} \left\langle \frac{\partial^2 \phi}{\partial u_2^2}, N(p) \right\rangle_{\mathbb{R}^3} - \left\langle \frac{\partial^2 \phi}{\partial u_1 \partial u_2}, N(p) \right\rangle_{\mathbb{R}^3}^2 \right).$$

Using Equation 3.1.7, this becomes

$$\begin{aligned} \det B &= \det \left( \frac{\partial \phi}{\partial u_1}, \frac{\partial \phi}{\partial u_2}, N(p) \right)^2 \left( \left\langle \frac{\partial \phi}{\partial u_1}, d_p N \left( \frac{\partial \phi}{\partial u_1} \right) \right\rangle_{\mathbb{R}^3} \left\langle \frac{\partial \phi}{\partial u_2}, d_p N \left( \frac{\partial \phi}{\partial u_2} \right) \right\rangle_{\mathbb{R}^3} \right. \\ &\quad \left. - \left\langle \frac{\partial \phi}{\partial u_1}, d_p N \left( \frac{\partial \phi}{\partial u_2} \right) \right\rangle_{\mathbb{R}^3}^2 \right). \end{aligned}$$

The first factor is greater than zero as  $\frac{\partial \phi}{\partial u_1}$ ,  $\frac{\partial \phi}{\partial u_2}$  and  $N(p)$  are linearly independent. To examine the second factor, let  $\kappa_1$  and  $\kappa_2$  be the principal curvatures for the orientation  $N$  with the corresponding directions of principal curvature  $X_1$  and  $X_2$ .  $X_1$  and  $X_2$  are orthonormal eigenvectors of  $d_p N$  with corresponding eigenvalues  $\kappa_1$  and  $\kappa_2$ . Let

$$A = \begin{pmatrix} a_1 & a_2 \\ b_1 & b_2 \end{pmatrix}$$

be the matrix describing the change of basis from  $\frac{\partial \phi}{\partial u_i}(u)$  to  $X_i$ , i.e.  $\frac{\partial \phi}{\partial u_1}(u) = a_1 X_1 + a_2 X_2$  and  $\frac{\partial \phi}{\partial u_2}(u) = b_1 X_1 + b_2 X_2$ . Inserting this, we get

$$\begin{aligned} &\left\langle \frac{\partial \phi}{\partial u_1}, d_p N \left( \frac{\partial \phi}{\partial u_1} \right) \right\rangle_{\mathbb{R}^3} \left\langle \frac{\partial \phi}{\partial u_2}, d_p N \left( \frac{\partial \phi}{\partial u_2} \right) \right\rangle_{\mathbb{R}^3} - \left\langle \frac{\partial \phi}{\partial u_1}, d_p N \left( \frac{\partial \phi}{\partial u_2} \right) \right\rangle_{\mathbb{R}^3}^2 \\ &= \langle a_1 X_1 + a_2 X_2, a_1 \kappa_1 X_1 + a_2 \kappa_2 X_2 \rangle \cdot \langle b_1 X_1 + b_2 X_2, b_1 \kappa_1 X_1 + b_2 \kappa_2 X_2 \rangle \\ &\quad - \langle a_1 X_1 + a_2 X_2, b_1 \kappa_1 X_1 + b_2 \kappa_2 X_2 \rangle^2 \\ &= (a_1^2 \kappa_1 + a_2^2 \kappa_2)(b_1^2 \kappa_1 + b_2^2 \kappa_2) - (a_1 b_1 \kappa_1 + a_2 b_2 \kappa_2)^2 \end{aligned}$$

A short calculation reveals that this is equal to  $K(p) \det(A)^2$ , where  $K(p) = \kappa_1 \kappa_2$  is the

Gaussian curvature of  $M$  in  $p$ . The expression  $\det(A)^2$  is greater than zero since  $A$  describes a change of basis. Altogether, we obtain  $\text{sgn}(\det B) = \text{sgn}(K(p))$ .

Hence, our assumption  $\det B > 0$  is fulfilled in all elliptic points. In all hyperbolic and parabolic points Raviv et al. define  $h = 0$ . As  $\det B$  is invariant under equi-affine transformations and  $\text{sgn}(\det B) = \text{sgn}(K(p))$ , we get that under equi-affine transformations elliptic, hyperbolic and parabolic points are mapped to elliptic, hyperbolic and parabolic points, respectively. Therefore,  $h$  defines an equi-affine invariant symmetric bilinear form on the tangent space  $T_p M$  for every point  $p$  of the regular surface  $M$ .

The next step is to construct a metric from  $h$ . Let us at first consider elliptic points. Raviv et al. propose in [Ra10] and [Ra14] to project  $h$  on the space of positive definite matrices. Considering the symmetric matrix  $H$  defined as

$$H_{ij} = h \left( \frac{\partial \phi}{\partial u_i}(u), \frac{\partial \phi}{\partial u_j}(u) \right),$$

and characterizing the bilinear form  $h$ , they write

$$H = U \Lambda U^T$$

where  $U$  is orthogonal and  $\Lambda = \text{diag}\{\gamma_1, \gamma_2\}$ . They define the symmetric positive definite metric  $\bar{H}$  by

$$\bar{H} = U |\Lambda| U^T.$$

In hyperbolic and parabolic points they set  $\bar{H} = 0$ . If all points of the regular surface  $M$  are elliptic,  $\bar{H}$  defines a valid Riemannian metric on  $M$  that is equi-affine and parametrization invariant. For all other regular surfaces it defines a valid Riemannian metric on elliptic regions while hyperbolic and parabolic regions are ignored. In our implementation, we handle hyperbolic points like elliptic points, only using the absolute value of  $\det B$  in Equation 3.1.6, such that  $|\det B|^{-1/4}$  is a real number. It is not clear why Raviv et al. set the metric to zero for hyperbolic points. Using the metric for car parts, which often have many hyperbolic points, numerical observations support our procedure.

The equi-affine invariant Laplace-Beltrami operator is defined using  $\bar{H}$  as metric in the usual definition of the Laplace-Beltrami operator 3.1.13.

### 3.1.3 Fokker-Planck operator

Apart from the Laplace-Beltrami operator for the induced Euclidean metric, Iza-Teran uses in [Iza17] and [IG17] a Fokker-Planck operator. He refers to the operator as "operator for point clouds" or "operator of independent components". It comes from the context of nonlinear independent component analysis (NICA) [SC08]. However, Iza-Teran uses it in a different way. In this section, I will give a short overview how the operator is motivated and built in [SC08] before I will explain how Iza-Teran uses it in our context.

#### General setting

The underlying model in Singer's and Coifman's construction of the operator in [SC08] is the following:

Given *observable* data points  $y^i \in \mathbb{R}^n$ , they assume that these points are the images of points  $x^i \in \mathbb{R}^m$ , lying in a lower dimensional *parameter space*,  $m \leq n$ , under a non-linear mapping  $f : \mathbb{R}^m \rightarrow \mathbb{R}^n$ , *i.e.*

$$y^i = f(x^i), \quad i = 1, \dots, N.$$

The data points  $x^i \in \mathbb{R}^m$  in the parameter space are samples of a stochastic process  $x = (x_1, \dots, x_m) \in \mathbb{R}^m$  whose components are independent stochastic Itô processes, *i.e.*

$$dx_j = a_j(x_j)dt + b_j(x_j)d\omega_j, \quad j = 1, \dots, m,$$

where  $a_j$  and  $b_j$  are unknown drift and noise coefficients, and  $\omega_j$  are independent  $\delta$ -correlated white noises.

Their objective is to find for each observed sample  $y^i = f(x^i)$  the underlying parameters  $x^i = (x_1^i, \dots, x_m^i)$ . In order to achieve this, Singer's and Coifman's first step is to approximate the distance of the samples in the parameter space. They show that for the Jacobian  $J(x^i) \in \mathbb{R}^{n \times m}$ ,  $J(x^i)_{j\ell} = \frac{\partial f_j}{\partial x_\ell}(x^i)$ , of the map  $f$  at a point  $x^i$  can be assumed

$$C(y^i) = J(x^i)J(x^i)^T,$$

where  $C(y^i)$  is the covariance matrix of the stochastic process  $(y_1, \dots, y_n) = y = f(x)$  at the point  $y^i = f(x^i)$ , *i.e.*

$$C_{j\ell}(y^i) = \text{Cov}(y_j^i, y_\ell^i), \quad j, \ell \in \{1, \dots, n\}.$$

Next, they show that the square of the Euclidean distance of two samples  $x^i$  and  $x^k$  in the

parameter space can be written as

$$\begin{aligned} \|x^i - x^k\|^2 &= \frac{\|J^{-1}(y^i)(y^i - y^k)\|^2 + \|J^{-1}(y^k)(y^i - y^k)\|^2}{2} + O(\|y^i - y^k\|^4) \\ &= \frac{1}{2} (y^i - y^k)^T \left( J^{-T} J^{-1}(y^i) + J^{-T} J^{-1}(y^k) \right) (y^i - y^k) + O(\|y^i - y^k\|^4) \\ &= \frac{1}{2} (y^i - y^k)^T \left( C(y^i)^{-1} + C(y^k)^{-1} \right) (y^i - y^k) + O(\|y^i - y^k\|^4), \end{aligned} \quad (3.1.8)$$

where  $y^i = f(x^i)$  and  $y^k = f(x^k)$ .

Singer and Coifman show that the discrete normalized graph Laplacian for the Gaussian kernel

$$W_{ij} = \exp \left( - \frac{(y^i - y^k)^T \left( C(y^i)^{-1} + C(y^k)^{-1} \right) (y^i - y^k)}{4\varepsilon} \right) \quad (3.1.9)$$

converges for  $N \rightarrow \infty$  to a backward Fokker-Planck operator on the parameter space which separates into  $n$  one-dimensional components. This implies that for each component  $j \in \{1, \dots, m\}$  of the parameter space exists a unique eigenfunction  $\psi_{i_j}$  of the operator, that depends only on the  $j$ -th component  $x_j$  of the data points in the parameter space. Moreover, this dependence is strictly monotone.

Singer and Coifman assume that the  $i_j$ -th eigenvector of the operator for a fixed number  $N$  of data points approximates the  $i_j$ -th eigenfunction of the operator for  $N \rightarrow \infty$ . Thus, its  $k$ -th entry approximates a scaled version of the  $j$ -th entry  $x_j^k$  of the parameter vector  $x^k$  which was mapped to the observed data point  $y^k$ .

In praxis, calculating the covariance matrices  $C(y^i)$  is problematic. If we have the possibility to run several short simulations (simulation bursts) of a small enough time length  $\delta > 0$ , all initiating in  $x^i$ , we can approximate it using the sample covariance of the resulting point cloud  $y_1^i, \dots, y_M^i$

$$C_{i,\delta} = \frac{1}{M} \sum_{j=1}^M (y_j^i - y^i)(y_j^i - y^i)^T \quad (3.1.10)$$

and

$$C(y^i) = \frac{d+2}{\delta^2} C_{i,\delta} + O(\delta), \quad (3.1.11)$$

where  $d = \dim M_X = \dim M_Y$  is the dimension of the manifold on that the data points  $x^i$  in the parameter space and the observable data points  $y^i$ , respectively, lie. For a proof, see [SC08]. However, we often do not have the possibility to run such simulation bursts.

In [SC08], Singer and Coifman illustrate the approach with the following example. The para-

meter domain is the unit square  $[0, 1] \times [0, 1] \subset \mathbb{R}^2$ , the stochastic process for the parameters  $(x_1, x_2)$  is the Brownian motion with reflection at the boundary and the map  $f$  is given by

$$y_1 = x_1 + x_2^3, \quad y_2 = x_2 - x_1^3.$$

The operator described above approximates the Laplacian of the unit square, whose eigenvalues are  $\lambda_{n,m} = \pi^2(n^2 + m^2)$ ,  $n, m \in \mathbb{N}_0$ , with the corresponding eigenfunctions  $\phi_{n,m}(x_1, x_2) = \cos(n\pi x_1) \cos(m\pi x_2)$ . In particular  $\phi_{1,0}$  depends only on  $x_1$  and is strictly monotonically decreasing. Given only an observable point  $y = f(x)$  and the value of the eigenfunction  $\phi_{1,0}$  at this point, we can recover the component  $x_1$  up to the scaling by  $\cos(\pi \cdot)$ . The same holds for the second component  $x_2$  using  $\phi_{0,1}$ .

For my work, I used an implementation of the Fokker-Planck operator, following Iza-Teran's description in [IG17], which differs slightly from the normalization presented in Iza-Theran's thesis [Iza17]. Inspired by the normalization with  $\alpha = \frac{1}{2}$  in Coifman's work on Diffusion maps [CL06], Iza-Teran normalizes the kernel  $W$  from Equation 3.1.9 using the following steps. First, he uses a density normalization

$$W_{dens} = D^{-\frac{1}{2}} W D^{-\frac{1}{2}} \tag{3.1.12}$$

of the kernel  $W$  as in [TC14], where  $D$  is a diagonal matrix with elements

$$D_{ii} = \sum_{j=1}^{N_h} W_{ij}.$$

Next, the matrix  $W_{dens}$  is transformed into another symmetric matrix

$$W_{stoch} = \tilde{D}^{-\frac{1}{2}} W_{dens} \tilde{D}^{-\frac{1}{2}} \tag{3.1.13}$$

where  $\tilde{D}$  is the diagonal matrix with elements

$$\tilde{D}_{ii} = \sum_{j=1}^{N_h} (W_{dens})_{ij}.$$

Iza-Teran uses the eigenvectors of that matrix in his numerical experiments.

### Our application

In the invariant operator approach, we want to represent elements of the space  $L^2(M)$  in the

spectral domain of an operator. Here,  $M$  is a reference embedding of the simulated object, in our case a regular surface in  $\mathbb{R}^3$ . Before we continue, it is important to notice that we want to build an operator on  $M$  and not for example on the space of embeddings.

A natural way to extend Singer's and Coifman's approach to the analysis of car crash simulations is to consider the different embeddings of the car part in the simulation bundle as observable data points  $y^i \in Emb(M, \mathbb{R}^3)$  or in the discrete case as observable data points  $y^i \in \mathbb{R}^{3N}$ , where  $N$  is the number of nodes used in the discretization of the part. In this setting, the parameter space is closely related to the space of physical parameters of the simulation bundle. Additionally, time is a parameter. The mapping  $f$  between parameter space and observable space is given by the solution of the partial differential equations underlying the simulation.

Under the assumption that the physical parameters vary according to independent stochastic Itô processes, this extension could fit in Singer's and Coifman's setting. However, it is of no interest for our application. First, we know the physical parameters for each simulation and do not need to approximate them. Second, nor are we interested in an operator on the space of embeddings of the car part, nor in an operator on the space of physical parameters. For the invariant operator approach, we need an operator on the regular surface  $M$  given by a reference embedding of the car part.

Therefore, Iza-Teran proceeds differently. Given  $N$  points  $y_1, \dots, y_N \in \mathbb{R}^3$  on a reference embedding  $M$  of the car part, he calculates for each point  $y_i$  the sample covariance matrix  $C_{i,\delta}$  from Equation 3.1.10 for the point cloud  $\{y_i^j\}_{j=1}^{\#\text{embeddings}}$  formed by the  $i$ -th points of embeddings of the car part for different physical parameters or different timesteps.

Given the matrices  $C_{i,\delta}$ , he chooses a  $\delta$  to calculate the matrix  $C_i$  from Equation 3.1.11. Following along as Singer and Coifman, he uses the expression

$$\frac{1}{2} (y_i - y_k)^T \left( C(y_i)^{-1} + C(y_k)^{-1} \right) (y_i - y_k)$$

from Equation 3.1.8 as new notion of distance between the points  $y_i$  and  $y_k$ ,  $i, k \in \{1, \dots, N\}$ .

While this certainly gives a new notion of distance between the points  $y_i$  of the regular surface  $M$ , it does not seem to fit in Singer's and Coifman's setting: The points  $y_i$  lie all on a reference embedding  $M$  of the car part. They only differ in their intrinsic position on the car part. Let us assume that they are the images of points  $x_i$  in a parameter space under a nonlinear map  $f$ , *i.e.*  $f(x_i) = y_i$  as in Singer's and Coifman's setting. It is not clear what the

parameter space and the map should look like. It is solely clear that an interpretation of the parameter space as the space of physical parameters and time and of the map as the solution of the partial differential equations underlying the simulations is not possible. However, to approximate the Jacobian of  $f$  in  $x_i$ , Iza-Teran computes the sample covariance matrix of the point cloud  $\{y_i^j\}_{j=1}^{\#\text{embeddings}}$ , formed by the  $i$ -th points of embeddings of the car part for different physical parameters or timesteps. The assumption that those points can be used to approximate the Jacobian of  $f$ , a map that is independent of the physical parameters and time, is *at least* questionable.

The interpretation of the constructed operator as operator of independent components is no longer justified. We should think of the operator as a Laplace-Beltrami operator, or - depending on the normalization, compare to Coifman's work on Diffusion maps [CL06] - a Fokker-Planck operator on the regular surface  $M$ , which does not use the induced Euclidean metric but a different notion of distance given by

$$d(y_i, y_k) = \frac{1}{2} (y_i - y_k)^T (C_{i,\delta}^{-1} + C_{k,\delta}^{-1}) (y_i - y_k), \quad (3.1.14)$$

where  $C_{i,\delta}^{-1}$  are the pseudoinverses of  $C_{i,\delta}$ .

In the computation of  $C_{i,\delta}$ , Iza-Teran uses the  $i$ -th points  $y_i^j$  of the embeddings for different physical parameters and timesteps. If the position of the  $i$ -th point varies strongly between the embeddings, *i.e.* it depends strongly on the choice of physical parameters, the absolute values in the matrix  $C_{i,\delta}$  will be bigger than for points with less variation. Hence, the distances around points whose positions depend strongly on the choice of physical parameters shrink in relation to distances around points whose positions depend less strongly on the choice of physical parameters. The parameter  $\delta$  in the computation of the matrices  $C_i$  controls the amount of shrinkage.

## 3.2 Numerical Evaluation of the Operators

In this section, I will present algorithms for the numerical computation of the eigenbases of the above defined operators. For the computation of the Laplace-Beltrami operator using the induced Euclidean metric and for the computation of the Fokker-Planck operator, we follow the algorithms presented in [Iza17]. For theory on the convergence of the discrete operators to the continuous ones, I refer to Iza-Teran's work [Iza17].

### 3.2.1 Laplace-Beltrami operator

Let  $(M, g)$  be a regular surface and let  $\Delta$  be the corresponding Laplace-Beltrami operator. Given a mesh  $K$  of vertices  $V$  and faces  $F$  approximating the surface, we define the mesh Laplace operator by

$$L_k^h f(w) = \frac{1}{4\pi h^2} \sum_{t \in F} \frac{\text{Area}(t)}{\#V(t)} \sum_{v \in V(t)} \exp\left(-\frac{d_G(v, w)^2}{4h}\right) (f(v) - f(w)) \quad (3.2.1)$$

for all  $w \in V$ , all  $f : V \rightarrow \mathbb{R}$ . Here,  $V(t)$  is the set of vertices of the face  $t$ ,  $d_G(v, w)$  denotes the graph distance between the vertices  $v$  and  $w$  with respect to the Riemannian metric  $g$  and  $h$  is a parameter controlling the size of the local neighbourhoods of the vertices.

Algorithm 1 describes the general computation of the eigenvector basis of the mesh Laplace operator. It introduces a parameter  $\rho$ . All summands in Equation 3.2.1 for which  $\exp\left(-\frac{d_G(v, w)^2}{4h}\right)$  is under a certain threshold controlled by the parameter  $\rho$  are ignored. Choosing a small  $\rho$  speeds up the computation. For a sufficiently large parameter  $\rho$ , the operator  $L$  from Algorithm 1 coincides with the operator from Equation 3.2.1.

---

**Algorithm 1** Spectral decomposition of the mesh Laplace operator.

---

**Input:** A regular surface given as triangular mesh  $M$  with  $N_h$  points and  $N_f$  faces.

**Parameter:**  $n_{ev}$ : Number of eigenvectors to return,  $h$ : controlling the size of local neighbourhoods,  $\rho$ : controlling up to what distance vertices are included in Equation 3.2.1.

**Output:** First  $n_{ev}$  greatest eigenvectors of the mesh Laplace operator.

Initialize array  $\text{area}[N_h]$  with values 0.

```

5: for  $k = 1, \dots, N_f$  do
    for  $i = 1, 2, 3$  do
         $\text{area}[\text{index of } i\text{-th vertex of } k\text{-th face}] += (\text{area of } k\text{-th face})/3$ 
    end for
end for
10: for  $k = 1, \dots, N_h$  do
     $[\text{ids}, \text{dists}] = \text{graphdist}(k, M, \rho \cdot \sqrt{h})$   $\triangleright$  distances to all nodes with  $d_G(k, l) < \rho \cdot \sqrt{h}$ .
    for each  $l, d \in [\text{ids}, \text{dists}]$  do
         $W[k, l] = \text{area}[k] \cdot \text{area}[l] \cdot \exp(-d^2/(4h))/(4\pi h^2)$ 
    end for
15: end for
     $D = \text{diag}(W \cdot (1, \dots, 1))$ 
     $L = W - D$ 
     $[U, E] = \text{eigen}(L, n_{ev})$ 
return greatest  $n_{ev}$  eigenvectors  $U$  of  $L$ .

```

---

For the Laplace Beltrami operator using the induced Euclidean metric, I use software published by Jian Sun on Github<sup>3</sup>. Instead of the graph distance, it uses a shortest path algorithm for triangular surface meshes to approximate the geodesic distance of two nodes.

For the Laplace Beltrami operator using the equi-affine invariant metric, the first step is to calculate the edge lengths and the area with respect to the equi-affine invariant metric. I describe those calculations below. After those calculations, Algorithm 1 can be applied using, for instance, Dijkstra’s algorithm to compute the graph distances for the new edge lengths.

### Equi-affine invariant metric

In this section, I will describe the numerical approximation of the equi-affine invariant metric defined in Section 3.1.2. The regular surface  $M$  must be given as triangular mesh. I will follow Raviv et al.’s description in [Ra10] and [Ra14], adding several details including the process of unfolding a given triangle patch to the plane and an explanation how the obtained estimate of the metric tensor can be used to approximate the equi-affine invariant edge lengths.

For each triangle  $T$  of the surface, we calculate a constant approximation of the metric tensor  $\bar{H}$ . To do so, we need a local parametrization of the regular surface around  $T$ , *i.e.* a map  $\phi$  from a subset  $U$  of  $\mathbb{R}^2$  to a subset  $V \cap M \subset \mathbb{R}^3$  of the regular surface around  $T$ . To construct such a parametrization, we consider a patch of four triangles consisting of  $T$  and the three neighbouring triangles. For now, we assume that  $T$  is not at the boundary of the mesh.

To get a 2-dimensional parameter domain  $U$ , we unfold the triangle patch to the plane and do an affine transformation, such that  $T$  becomes the unit triangle with vertices  $u^1 = (0, 0)$ ,  $u^2 = (1, 0)$  and  $u^3 = (1, 1)$ . See Figure 3.4 for an illustration. Next, a quadratic para-

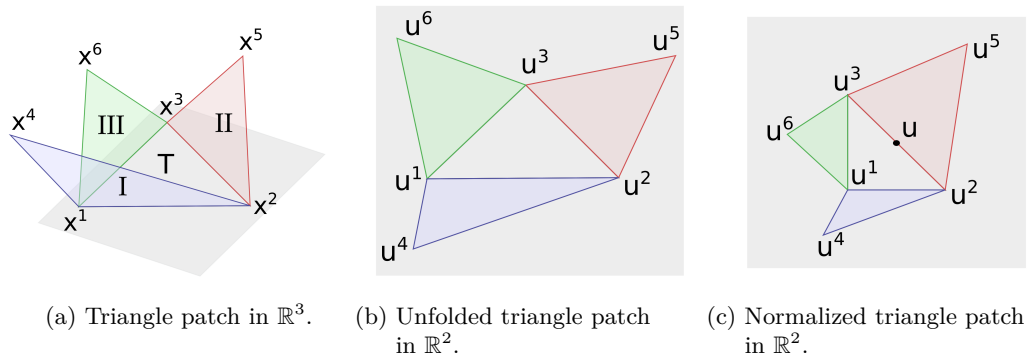


Figure 3.4: Unfolding and normalizing a triangle patch. Notations for Algorithm 2.

<sup>3</sup><https://github.com/areslp/matlab/tree/master/MeshLP/MeshLP>

metrization  $\phi$  of the surface around  $T$  is calculated solving the linear equation system

$$\phi_j(u_1^i, u_2^i) = c_j^{(0)} + c_j^{(1)}u_1^i + c_j^{(2)}u_2^i + c_j^{(3)}u_1^i u_2^i + c_j^{(4)}(u_1^i)^2 + c_j^{(5)}(u_2^i)^2 = X_j^i$$

for all  $j = 1, 2, 3$  and  $i = 1, \dots, 6$ , where  $(u_1^i, u_2^i)$  and  $(X_1^i, X_2^i, X_3^i)$  are the six corners of the four unfolded and normalized triangles in  $\mathbb{R}^2$  and of the original triangles in  $\mathbb{R}^3$ , respectively.  $\phi$  is the unique quadratic map  $\mathbb{R}^2 \rightarrow \mathbb{R}^3$  mapping the six corners of the unfolded and normalized triangles to the corresponding corners of the original triangles in  $\mathbb{R}^3$ . We use it as a local parametrization of the regular surface around  $T$ . The proceeding is summarized in Algorithm 2.

---

**Algorithm 2** Unfold a triangle patch to calculate the coefficients of a quadratic approximation of a local parametrization of a regular surface.

---

**Input:** A triangle  $T$  in a triangular mesh  $K$ .

**Output:** Coefficient matrix  $C$ .

▷ Unfold the 3 triangles around  $T$  to the plane. See Figure 3.4 for the notation.

$$u^1 = (0, 0)^T$$

$$5: u^2 = (\|X^1 - X^2\|, 0)^T \quad \triangleright \|\cdot\| \text{ denotes the Euclidean norm.}$$

$$u^3 = \|X^1 - X^3\| \cdot (\cos(\angle X^2 X^1 X^3), \sin(\angle X^2 X^1 X^3))^T$$

**if** triangle I is Null **then** ▷ Invert centre triangle. See Figure 3.5.

$$X^4 = X^1 + (X^2 - X^3)$$

**end if**

$$10: u^4 = \|X^1 - X^4\| \cdot (\cos(\angle X^4 X^1 X^2), -\sin(\angle X^4 X^1 X^2))^T$$

**if** triangle II is Null **then**

$$X^5 = X^2 + (X^3 - X^1)$$

**end if**

$$u^5 = u^2 + \|X^2 - X^5\| \cdot (-\cos(\angle X^3 X^2 X^1 + \angle X^5 X^2 X^3), \sin(\angle X^3 X^2 X^1 + \angle X^5 X^2 X^3))^T$$

15: **if** triangle III is Null **then**

$$X^6 = X^1 + (X^3 - X^2)$$

**end if**

$$u^6 = (\cos(\angle X^2 X^1 X^3 + \angle X^3 X^1 X^6), \sin(\angle X^2 X^1 X^3 + \angle X^3 X^1 X^6))$$

▷ Do a linear normalization such that  $u^1 = (0, 0)$ ,  $u^2 = (1, 0)$  and  $u^3 = (0, 1)$ .

$$20: N = (u^2 | u^3)^{-1}$$

**for**  $i = 1, \dots, 6$  **do**

$$u^i = N u^i$$

**end for**

Declare matrix  $P \in \mathbb{R}^{6 \times 6}$ . ▷ For the values of the polynomials  $1, u, v, uv, u^2, v^2$  at  $u^i$ .

25: **for**  $i = 1, \dots, 6$  **do**

$$\text{set } i\text{-th row of } P \text{ to } (1, u_1^i, u_2^i, u_1^i \cdot u_2^i, (u_1^i)^2, (u_2^i)^2).$$

**end for**

$$\text{solve linear system } PC = (X^1 | \dots | X^6)^T$$

**return** Coefficient matrix  $C \in \mathbb{R}^{6 \times 3}$ .

---

Given the parametrization  $\phi$ , we approximate the pre-metric tensor  $H$  at the point  $u = (1/2, 1/2)$ . To do that, we note

$$\begin{aligned}\frac{\partial\phi}{\partial u_1}(u) &= c^{(1)} + c^{(3)}u_2 + 2c^{(4)}u_1, \\ \frac{\partial\phi}{\partial u_2}(u) &= c^{(2)} + c^{(3)}u_1 + 2c^{(5)}u_2, \\ \frac{\partial^2\phi}{\partial u_1^2}(u) &= 2c^{(4)}, \\ \frac{\partial^2\phi}{\partial u_2^2}(u) &= 2c^{(5)}, \\ \frac{\partial^2\phi}{\partial u_1\partial u_2}(u) &= c^{(3)}\end{aligned}$$

and compute

$$B_{ij} = \det\left(\frac{\partial\phi}{\partial u_1}(u), \frac{\partial\phi}{\partial u_2}(u), \frac{\partial^2\phi}{\partial u_i\partial u_j}(u)\right)$$

for  $i, j = 1, 2$ . Next, we set

$$H = |\det(B)|^{-\frac{1}{4}}B,$$

where we assume for now that  $\det B \neq 0$ .

Given the approximation of the pre-metric tensor  $H$  in the triangle  $T$ , we calculate the eigendecomposition  $U\Lambda U^T = H$  and use  $\bar{H} = U|\Lambda|U^T$  as approximation of the metric tensor in  $T$ .

Next, we want to use  $\bar{H}$  to get an estimate of the equi-affine invariant edge lengths in  $T$ , *i.e.* an estimate of the equi-affine invariant distances between the vertices  $X^1, X^2$  and  $X^3$ .

In Definition 3.1.6, we defined the length of a curve  $c : [0, 1] \rightarrow M$  on a regular surface  $M$  with Riemannian metric  $h$  as

$$\ell(c) = \int_0^1 \sqrt{h_{c(t)}(\dot{c}(t), \dot{c}(t))} dt.$$

The vertices  $X^1, X^2$  and  $X^3$  of  $T$  correspond in the parameter domain  $U$  to the vertices  $u^1 = (0, 0)$ ,  $u^2 = (1, 0)$  and  $u^3 = (0, 1)$  of the unit triangle. In the following, we use circular indices, *i.e.*  $3 + 1 = 1$ .

Let  $\tilde{c}_i : [0, 1] \rightarrow M$ ,  $\tilde{c}_i(t) = u^i + t \cdot (u^{i+1} - u^i)$  be a curve along the  $i$ -th edge of the triangle in the parameter domain and  $c_i : [0, 1] \rightarrow M$  be the image of that curve under the parametrization  $\phi$ , *i.e.*  $c_i(t) = \phi(\tilde{c}_i(t))$ . Then  $c_i(0) = X^i$  and  $c_i(1) = X^{i+1}$ . To approximate the distances

between  $X^i$  and  $X^{i+1}$ , we consider the length of the curve  $c_i$ . To approximate, for example, the distance between  $X^1$  and  $X^2$ , we consider the curve  $\tilde{c}_1(t) = (0, 0) + t \cdot ((1, 0) - (0, 0)) = te_1$  and  $c_1 : [0, 1] \rightarrow M$ ,  $c_1(t) = \phi(\tilde{c}_1(t))$ . By the chain rule holds  $\dot{c}_1(t) = \frac{\partial \phi}{\partial u_1}$  and we get

$$\ell(c_1) = \int_0^1 \sqrt{h_{c_1(t)} \left( \frac{\partial \phi}{\partial u_1}(c_1(t)), \frac{\partial \phi}{\partial u_1}(c_1(t)) \right)} dt$$

which we approximate by  $\sqrt{\bar{H}_{11}}$ . Similarly, we get as approximations for the distances between  $X^2$  and  $X^3$  and between  $X^3$  and  $X^1$   $\sqrt{\bar{H}_{11} - 2\bar{H}_{12} + \bar{H}_{22}}$  and  $\sqrt{\bar{H}_{22}}$ , respectively.

Algorithm 3 summarizes the computation of the new edge lengths.

---

**Algorithm 3** Computation of the equi-affine invariant edge lengths for a triangle from the mesh.

---

**Input:** A triangle  $T$  in a triangular mesh  $M$ .

**Output:** Equi-affine invariant edge lengths of  $T$ .

Follow Algorithm 2 to get the coefficient matrix  $C = (c_1, \dots, c_6)^T \in \mathbb{R}^{6 \times 3}$  for a quadratic approximation of a local parametrization of the surface.

▷ Calculate first and second derivatives of the quadratic approximation  $\phi$  at the point  $u = (1/2, 1/2)^T$ .

$$\phi_1 = c_2 + 0, 5c_4 + 2 \cdot 0, 5c_5$$

$$\phi_2 = c_3 + 0, 5c_4 + 2 \cdot 0, 5c_6$$

$$\phi_{11} = 2c_5$$

$$\phi_{22} = 2c_6$$

$$\phi_{12} = c_4.$$

5: ▷ Calculate the pre-metric tensor  $H$ .

$$H(0, 0) = \det(\phi_1 | \phi_2 | \phi_{11})$$

$$H(1, 1) = \det(\phi_1 | \phi_2 | \phi_{22})$$

$$H(1, 0) = H(0, 1) = \det(\phi_1 | \phi_2 | \phi_{12})$$

**if**  $|\det H| < 1e-3$  **then**

$$H = \varepsilon \cdot Id_{2 \times 2}$$

**else**

$$H = |\det H|^{-\frac{1}{4}} H$$

10:  $U, E = \text{eigen}(H)$

▷ Such that  $U \text{diag}(E) U^T = H$

$$H = U \text{diag}(\text{abs}(E)) U^T$$

**end if**

▷ Calculate the equi-affine invariant edge lengths.

$$e_0 = \sqrt{H(0, 0)}$$

$$e_1 = \sqrt{H(0, 0) - 2H(0, 1) + H(1, 1)}$$

$$e_2 = \sqrt{H(1, 1)}$$

**return**  $e_0, e_1, e_2$ .

---

We follow this procedure for every triangle. For each edge  $e$  of an inner triangle  $T$ , we get two estimates for the distance between the vertices connected by the edge, one considering the triangle  $T$  and one considering the neighbouring triangle that shares the edge  $e$  with  $T$ . We choose the average of the two estimates. Notice that, in general, it is not clear if there exists an embedding of the vertices in  $\mathbb{R}^3$  such that the Euclidean distances between the vertices correspond to our estimates of the equi-affine invariant distances. It is not even guaranteed that the new edge length fulfil the triangle inequality, it is possible that the sum of the lengths of the two shorter edges is smaller than the length of the third edge.

Given the new edge lengths, we use Heron's formula to compute the area of the triangle. Heron's formula states that the area of a triangle with edge lengths  $a$ ,  $b$  and  $c$  is given by

$$A = \sqrt{s(s-a)(s-b)(s-c)},$$

where

$$s = \frac{a+b+c}{2}.$$

There are a few special cases and remarks concerning the above computations. In [Ra14], Raviv et al. consider only closed surfaces without boundary. However, the mesh discretizing the car part in our simulation bundle contains boundary triangles. If a triangle is at the boundary of the mesh, we invert it in the midpoint of each boundary edge to get a patch of four triangles. See Figure 3.5 for an example. Subsequently, we follow along as above.

Another special case is that  $\det B = 0$ , *i.e.* the triangle lies in an approximately parabolic region, compare Section 3.1.2. At such points, we set the continuous metric to zero. Numerically, we set

$$H = \varepsilon I = \varepsilon \begin{pmatrix} 1 & 0 \\ 0 & 1 \end{pmatrix}$$

for a small constant  $\varepsilon > 0$ . For a justification I refer to [Ra14].

To my knowledge, Raviv et al. did not examine the conditions on the mesh under which the discrete approximation of the metric converges to the continuous metric. An analysis of the convergence is out of scope of this thesis. Further works should treat this problem.

### 3.2.2 Fokker-Planck operator

The numerical computation of the Fokker-Planck operator and its eigendecomposition is described in Algorithm 4. As parameters, I used  $\varepsilon = 0.01$  and  $\delta = 0.1$  which produce

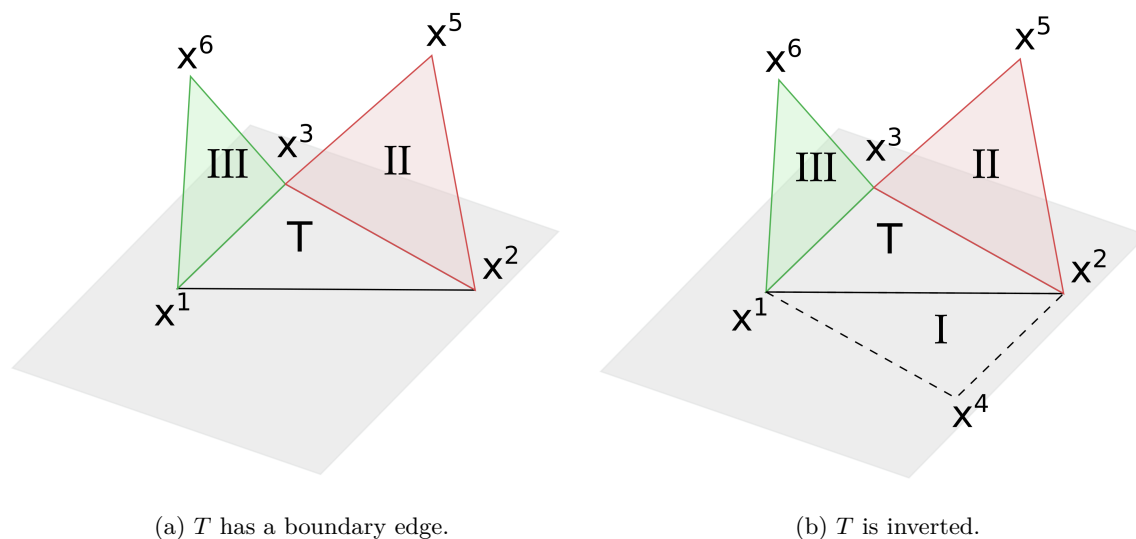


Figure 3.5: The centre triangle is inverted in the midpoint of each boundary edge to get a patch of four triangles.

similar results as presented in [IG17]. However, the operator depends strongly on the chosen parameters.

### 3.3 Invariance of operators

Iza-Teran calls his approach in [Iza17] and [IG17] "invariant operator approach". He states that the Laplace-Beltrami operator is invariant under isometries and the Fokker-Planck operator is invariant under a nonlinear transformation. However, he does not elaborate on what he means *in general* by calling an operator invariant. In fact, concretizing in what sense Iza-Teran's Fokker-Planck operator is invariant is difficult.

Further, Iza-Teran conjectures that the observed separation of effects can be explained using a known link between invariant operators and the representation of groups. However, the type of invariance used in this theory is another type of invariance than the one of the Laplace-Beltrami operator with respect to isometries.

In this section, we will examine and compare the different invariances.

#### 3.3.1 Invariant operator in the representation of groups

In [Iza17], Iza-Teran observes that the transformations upon variation of single spectral coefficients are predominantly isometric. He offers the following link between the representation

---

**Algorithm 4** Spectral decomposition of the Fokker-Planck operator.
 

---

**Input:** 1) reference simulation  $x$ : A surface embedded in  $\mathbb{R}^3$ , given as  $N_h$  points.  
 2) data set bundle  $\{x_j\}$ ,  $j = 1, \dots, m$ : Surfaces embedded in  $\mathbb{R}^3$ , each one given as  $N_h$  points.

**Parameter:**  $n_{ev}$ : number of eigenvectors to return,  $\varepsilon$ : controlling the size of local neighbourhoods,  $\delta$ : parameter in the approximation of the covariance matrix. In our setting,  $\delta$  controls the distortion of the Euclidean metric, see Section 3.1.3.

**Output:** First  $n_{ev}$  greatest eigenvectors of the operator.

```

for  $k = 1, \dots, N_h$  do
5:   Compute for each point  $x^k$  of  $x$  the sample covariance matrix  $C_{k,\delta}$  of the point cloud
       $\{x_j^k\}_{j=1}^m$  formed by the  $k$ -th points of the surfaces  $x_j$ , see Equation 3.1.10.
      Set  $C[k] =$  pseudoinverse of  $C_{k,\delta} \cdot \frac{1}{\delta}$ .
end for
for  $k = 1, \dots, N_h$  do
10:  for  $j = 1, \dots, N_h$  do
      Calculate the Gaussian kernel  $W[k, j]$  using Equation 3.1.9 and the pseudoinverses
      in  $C$ .
    end for
  end for
15: Let  $D_1$  be a diagonal matrix with  $D_1[ii] = \sum_{k=1}^{N_h} W[i, k]$ .
    Set  $W_{dens} = D_1^{-\frac{1}{2}} \cdot W \cdot D_1^{-\frac{1}{2}}$ .
    Let  $D_2$  be a diagonal matrix with  $D_2[ii] = \sum_{k=1}^{N_h} W_{dens}[i, k]$ .
    Set  $W_{stoch} = D_2^{-\frac{1}{2}} \cdot W_{dens} \cdot D_2^{-\frac{1}{2}}$ .
     $[U, E] = \text{eigen}(W_{stoch}, n_{ev})$ 
20: return greatest  $n_{ev}$  eigenvectors  $U$  of  $W_{stoch}$ .
  
```

---

of groups and invariant operators as a first theoretical approach to explain this. The following is based on [Sug90] and [Gal13].

**Theorem 3.3.1.** *Let  $F$  be the space of complex valued  $C^\infty$ -functions on the sphere  $S^2 \subset \mathbb{R}^3$ . A linear representation  $T_a$  of the rotation group  $SO(3)$  on  $F$  is defined by*

$$T_a f(x) = f(a \cdot x)$$

*for  $a \in SO(3)$  and  $f \in F$ . The Laplace-Beltrami operator  $\Delta_{S^2}$  on  $F$  commutes with  $T_a$ , i.e. for any  $a \in SO(3)$  and  $f \in F$  holds*

$$\Delta_{S^2}(T_a f) = T_a(\Delta_{S^2} f).$$

A linear representation of a Lie group  $G$  in a vector space  $V$  defines how an element from  $G$  acts on an element of  $V$ . Formally, it is a group homomorphism  $U : G \rightarrow GL(V)$  such that the map  $g \mapsto U(g)(u)$  is continuous for every  $u \in V$ . Here,  $GL(V)$  is the group of linear invertible maps from  $V$  to itself.

We note that the Laplace-Beltrami operator is invariant with respect to the rotation group in the sense that it *commutes* with the representation of the group in  $F$ .

**Theorem 3.3.2.** *The eigenvalues of  $\Delta_{S^2}$  are given by  $-k(k+1)$ ,  $k \in \mathbb{N}_0$ . The space  $H_k(S^2)$  of eigenfunctions for the eigenvalue  $-k(k+1)$  is spanned by  $\sin(k\theta)$  and  $\cos(k\theta)$ . It holds*

$$C^\infty(S^2) \subset L^2(S^2) = \bigoplus_{k=0}^{\infty} H_k(S^2).$$

Further, the representation  $T$  of  $SO(3)$  into  $H_k(S^2)$ , given by

$$T_a f(x) = f(a \cdot x)$$

for  $a \in SO(3)$  and  $f \in H_k(S^2)$  is irreducible.

A representation  $T$  of a group  $G$  in a vector space  $V$  is called irreducible, if it does not exist a non-trivial subspace  $W$  of  $V$  such that  $T$  defines a linear representation of  $G$  in  $W$ , *i.e.* it does not exist a subspace  $W \subset V$ ,  $W \neq \emptyset$ ,  $W \neq V$ , such that  $T_a(w) \in W$  for all  $w \in W$  and  $a \in G$ .

This expansion in irreducible subspaces yields two opportunities. Let  $f_i$  be elements of a Hilbert space  $H$ , for instance different embeddings of our car part interpreted as elements of  $L^2(M, \mathbb{R}^3)$ . Assume that there exists an element  $f \in H$  and a linear representation  $T$  of a Lie Group  $G$  such that all elements  $f_i$  are the result  $T_{a_i} f$  of the action of an element  $a_i$  on  $f$ . If we can decompose  $H$  into irreducible subspaces

$$H = \bigoplus_{k=0}^{\infty} H_k,$$

we know that if the projection of  $f$  on  $H_k$  is 0 for some  $k$ , so will be the projection of all  $f_i$  on  $H_k$ . We can therefore neglect the space  $H_k$  for the representation of our simulations. In practice this yields the possibility of a lossless dimensionality reduction. Moreover, given such an expansion, it suffices to consider the projection of the simulations  $f_i$  on a single  $H_k$  (for a  $k$  for that this projection is not 0) to be able to observe all group actions of  $G$  that distinguish between the different simulations.

However, I do not see how those theorems could be used to explain that the variation of different spectral coefficients in the invariant operator approach corresponds to *different* basic transformations, *i.e.* different group actions, when the theorem states for the above case, that actions of the group  $SO(3)$  act on all subspaces  $H_k$  in the *same* way.

### 3.3.2 Invariance of the Laplace-Beltrami operator

The Laplace-Beltrami operator is invariant with respect to isometries. To clarify in what sense, we first define what an isometry between regular surfaces is.

**Definition 3.3.3** (Isometry). *Let  $M_1$  and  $M_2$  be regular surfaces in  $\mathbb{R}^3$  with Riemannian metric  $g_1$  and  $g_2$ , respectively. A smooth map  $f : M_1 \rightarrow M_2$  is called isometry, if:*

1. *it is bijective and*
2. *for each  $p \in M_1$ , the differential*

$$d_p f : T_p M_1 \rightarrow T_{f(p)} M_2$$

*is a linear isometry with respect to the metrics  $g_i$ , *i.e.**

$$g_2^{f(p)}(d_p f(X), d_p f(Y)) = g_1^p(X, Y)$$

*for all  $X, Y \in T_p M_1$ .*

*If there exists such an isometry  $f$ , the surfaces  $(M_1, g_1)$  and  $(M_2, g_2)$  are called isometric.*

The differential  $d_p f$  is defined analogously as for functions  $f : M_1 \rightarrow \mathbb{R}$  in Equation 3.1.1.

Isometries are maps that preserve distances: The length of a curve  $c(\cdot)$  on  $(M_1, g_1)$  is identical to the length of the image of the curve under  $f$ ,  $f(c(\cdot))$ , on  $(M_2, g_2)$ .

At this point, note once more that there are different types of isometries. Given a regular surface  $M$  with Riemannian metric  $g$ , we can consider isometries  $g : M \rightarrow M$ . Those maps form a group  $G(M)$ . They can be thought of as reparametrizations of  $M$ .

In our application, we consider isometric transformations of different embeddings  $f \in \text{Emb}(M, \mathbb{R}^3)$  of our car part. We are interested in isometries acting on the embeddings  $f \in \text{Emb}(M, \mathbb{R}^3)$  by composition from the left, *i.e.* isometries  $g : f(M) \rightarrow g(f(M)) \subset \mathbb{R}^3$ , as for example translations and rotations.

While the isometric maps  $g : M \rightarrow M$  form a group  $G(M)$ , the isometric maps acting on  $Emb(M, \mathbb{R}^3)$  by composition from the left are hard to characterize. For each element  $f \in Emb(M, \mathbb{R}^3)$ , we can consider the set of isometries  $g : f(M) \rightarrow g(f(M)) \subset \mathbb{R}^3$  acting by composition from the left, but this set depends on the chosen element  $f$  and does not form a group.

Let us now examine in what sense the Laplace-Beltrami operator is invariant under isometries.

**Theorem 3.3.4** (Invariance under isometries). *Let  $(M_1, g_1)$  and  $(M_2, g_2)$  be regular surfaces,  $\Delta_{M_1}, \Delta_{M_2}$  the corresponding Laplace-Beltrami operators on  $C^\infty(M_1), C^\infty(M_2)$  and  $f : M_2 \rightarrow M_1$  an isometry. It holds*

$$(\Delta_{M_1} h) \circ f = \Delta_{M_2}(h \circ f)$$

for all  $h \in C^\infty(M_1)$ .

*Proof.* Let  $p \in M_1$ ,  $(U, \phi, V)$  be a local parametrization of  $M_1$  around  $p$ ,  $\tilde{u} \in U$  such that  $\phi(\tilde{u}) = p$ . The Laplace-Beltrami operator acting on a function  $h \in C^\infty(M_1)$  can in local coordinates be written as

$$\Delta_{M_1} h(p) = \frac{1}{\sqrt{\det G_1(\tilde{u})}} \sum_{i,j=1}^2 \frac{\partial}{\partial u^i} \left( G_1^{ij}(\tilde{u}) \sqrt{\det G_1(\tilde{u})} \frac{\partial(h \circ \phi)}{\partial u^j}(\tilde{u}) \right),$$

where  $(G_1)_{ij}(\tilde{u}) = g_1(\frac{\partial \phi}{\partial u_i}(\tilde{u}), \frac{\partial \phi}{\partial u_j}(\tilde{u}))$  and  $G_1^{ij}$  are the entries of the inverse matrix. See for example [Gri09] for a proof.

As  $f$  is smooth and bijective,  $(U, f^{-1} \circ \phi, f^{-1}(V))$  is a local parametrization of  $M_2$  around  $f^{-1}(p) \in M_2$  and  $(f^{-1} \circ \phi)(\tilde{u}) = f^{-1}(p)$ . We obtain

$$\begin{aligned} \Delta_{M_2}(h \circ f)(f^{-1}(p)) &= \frac{1}{\det G_2(\tilde{u})} \sum_{i,j=1}^2 \frac{\partial}{\partial u^i} \left( G_2^{ij}(\tilde{u}) \sqrt{\det G_2(\tilde{u})} \frac{\partial(h \circ f \circ f^{-1} \circ \phi)}{\partial u^j}(\tilde{u}) \right) \\ &= \frac{1}{\det G_2(\tilde{u})} \sum_{i,j=1}^2 \frac{\partial}{\partial u^i} \left( G_2^{ij}(\tilde{u}) \sqrt{\det G_2(\tilde{u})} \frac{\partial(h \circ \phi)}{\partial u^j}(\tilde{u}) \right). \end{aligned}$$

Further, by the second property in Definition 3.3.3, we obtain that for all  $u \in U$

$$\begin{aligned}
 (G_2)_{ij}(u) &= g_2 \left( \frac{\partial(f^{-1} \circ \phi)}{\partial u_i}(u), \frac{\partial(f^{-1} \circ \phi)}{\partial u_j}(u) \right) \\
 &= g_2 \left( d_p f^{-1} \left( \frac{\partial \phi}{\partial u_i}(u) \right), d_p f^{-1} \left( \frac{\partial \phi}{\partial u_j}(u) \right) \right) \\
 &= g_1 \left( \frac{\partial \phi}{\partial u_i}(u), \frac{\partial \phi}{\partial u_j}(u) \right) \\
 &= (G_1)_{ij}(u).
 \end{aligned}$$

Using this, it follows

$$\begin{aligned}
 \Delta_{M_2}(h \circ f)(f^{-1}(p)) &= \frac{1}{\sqrt{\det G_1(\tilde{u})}} \sum_{i,j=1}^2 \frac{\partial}{\partial u^i} \left( G_1^{ij}(\tilde{u}) \sqrt{\det G_1(\tilde{u})} \frac{\partial(h \circ \phi)}{\partial u^j}(\tilde{u}) \right) \\
 &= \Delta_{M_1} h(p)
 \end{aligned}$$

which proves the theorem. □

The theorem can either be applied to the Laplace-Beltrami operator using the induced Euclidean metric or to the Laplace-Beltrami operator using the equi-affine invariant metric. However, an isometry with respect to the Euclidean metric is in general not an isometry with respect to the equi-affine invariant metric and vice versa. To see this, let us consider a simple example given similarly but with a small mistake in [Ra14].

Consider the regular surfaces given by the parametrizations

$$\begin{aligned}
 M_1(u, v) &= (u, v, u^2 + v^2) \\
 M_2(u, v) &= \left( 2u, \frac{v}{2}, u^2 + v^2 \right)
 \end{aligned}$$

depicted in Figure 3.6.

Consider the smooth, bijective map  $f : M_1 \rightarrow M_2$ ,  $f(x) = Ax$  with

$$A = \begin{pmatrix} 2 & 0 & 0 \\ 0 & \frac{1}{2} & 0 \\ 0 & 0 & 1 \end{pmatrix}.$$

As it is an equi-affine transformation, we expect it to be an isometry with respect to the

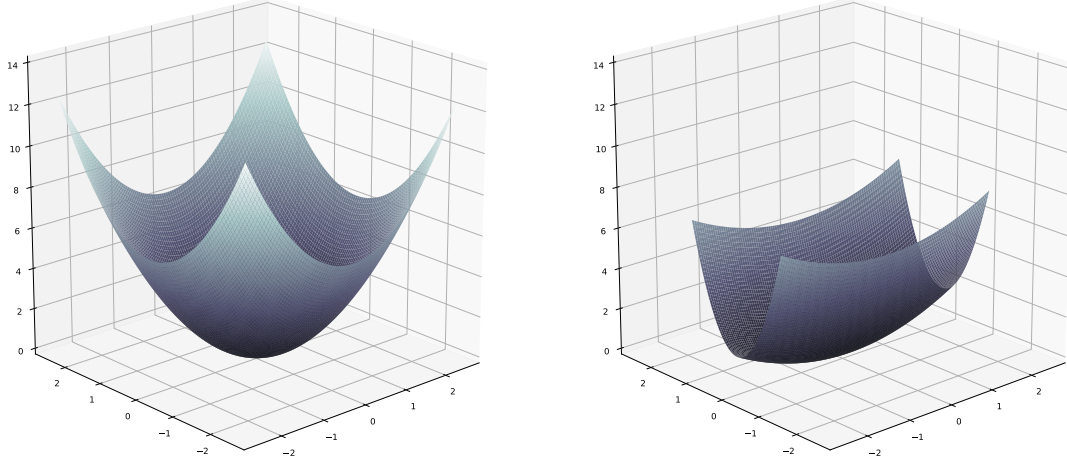


Figure 3.6: Two surfaces that are isometric with respect to the equi-affine invariant metric.

equi-affine invariant metric.

Let  $p \in M_1$ ,  $p = M_1(u, v)$ . Following Section 3.1.2, the equi-affine invariant metric in  $p$  with respect to the basis  $B_1 = \{\frac{\partial M_1}{\partial u}(u, v), \frac{\partial M_1}{\partial v}(u, v)\}$  of the tangent space  $T_p M_1$  is given by

$$G = \begin{pmatrix} \sqrt{2} & 0 \\ 0 & \sqrt{2} \end{pmatrix}.$$

The point  $p \in M_1$  is mapped to a point  $f(p) \in M_2$  with  $f(p) = M_2(u, v)$ . Further,

$$d_p f\left(\frac{\partial M_1}{\partial u}(u, v)\right) = \frac{d}{dt}(f(M_1(u+t, v)))|_{t=0} = \frac{d}{dt}(M_2(u+t, v))|_{t=0} = \frac{\partial M_2}{\partial u}(u, v)$$

and analogously

$$d_p f\left(\frac{\partial M_1}{\partial v}(u, v)\right) = \frac{\partial M_2}{\partial v}(u, v).$$

Calculating the equi-affine invariant metric in  $f(p)$  with respect to the basis  $B_2 = \{\frac{\partial M_2}{\partial u}(u, v), \frac{\partial M_2}{\partial v}(u, v)\}$  yields again the matrix  $G$ , therefore,  $f$  is indeed an isometry with respect to the equi-affine invariant metric. On the other hand,  $f$  is not an isometry with respect to the Euclidean metric, as the induced Euclidean metric in  $p \in M_1$  with respect to the basis  $B_1$  is given by

$$G_1 = \begin{pmatrix} 1 + 4u^2 & 4uv \\ 4uv & 1 + 4v^2 \end{pmatrix},$$

while the induced Euclidean metric in  $f(p) \in M_2$  with respect to the basis  $B_2$  is given by

$$G_2 = \begin{pmatrix} 4 + 4u^2 & 4uv \\ 4uv & \frac{1}{4} + 4v^2 \end{pmatrix}.$$

To illustrate the invariance of the Laplace-Beltrami operator in more detail and to bring out the difference between the operator for the induced Euclidean metric and the one for the equi-affine invariant metric, we consider one more example. I computed the Laplace-Beltrami operators for a given embedding of the car part and a transformed embedding. The transformation is given by  $f(x) = Ax$  with

$$A = \begin{pmatrix} 1 & 2 & 0 \\ 1 & 3 & 0 \\ 0 & 0 & 1 \end{pmatrix}.$$

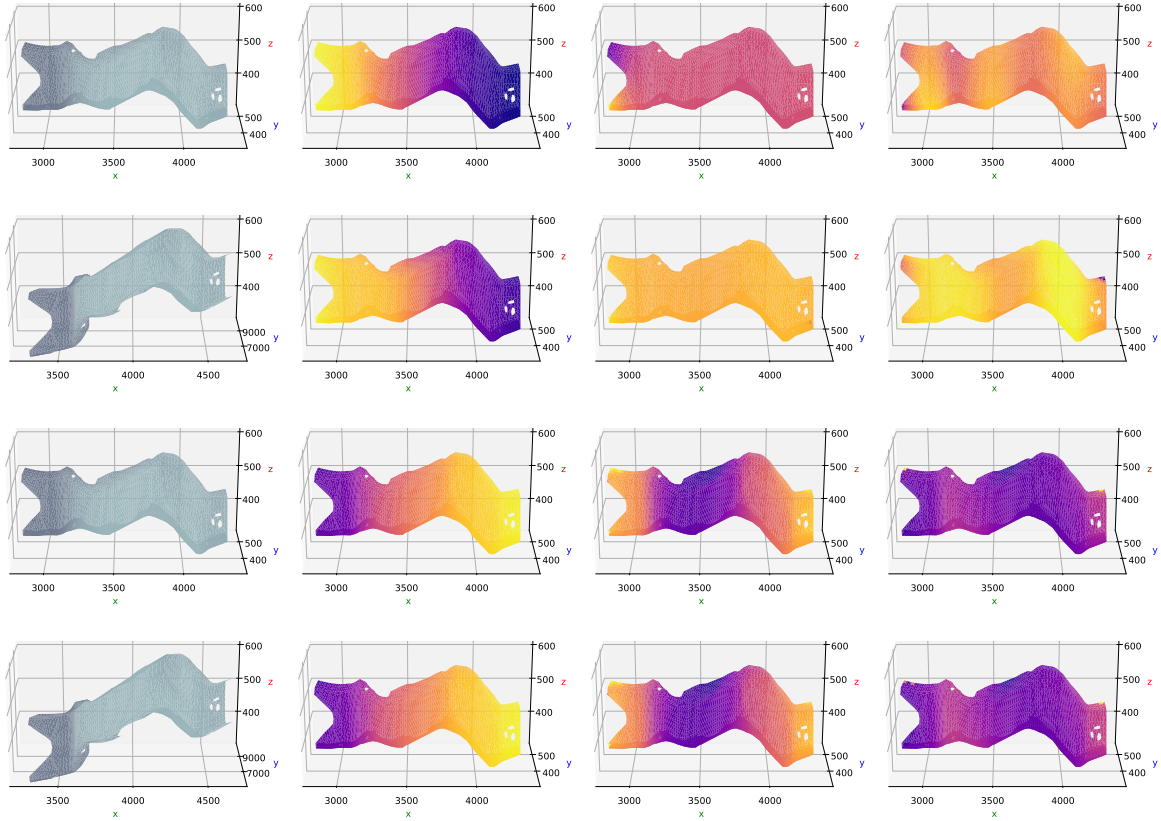
The first column of Figure 3.7 shows the original shape and the transformed shape. The first and third rows of the remaining columns show the second, fifth and tenth eigenvectors of the Laplace-Beltrami operator using the induced Euclidean metric and the equi-affine invariant metric on the original shape. The second and fourth rows show the corresponding eigenvectors for the operators on the transformed shape. To facilitate the comparison between the eigenvectors for the original and the transformed shape, the eigenvectors for the transformed shape are overlaid onto the untransformed shape.

We observe that the eigenvectors of the Laplace-Beltrami operator using the equi-affine invariant metric for the original and the transformed shape are identical. This is because the transformation is an isometry with respect to the equi-affine invariant metric since  $\det A = 1$ .

I picked the second, fifth and tenth eigenvectors since the eigenvectors in between are for the most part constant, making it more difficult to see the invariance although it is still present. A similar example was given in Figure 6 of [Ra14] using the shape of a centaur instead of a car part.

Now that we have an idea in what sense the Laplace-Beltrami operator is invariant under isometries, let us compare it to the invariance in Theorem 3.3.1 from the context of the representation of groups.

In that context, we had a function space  $F$ , a Laplace-Beltrami operator acting on that space,  $\Delta : F \rightarrow F$ , a Lie group  $G$  and a linear representation  $T$  of  $G$ , describing how an element of  $G$  acts on an element of  $F$ . The Laplace-Beltrami operator was invariant under actions from



(a) Original and transformed shape. (b) 2nd eigenvectors. (c) 5th eigenvectors. (d) 10th eigenvectors.

Figure 3.7: First and second rows: Eigenvectors of the Laplace-Beltrami operator using the induced Euclidean metric on the original and the transformed shape, respectively. Third and fourth rows: Same for the Laplace-Beltrami operator using the equi-affine invariant metric. All eigenvectors are overlaid onto the original shape.

$G$  in the sense that  $\Delta$  and  $T$  commuted.

In our application, we interpret all simulation data as functions on a regular surface  $M$  which is a reference embedding of the car part. The function space  $F$  should be the space  $C^\infty(M)$ . The Laplace-Beltrami operator  $\Delta_M$  acts on  $C^\infty(M)$ . Choosing as group  $G$  the group  $G(M)$  of isometries  $g : M \rightarrow M$ , the natural definition of the action of an element  $g$  of  $G$  on  $f \in C^\infty(M)$  is

$$T_g f(x) = f \circ g(x).$$

From Theorem 3.3.4 follows  $\Delta_M T_g f(\cdot) = T_g \Delta_M f(\cdot)$ , *i.e.* the Laplace-Beltrami operator commutes with the actions of  $G$  and is therefore in the same sense invariant under isometries as it is in Theorem 3.3.1 invariant under rotations.

However, a problem occurs. The above link between the invariance of the Laplace-Beltrami operator with respect to isometries and the representation of groups is only valid for isometries acting on  $Emb(M, \mathbb{R}^3)$  by composition from the *right*. To use the theory from the representation of groups for Iza-Teran's observations concerning the separation of effects, we would need a similar representation for isometries acting by composition from the *left*. Nevertheless, we saw above that those isometries are hard to characterize and do not form a group.

### 3.3.3 Invariance of the Fokker-Planck operator

Iza-Teran motivates the use of the Fokker-Planck operator by its invariance under a nonlinear transformation without elaborating on what he means by that. In this section, we will examine in what sense the Fokker-Planck operator might be considered invariant.

The (observable) data points  $y_i \in \mathbb{R}^n$  in Singer's and Coifman's setting in [SC08], which we considered in Section 3.1.3, are the images of points  $x_i \in \mathbb{R}^m$ ,  $m \leq n$ , in an unobservable parameter space under a nonlinear map  $f$ . Instead of building an operator on the manifold of the observable data points, Singer and Coifman build an operator on the manifold of the unobservable points  $x_i$ . In the construction of the operator, they approximate the distance of the unobservable points. The resulting operator is asymptotically independent of  $f$ , in the sense that it would not depend on  $f$ , if one was able to calculate the exact distances of the unobservable points. On the other hand, an operator as the Laplace-Beltrami operator, built on the manifold of the observable data points  $y_i$ , depends on  $f$ . Notice however, that this invariance of the Fokker-Planck operator is a different kind of invariance than the invariance of the Laplace-Beltrami operator with respect to isometries and the invariance of an operator in the representation of groups. Remember further from Section 3.1.3, that Iza-Teran uses the ideas from [SC08] in a way that does not allow a model of the data points as images of unobservable parameters under a nonlinear map as in Singer's and Coifman's settings.

Nevertheless, the way Iza-Teran builds the operator, it possesses the following property.

**Theorem 3.3.5** (Invariance of the Fokker-Planck operator). *Given a set of points  $X = \{x_1, \dots, x_n\} \subset \mathbb{R}^m$  and an injective map  $f : X \rightarrow \mathbb{R}^n$ , let  $Y_1, \dots, Y_n$  be multivariate random variables with values in  $\mathbb{R}^n$ , finite expectations and finite variances. Consider the multivariate random variables  $Z_i = f(x_i) + Y_i \in \mathbb{R}^n$ . Using for each  $i$  the covariance matrices of  $Z_i$  for the construction of the operator in Algorithm 4, the resulting operator is independent of the map  $f$ .*

*Proof.* The theorem follows directly from the formula of the covariance of a multivariate

random variable. It holds

$$\begin{aligned}
\text{Var}[Z_i] &= \mathbb{E}[(Z_i - \mathbb{E}[Z_i])(Z_i - \mathbb{E}[Z_i])^T] \\
&= \mathbb{E}[(f(x_i) + Y_i - f(x_i) - \mathbb{E}[Y_i])(f(x_i) + Y_i - f(x_i) - \mathbb{E}[Y_i])^T] \\
&= \mathbb{E}[(Y_i - \mathbb{E}[Y_i])(Y_i - \mathbb{E}[Y_i])^T] \\
&= \text{Var}[Y_i].
\end{aligned}$$

Therefore, the covariance of the  $Z_i$  and hence the construction of the operator is independent of  $f$ .  $\square$

To obtain an invariance of the operator in Iza-Teran's setting, we can proceed as follows. Let the points  $x_i \in \mathbb{R}^3$  be the mesh points of the car part at a timestep  $t_0$  in a reference simulation. For the construction of the sample covariance matrices  $C_{k,\delta}$ , we use the mesh points from all simulations at a timestep  $t_1 > t_0$ . We assume that the deformation of the car part between the reference state at timestep  $t_0$  and the different states at timestep  $t_1$  can be modelled as a combination of a deterministic nonlinear transformation due to the proceeding in time and a stochastic component due to the change of the physical parameters. By Theorem 3.3.5, the operator does not depend on the deterministic nonlinear transformation.

Note however, that this is again a different type of invariance than the invariance of the Laplace-Beltrami operator under isometries and the invariance of operators in the representation of groups.

In Section 3.1.3, we saw that the operator can be interpreted as a Laplace-Beltrami operator for a different "covariance metric". In this setting, it is invariant under isometries with respect to the covariance metric in the sense of Section 3.3.2.

### 3.4 Separation of effects

In the invariant operator approach, we represent an element  $f \in \text{Emb}(M, \mathbb{R}^3)$  in the spectral domain of, for instance, the Laplace-Beltrami operator as

$$\begin{pmatrix} f_x \\ f_y \\ f_z \end{pmatrix} = \sum_{i=1}^{\infty} \alpha^i \psi_i, \quad \text{where } \alpha^i = \begin{pmatrix} \langle f_x, \psi_i \rangle_{L^2(M)} \\ \langle f_y, \psi_i \rangle_{L^2(M)} \\ \langle f_z, \psi_i \rangle_{L^2(M)} \end{pmatrix}.$$

Numerical observations from [Iza17] and [IG17] suggest that variations of the spectral coefficients  $\alpha^i$  correspond to different basic transformations, referred to as "independent defor-

mation modes”. Being able to analyse different aspects of a transformation separately can be interesting for the engineer. Ignoring on the other hand certain aspects of a transformation neglecting the corresponding spectral coefficients is of high interest for shape recognition since there are many basic transformations of a shape that should not influence its classification.

For the numerical analysis of the separation of effects, consider the following procedures:

1. Calculate the eigenvectors  $\psi_i$ ,  $i = 1, \dots, N$  of one of the above presented operators. Project the coordinate functions  $f_x$ ,  $f_y$  and  $f_z$  of an embedding of the car part on the eigenvectors to write

$$f_x = \sum_{i=1}^N \alpha_i^x \psi_i \quad \text{with} \quad \alpha_i^x = \langle f_x, \psi_i \rangle$$

and analogously for  $f_y$  and  $f_z$ . Choose a spectral coefficient  $J \in \{1, \dots, N\}$ . Modify one or more of the coefficients  $a_J^x$ ,  $a_J^y$  and  $a_J^z$ . Leave all other coefficients fixed. An example for this procedure was already given in Figure 3.1.

2. Calculate the eigenvectors  $\psi_i$ ,  $i = 1, \dots, N$ , of one of the above presented operators. Project the coordinate functions  $f_x^j$ ,  $f_y^j$  and  $f_z^j$  of several embeddings  $x^j$ ,  $j = 1, \dots, M$  of the car part at different timesteps and in different simulations on the eigenvectors. Choose a spectral coefficient  $J \in \{1, \dots, N\}$  (for instance the one with the highest variance), compute the minimal and maximal spectral coefficients from all  $M$  simulations and linearly interpolate between them. Leave all other coefficients fixed.

The second procedure can be seen as special case of the first one. It differs only in that a projection coefficient for variation may be chosen with respect to the variability of the data and in that the given data yields an interval for the variation of the coefficient. In praxis, this procedure might be the more interesting one, as it respects which of the projection coefficients is most important to represent the changes between the simulations for different parameters and allows to examine what type of transformation the coefficient represents. However, to understand what actually causes the observations of a separation of effects, we will consider in the following only the first procedure.

Iza-Teran conjectures in [Iza17] and [IG17] a link between the invariances of the used operator and the basic transformations observed upon variation of the spectral coefficients. In the first part of this section, we will follow the above procedure for all three presented operators and compare the results to investigate this conjecture. In the second part of this section, we will examine the reasons for the numerical observations.

### 3.4.1 Numerical observations

Figures 3.8 to 3.11 show the simultaneous variation of the  $x$ -,  $y$  and  $z$ - components of different spectral coefficients for an embedding of the car part. The Fokker-Planck operator was calculated using as reference embedding the embedding of the car part at timestep 7 in a reference simulation. The embeddings of all 116 simulations at timestep 7 were used to form the point clouds.

For all operators, the first spectral coefficient seems to correspond to a translation. We observe this in Figure 3.8.

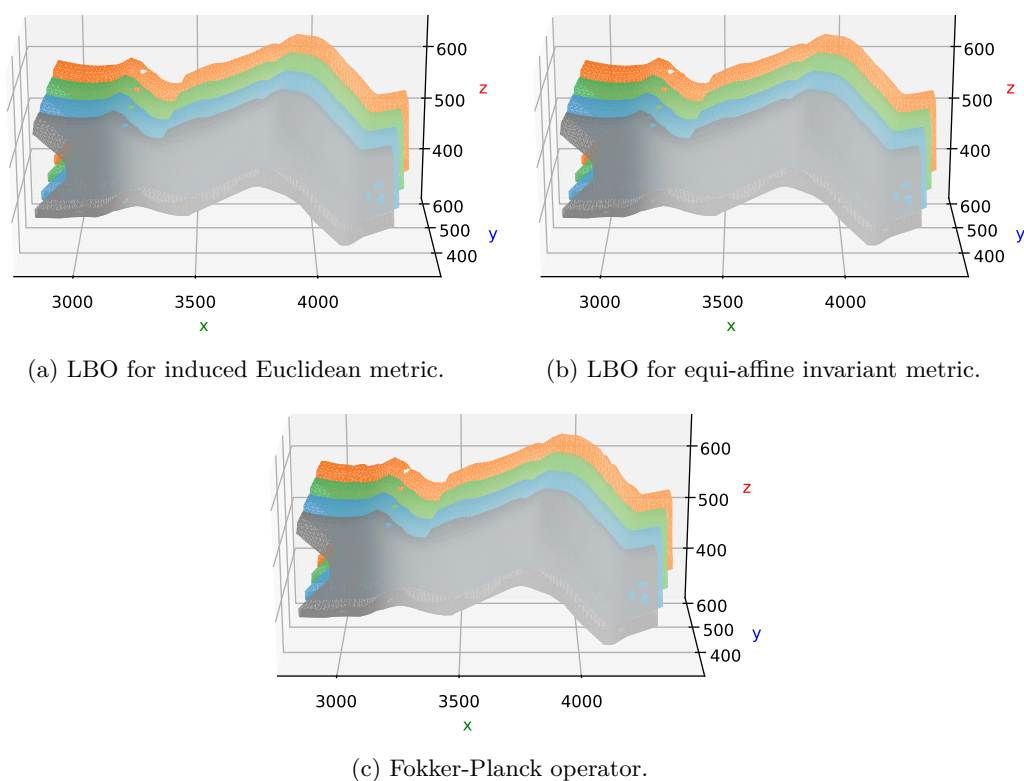


Figure 3.8: Stepwise increase of the first spectral coefficients seems to correspond to a translation.

For all operators, the second coefficient seems to correspond to a rotation. This is shown in Figure 3.9.

For the Laplace-Beltrami operator using the induced Euclidean metric, the third coefficient corresponds to a bending of the car part. This is illustrated in Figure 3.10. The behaviour for the Laplace-Beltrami operator using the equi-affine invariant metric and for the Fokker-Planck

operator is due to the fact that the support of the third eigenfunction of those operators is very small. I will further expand on this in the next section.

In Figure 3.11 we see the variation of the fifth spectral coefficient. For the Laplace-Beltrami operator using the induced Euclidean metric, it corresponds to a local deformation on the left side of the car part. For the Laplace-Beltrami operator using the equi-affine invariant metric, it corresponds to a bending, similar to the bending observed in Figure 3.10. The behaviour for the Fokker-Planck operator is again due to a small support of the fifth eigenfunction.

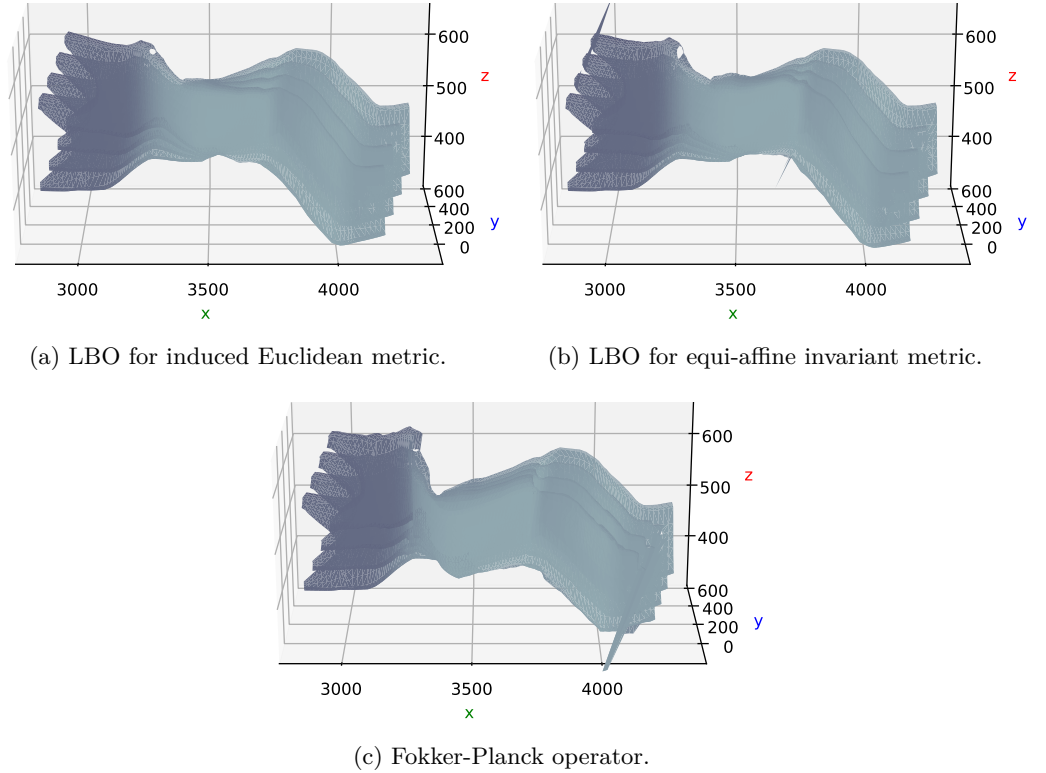


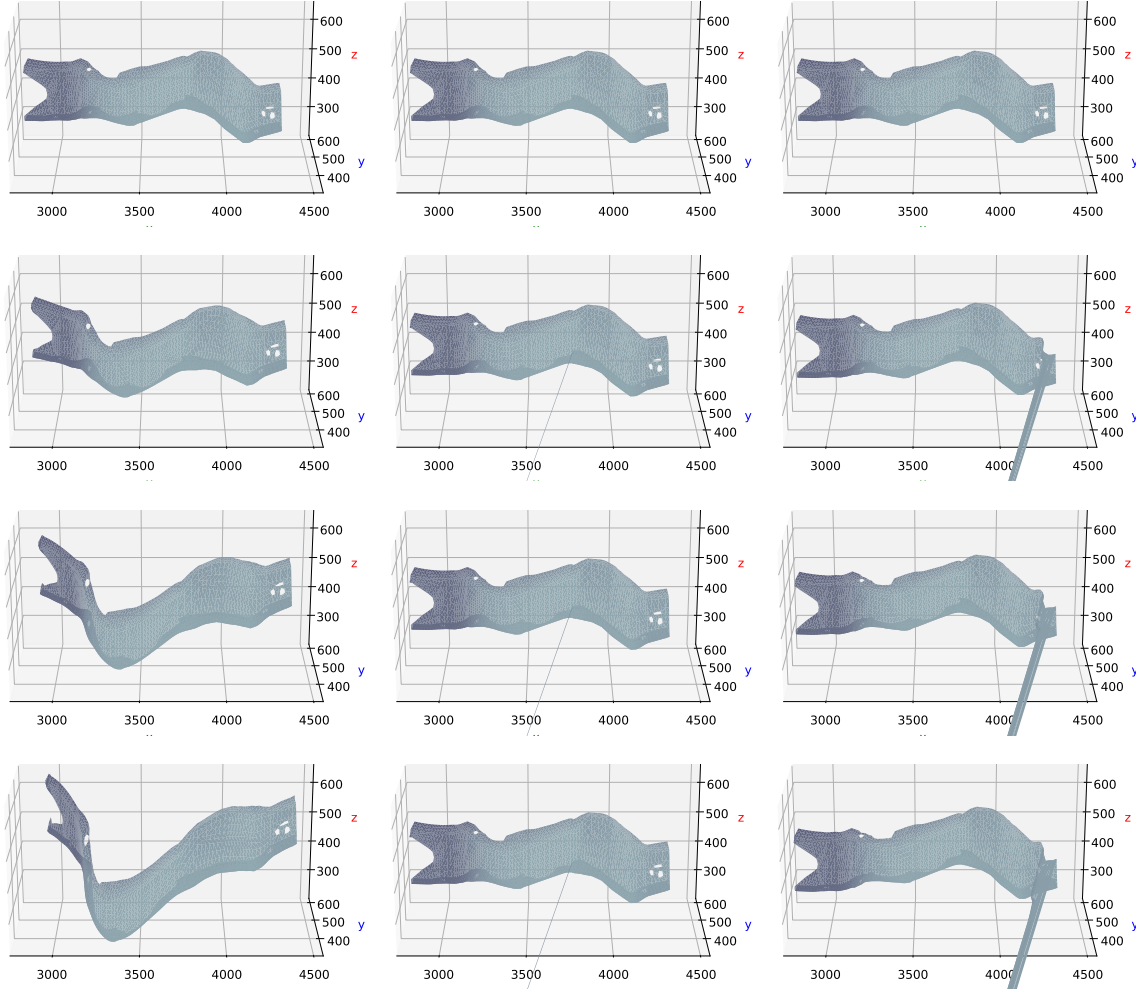
Figure 3.9: Stepwise increase of the second spectral coefficients seems to correspond to a rotation.

### 3.4.2 Theoretical framework

In the invariant operator approach, we write the coordinate functions of an embedding of the car part as finite linear combination of the eigenvectors  $\{\psi_i\}_{i=1}^N$  of an invariant operator,

$$\begin{pmatrix} f_x \\ f_y \\ f_z \end{pmatrix} = \sum_{i=1}^N \alpha^i \psi_i, \quad \text{where } \alpha^i = \begin{pmatrix} \langle f_x, \psi_i \rangle_{\mathbb{R}^N} \\ \langle f_y, \psi_i \rangle_{\mathbb{R}^N} \\ \langle f_z, \psi_i \rangle_{\mathbb{R}^N} \end{pmatrix} \quad (3.4.1)$$

and where  $N$  is the number of nodes of the discretization.



(a) LBO for induced Euclidean metric.

(b) LBO for equi-affine invariant metric.

(c) Fokker-Planck operator.

Figure 3.10: Rowwise increase of the third spectral coefficients. In the first column we observe a bending. In the second and third columns we observe strongly local deformations.

Increasing the  $x$ -component  $a_x^J$  of the  $J$ -th spectral coefficient corresponds to an addition of the  $J$ -th basis function  $\psi_J$  to the  $x$ -coordinates of the embedding. This holds analogously for the  $y$ - and  $z$ - components of the spectral coefficient.

To understand why we observe certain transformations when we vary the spectral coefficients, we need to look at the eigenfunctions  $\psi_i$  of the operators.

To explain how the shape of the eigenfunctions relates to the observed transformations, we

consider in this section the Laplace-Beltrami operator for the induced Euclidean metric, the same thoughts apply to the other operators.

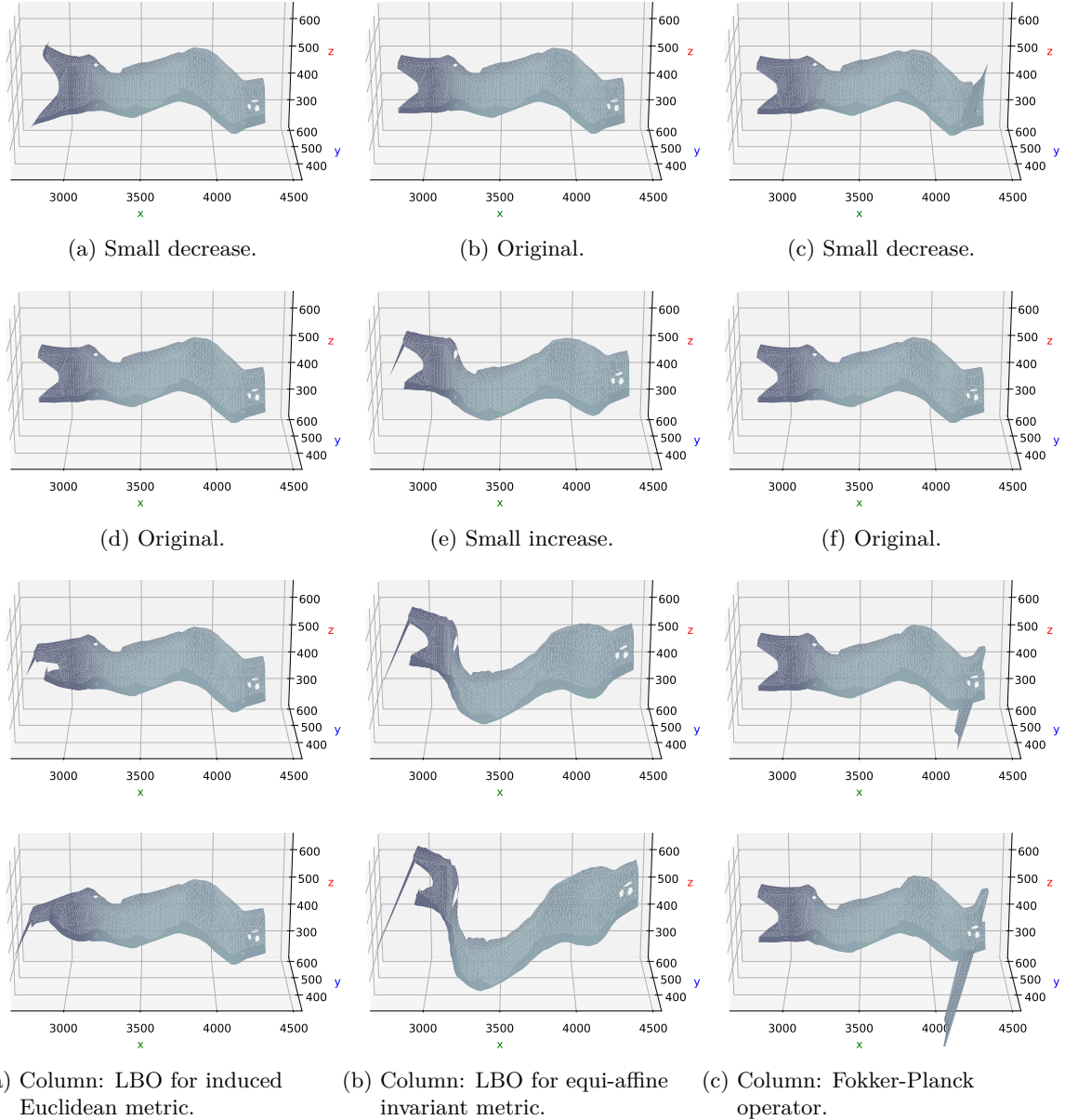


Figure 3.11: Rowwise increase of the fifth spectral coefficients starting with the original and the reduced coefficients, respectively. In the first column, we observe a local deformation. In the second column, we observe a bending, similar to the bending in Figure 3.10. The deformation in the third column is similar to the local deformations in Figure 3.10.

Figure 3.12 shows the first, second, third and fifth eigenvectors of the operator on the embed-

ding of the car part from the previous section. For better visualisation, the eigenfunctions are scaled to the interval  $[0, 1]$  such that the full width of the colour map is used. The problem of this scaling is that the original variance of the eigenfunctions is lost. In fact, the first eigenfunction is nearly constant. The difference between the function values at points with small  $x$ -value and points with large  $x$ -value is much smaller than for the second eigenfunction. Knowing the eigenfunctions, we can explain the observed transformations. The first eigen-

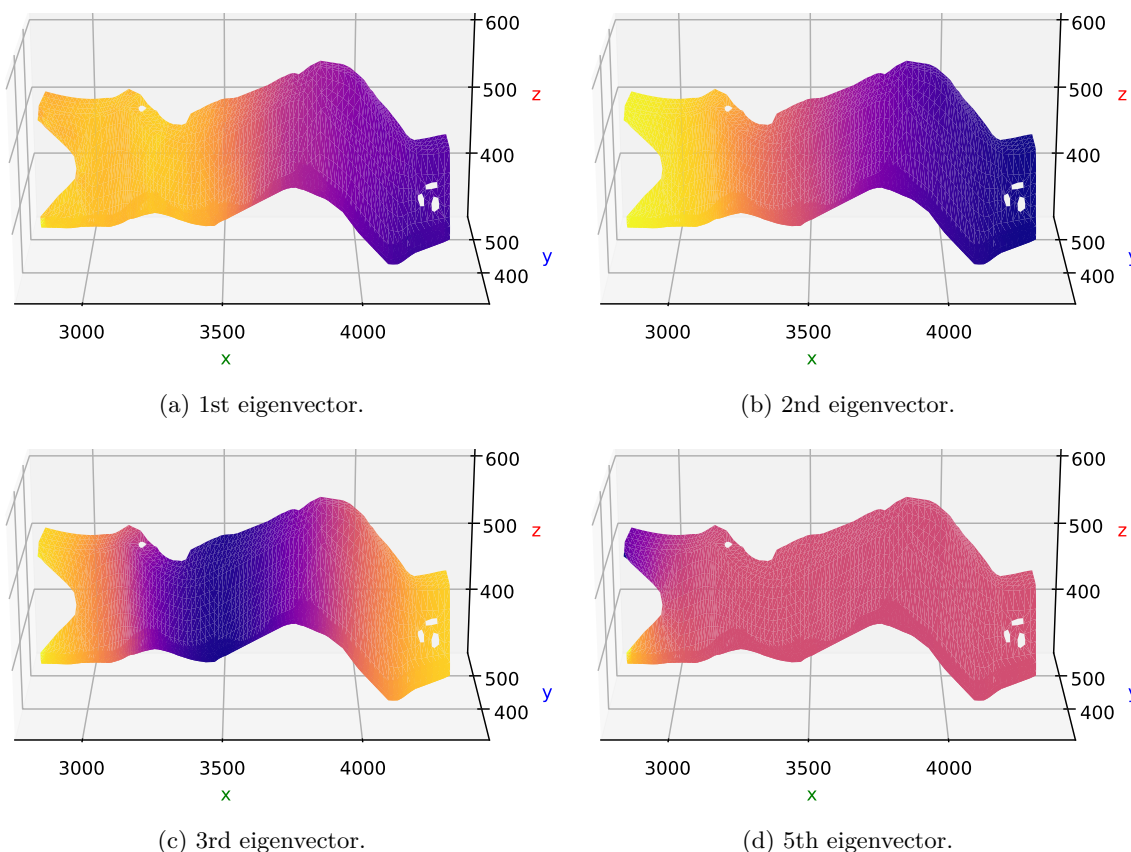


Figure 3.12: Eigenvectors of the Laplace-Beltrami operator using the induced Euclidean metric. Scaled to the interval  $[0, 1]$  to use the full range of the colour map.

function is nearly constant. Increasing the  $x$ -component  $a_x^1$  in Equation 3.4.1, we increase the  $x$ -coordinate of each point by approximately the same amount, causing a translation of the car part in the  $x$ -direction. Analogously, this holds for the  $y$ - and  $z$ -components. This explains the translation in Figure 3.8.

In Figure 3.9, we observed that a variation of the second spectral coefficient seems to correspond to a rotation. How can the form of the second eigenfunction explain this observation? In Figure 3.12, we see that the second eigenfunction decreases in the  $x$ -direction. Figure

3.13 shows a plot of the  $x$ -coordinates of the nodes of the embedding against the value of the second eigenfunction. It underlines the monotone dependence. If we increase the  $y$ -

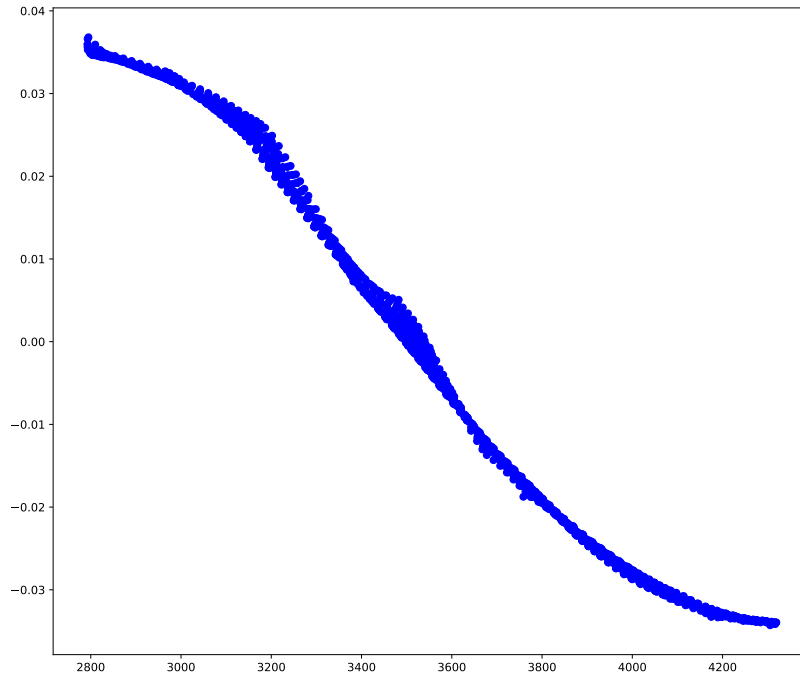


Figure 3.13: Plot of the  $x$ -coordinates of the nodes of the embedded car part against the value of the second eigenfunction.

component  $a_y^2$  of the second spectral coefficient, *i.e.* add a factor of the second eigenfunction to the  $y$ -coordinates of the embedding, the  $y$ -coordinates of points with small  $x$ -coordinate increase while the  $y$ -coordinates of points with large  $x$ -coordinate decrease. Increasing at the same time the  $x$ -component  $a_x^2$  of the second spectral coefficient, the  $x$ -coordinates of points with small  $x$ -coordinate increase, while the  $x$ -coordinates of points with large  $x$ -coordinate decrease. If the increase is small enough, the combination corresponds visually to a rotation of the embedding in the  $x$ - $y$ -plane around the centre of the part. However, increasing the coefficients further, the  $x$ - and  $y$ -coordinates of points with initially small  $x$ -coordinate continue increasing while the  $x$ - and  $y$ -coordinates of points with initially large  $x$ -coordinate continue decreasing, breaking the illusion that an increase of the second projection coefficient corresponds to a rotation. Similarly, reducing the size of the  $x$ -component of the second spectral coefficient, the  $x$ -coordinates of points with small  $x$ -coordinate become even smaller, while the  $x$ -coordinates of points with already large  $x$ -coordinate become even larger, leading to a stretching of the part, not to a rotation.

In the same way, the bending of the car part and the local deformation observed in Figures

3.10 and 3.11 can be explained. In Figure 3.12, we see that the third eigenfunction of the Laplace-Beltrami operator is large for points with small and with large  $x$ -coordinate and small for points in the middle. Increasing the  $z$ -component  $a_z^3$  of the third projection coefficient, we increase the  $z$ -component of the points at the left and the right of the beam and decrease the  $z$ -component of the points in the middle. This is the first ingredient for the observed bending. Increasing the  $x$ -component  $a_x^3$ , we increase the  $x$ -component for points that were initially on the left and the right of the beam and decrease the  $x$ -component of the points that were initially in the middle. This leads to a stretching of the part on the right and the bending on the left as the points that were initially in the middle move to the left and the points that were initially on the left move to the right. While the bending seems to be at first sight a physically reasonable deformation, it does not respect any physical constraints: Parts of the beam are stretched, others crushed, intrinsic distances change and at the latest when we increase the spectral coefficients further or when we decrease them, the visual impression of a physically reasonable deformation breaks.

Iza-Teran conjectures in [Iza17] that the observed separation of effects upon variation of the coefficients  $\alpha^i$  can mathematically be expressed as movements along orbits of  $Emb(M, \mathbb{R}^3)$ . Indeed, a variation of the  $J$ -th spectral coefficients of an element  $f \in Emb(M, \mathbb{R}^3)$  corresponds to a movement along the orbit

$$\{f + \alpha^J \psi_J \mid \alpha^J \in \mathbb{R}^3\},$$

where  $\psi_J : M \rightarrow \mathbb{R}$  is the  $J$ -th eigenfunction of the used operator. The set  $\{\psi_{i_1}\} \times \{\psi_{i_2}\} \times \{\psi_{i_3}\}$ ,  $i_j \in \mathbb{N}$ , builds a basis of the whole space  $L^2(M, \mathbb{R}^3)$ . Consequently, the orbits are in general no subset of  $Emb(M, \mathbb{R}^3)$ . Further, the orbit actions are in general not isometric. Indeed, given two arbitrary points  $p_1$  and  $p_2$  on  $M$  and an eigenfunction  $\psi_i$  such that  $\psi_i(p_1) \neq \psi_i(p_2)$ , we can modify the  $i$ -th spectral coefficient such that the points  $p_1$  and  $p_2$  have the same embedding coordinates. This modification is unique. However, if we do not fix the points  $p_1$  and  $p_2$ , there are many variations of spectral coefficients that cause two different points on  $M$  to have the same embedding coordinates in  $\mathbb{R}^3$ . In our application, this means that in general occur (physically impossible) crossing of the car part upon variation of the spectral coefficients.

Concerning the example of rotations, it is impossible that a single spectral coefficient represents a rotation. In general, we need to modify all  $N$  projection coefficients to represent any affine transformation  $g : \mathbb{R}^3 \rightarrow \mathbb{R}^3$ ,  $g(x) = Ax + b$  exactly: We apply  $g$  to our embedding from Equation 3.4.1, to get for the coordinate functions  $\tilde{f}_x$ ,  $\tilde{f}_y$  and  $\tilde{f}_z$  of the transformed

embedding

$$\begin{aligned}
 \begin{pmatrix} \tilde{f}_x \\ \tilde{f}_y \\ \tilde{f}_z \end{pmatrix} &= A \begin{pmatrix} f_x \\ f_y \\ f_z \end{pmatrix} + b \\
 &= \left( \sum_{i=1}^N (A\alpha^i) \psi_i \right) + b \\
 &= (A\alpha^1 + c^{-1}b)\psi_1 + \sum_{i=2}^N (A\alpha^i) \psi_i,
 \end{aligned} \tag{3.4.2}$$

where we assumed for the last equality that  $\psi_1$  is constant with entries  $c$ .

Thus, any affine transformation is up to the translation term visible in every projection coefficient. No finite number of projection coefficients can represent an affine transformation if it is not simply a translation.

Aside from the numerical observation of the orbits, Iza-Teran made the following experiment: He calculated the variance of the spectral coefficients for rotations of the embedding. Doing that, he observed that there are only a few coefficients with high variance. However, this is not because only a few spectral coefficients are affected by rotations or certain coefficients are better suited to represent rotations than others. From Equation 3.4.2, we know that the spectral coefficients of the rotated embeddings lie on spheres, where the radius of the sphere is the Euclidean norm of the spectral coefficient of the original embedding. Thus, the variance of a spectral coefficient under rotations depends only on the Euclidean norm of the coefficient for the original embedding. Most of the coefficients vary only weakly, because only a few spectral coefficients for the original embedding have a large Euclidean norm. This is due to the strong decay of the spectral coefficients treated in the next section.

Similarly, Iza-Teran observes in [Iza17] that for the example from Section 2.1 of a car crash simulation bundle exist only a few spectral coefficients with high variance. This is illustrated by Figure 3.14 showing the variance of the 1714 spectral coefficients for the 116 embeddings at timestep 7. However, this is again not because only a few spectral coefficients are affected by the transformations between the reference embedding and the other embeddings of the car part or because a few coefficients are better suited to represent those transformations.

The variance of a coefficient is again mainly due to the norm of the coefficient for the original embedding. This can be seen in Figure 3.15, which shows the variance of the 1714 spectral coefficients for the 116 embeddings at timestep 7 after scaling each coefficient to the interval

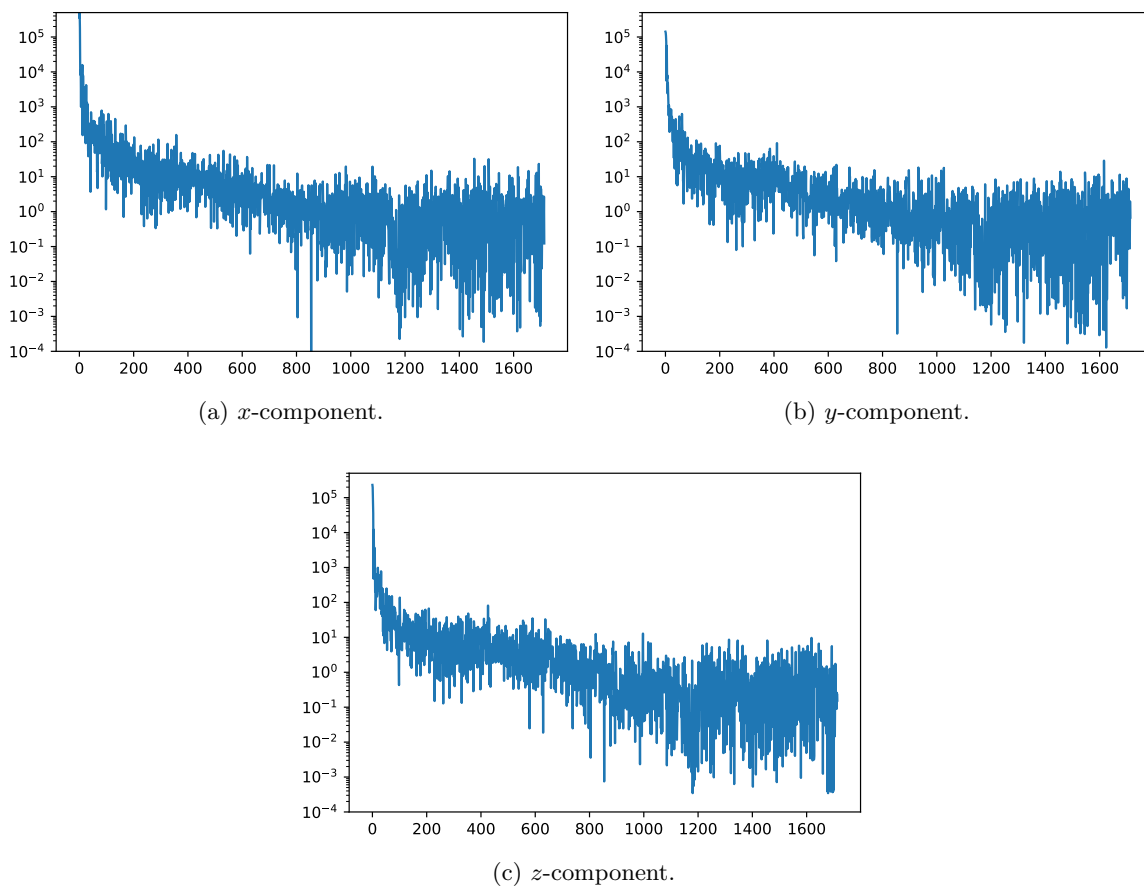


Figure 3.14: Variance of the spectral coefficients of the embeddings from the car crash simulation bundle from Section 2.1 at timestep 7.

$[0, 1]$ . Again, most of the coefficients vary only weakly, because only a few spectral coefficients for the original embedding have a large Euclidean norm. This is once again due to the strong decay of the spectral coefficients treated in the next section.

### 3.5 Decay of the spectral coefficients

Apart from the separation of effects, Iza-Teran observes in [Iza17] and [IG17] a strong decay of the spectral coefficients. Further, he motivates a decay estimate for the spectral coefficients of the Fokker-Planck operator.

In the first part of this section, we will numerically observe and compare the decay of the spectral coefficients of the different operators. In the second part, we will come across a problem in Iza-Teran's estimate for the decay of the spectral coefficients of the Fokker-Planck operator. Further, we will prove a decay estimate for the spectral coefficients of the Laplace-

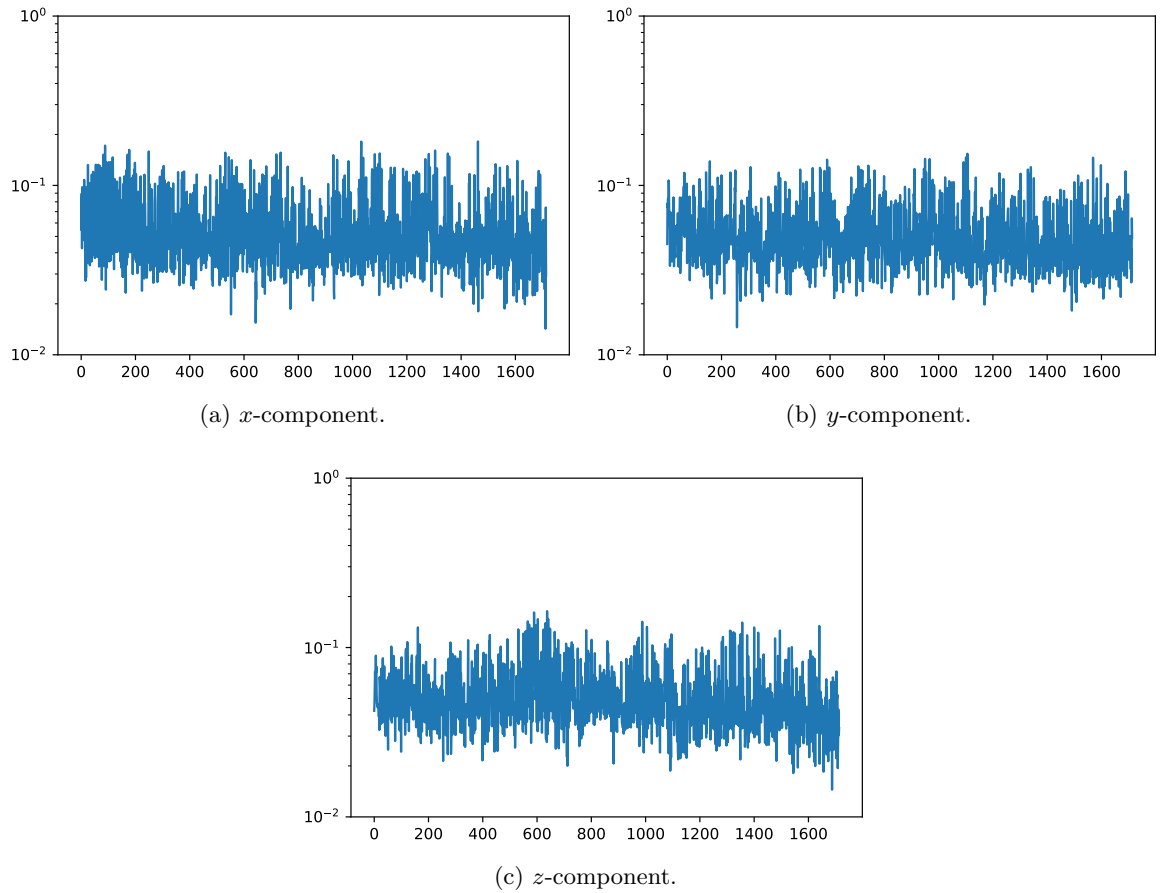


Figure 3.15: Scaled variance of the spectral coefficients of the embeddings from the car crash simulation bundle from Section 2.1 at timestep 7.

Beltrami operator following ideas from Aflalo, Brezis et al. in [Afl16] and [BG17]. Those thoughts yield an optimality result for the representation of functions in the spectral domain of the Laplace-Beltrami operator. Since Taubin’s publication [Tau95] in 1995 and Karni’s and Gotsman’s publication [KG00] in 2000, the spectral domain of Laplacians was in many publications used for the compression of mesh geometries. However, a theoretical foundation for the proceeding had long been missing.

### 3.5.1 Numerical observations

In this section, we will consider once again the embeddings of our car part at timestep 7 in the 116 crash simulations from the simulation bundle presented in Section 2.1.

Figure 3.16 shows the decay of the absolute value of the spectral coefficients for every tenth of the 116 embeddings. The plots for the other embeddings look similar. We observe for all three

operators a strong decrease of the first spectral coefficients. However, while the coefficients for the Laplace-Beltrami operators keep decreasing, the coefficients of the Fokker-Planck operator stagnate or even start increasing again. While the first spectral coefficients for the Laplace-Beltrami operator are in the order of  $10^4$ , after the first two hundred, the coefficients are in the order of  $10^1$ , decreasing only slowly further. However, the eigenvectors are of length 1714 and normed such that the size of each entry is in the end on average in the order of  $10^{-2}$ . This underlines the small influence of the trailing eigenvectors in the representation of the embeddings using the Laplace-Beltrami operator eigenbases. For the Fokker-Planck operator, the influence of the trailing eigenvectors seems to be higher.

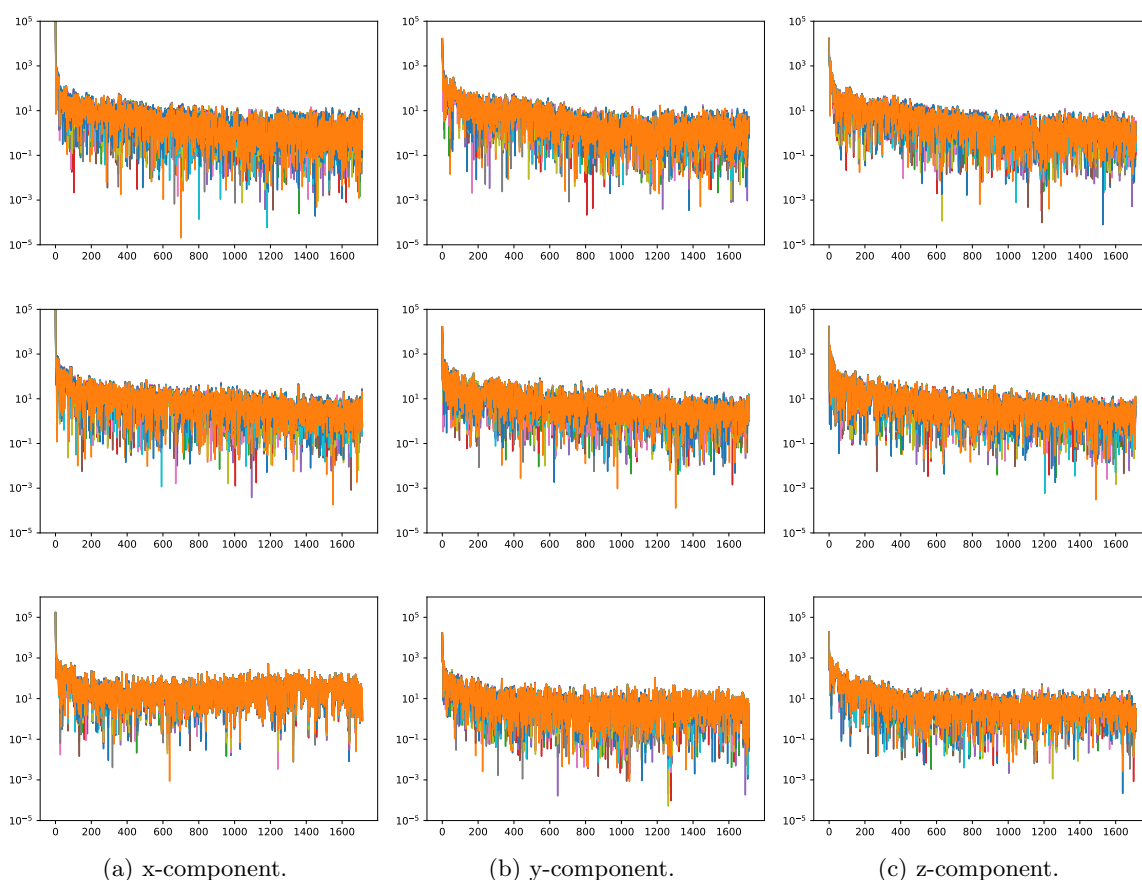


Figure 3.16: Absolute value of the spectral coefficients for every tenth of 116 simulations. First row: Laplace-Beltrami operator using the induced Euclidean metric, second row: Laplace-Beltrami operator using the equi-affine invariant metric, third row: Fokker-Planck operator.

Figure 3.17 shows the reconstruction of an embedding of the car part using only the first 30, the first 300 and all 1714 eigenvectors of the different operators. The result confirms that

the first eigenvectors are of much higher importance for the representation of the embedding than the trailing eigenvectors. As Figure 3.16 suggests, the reconstruction using the Laplace-Beltrami operators, especially of the operator for the induced Euclidean metric, seems to be better suited for a low-dimensional representation of the embeddings.

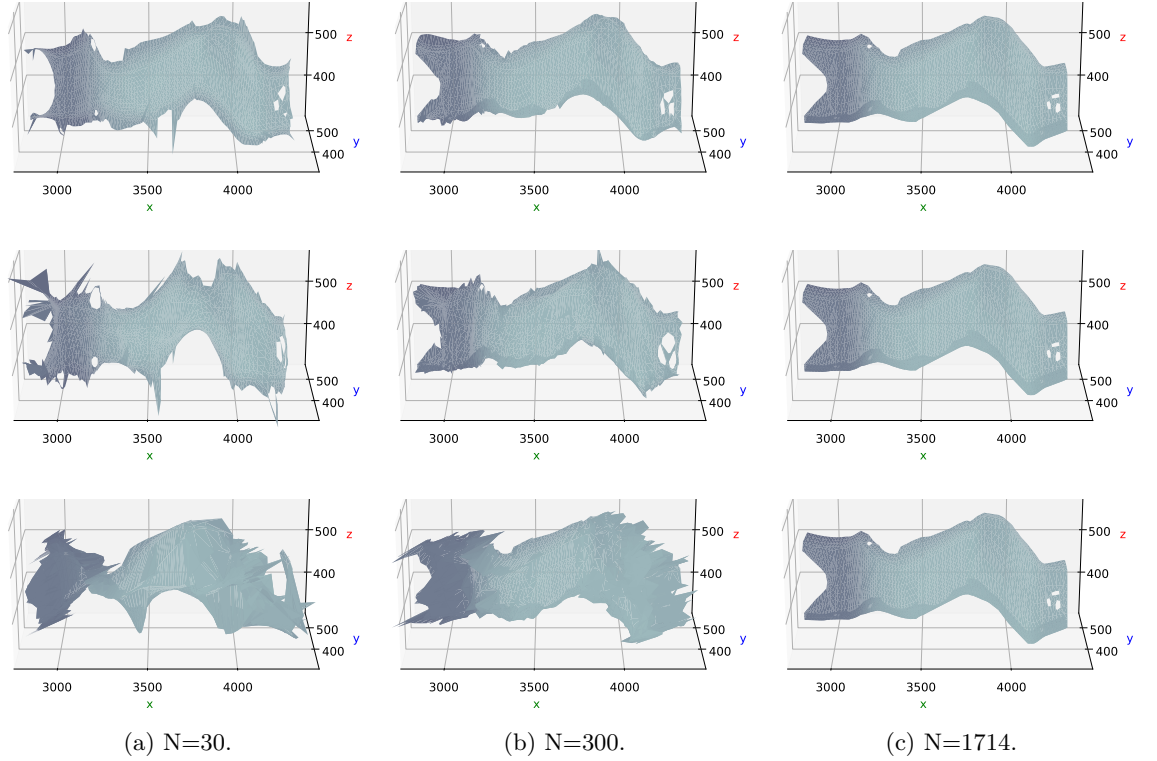


Figure 3.17: Reconstruction using  $N$  eigenvectors. First row: Laplace-Beltrami operator using the induced Euclidean metric, second row: Laplace-Beltrami operator using the equi-affine invariant metric, third row: Fokker-Planck operator.

### 3.5.2 Theoretical framework

In the last section, we observed a strong decay of the spectral coefficients for the embeddings of the car part from our example simulation bundle.

In [Iza17], Iza-Teran states a theorem concerning the decay of the spectral coefficients of the Fokker-Planck operator. However, to prove the statement, he assumes that his Fokker-Planck operator approximates a backward Fokker-Planck operator on some unobservable parameter space as the operator in Singer's and Coifman's setting does. In Section 3.1.3, we saw that this assumption is questionable.

Instead of Iza-Teran's approach to explain the decay of the spectral coefficients, we will follow ideas from [Afl16] and [BG17] to prove an optimality and a decay estimate for the Laplace-Beltrami operator.

In Section 3.1.3, we saw that Iza-Teran's Fokker-Planck operator can be interpreted as a Laplace-beltrami operator for a different metric. Therefore, the results apply as well to this operator.

From Section 3.1.1, we know that for a compact Riemannian manifold  $(M, g)$  exists an orthonormal basis of  $L^2(M)$  consisting of eigenfunctions  $\{\psi_i\}$ ,  $i \in \mathbb{N}$  of the negative Laplace-Beltrami operator  $-\Delta$  with corresponding eigenvalues  $0 \leq \lambda_1 \leq \lambda_2 \leq \dots$  and  $\lambda_i \rightarrow \infty$ .

We prove the following theorem concerning the maximal  $L^2$ -error for an approximation of a function using only the first  $k \in \mathbb{N}$  spectral coefficients.

**Theorem 3.5.1** ( *$L^2$ -error estimate for Laplace-Beltrami operator eigenfunction approximation*). *Let  $(M, g)$  be a compact Riemannian manifold with corresponding gradient  $\nabla$  and Laplace-Beltrami operator  $\Delta$ . Let  $\{\psi_i\}$ ,  $i \in \mathbb{N}$  be an orthonormal basis of  $L^2(M)$  of eigenfunctions of  $-\Delta$  as above. Let  $B$  be the class of all (ordered) orthonormal bases of  $L^2(M)$ , where for  $b \in B$  we write  $b = (b_1, b_2, \dots)$ . Then for all  $k \in \mathbb{N}$  with  $\lambda_{k+1} > 0$  holds*

$$\left\| f - \sum_{i=1}^k \langle f, \psi_i \rangle \psi_i \right\| = \frac{\|\nabla f\|}{\sqrt{\lambda_{k+1}}} \quad (3.5.1)$$

for all  $f \in H^{2,2}(M)$ . Further, if for  $b \in B$  holds

$$\left\| f - \sum_{i=1}^k \langle f, b_i \rangle b_i \right\| \leq \frac{\|\nabla f\|}{\sqrt{\lambda_{k+1}}} \quad (3.5.2)$$

for all  $k \in \mathbb{N}$  and  $f \in H^{2,2}(M)$ , then  $b$  is an orthonormal basis of eigenfunctions of  $-\Delta$  with corresponding eigenvalues  $\{\lambda_i\}_{i \in \mathbb{N}}$ . Here  $\|\cdot\|$  and  $\langle \cdot, \cdot \rangle$  denote the standard  $L^2$ -norm and inner product.

Note that Parseval's identity states that

$$\left\| f - \sum_{i=1}^k \langle f, \psi_i \rangle \psi_i \right\|^2 = \sum_{i=k+1}^{\infty} |\langle f, \psi_i \rangle|^2$$

such that the theorem yields as well a decay estimate for the sum of the trailing spectral coefficients.

Aflalo and Kimmel state in [AK13] that there exists a constant  $c$  such that for the eigenvalues  $\lambda_k$  of the negative Laplace-Beltrami operator holds  $\lambda_k \approx ck$  as  $k \rightarrow \infty$ . Together with Theorem 3.5.1, this implies that for the sum of the squared trailing spectral coefficients of a function  $f \in H^{2,2}(M)$ , and hence (using Parseval's identity) for the squared  $L^2$ -approximation error, holds

$$\sum_{i=k+1}^{\infty} |\langle f, \psi_i \rangle|^2 \leq \frac{c \|\nabla f\|^2}{k}$$

for a constant  $c$  independent of  $f$ .

*Proof of Theorem 3.5.1:* First, we note that by the Divergence Theorem 3.1.12 holds

$$\|\nabla f\|^2 = -\langle \Delta f, f \rangle.$$

We continue with the proof of Equation 3.5.1:

$\geq$ : Let  $f = \frac{c}{\sqrt{\lambda_{k+1}}} \psi_{k+1} \in H^{2,2}(M)$  for  $c > 0$ . Then

$$\|\nabla f\|^2 = \langle -\Delta f, f \rangle = c^2.$$

Further

$$\left\| f - \sum_{i=1}^k \langle f, \psi_i \rangle \psi_i \right\|^2 = \|f - 0\|^2 = \frac{c^2}{\lambda_{k+1}}.$$

$\leq$ : Let  $f \in H^{2,2}(M)$ , then

$$\begin{aligned} \|\nabla f\|^2 &= \langle -\Delta f, f \rangle \\ &= \left\langle \sum_{i \in \mathbb{N}} \lambda_i \langle f, \psi_i \rangle \psi_i, \sum_{i \in \mathbb{N}} \langle f, \psi_i \rangle \psi_i \right\rangle \\ &= \sum_{i \in \mathbb{N}} \lambda_i \langle f, \psi_i \rangle^2 \\ &\geq \sum_{i=k+1}^{\infty} \lambda_i \langle f, \psi_i \rangle^2 \\ &\geq \lambda_{k+1} \sum_{i=k+1}^{\infty} \langle f, \psi_i \rangle^2. \end{aligned}$$

With that, we conclude

$$\begin{aligned} \left\| f - \sum_{i=1}^k \langle f, \psi_i \rangle \psi_i \right\|^2 &= \left\| \sum_{i=k+1}^{\infty} \langle f, \psi_i \rangle \psi_i \right\|^2 \\ &= \sum_{i=k+1}^{\infty} \langle f, \psi_i \rangle^2 \\ &\leq \frac{\|\nabla f\|^2}{\lambda_{k+1}}. \end{aligned}$$

For the proof of Equation 3.5.2, we use the following Lemma:

**Lemma 3.5.2.** *Let  $b \in B$ . Assume*

$$\left\| f - \sum_{i=1}^n \langle f, \psi_i \rangle \psi_i \right\| \leq \frac{\|\nabla f\|}{\sqrt{\lambda_{n+1}}} \quad (3.5.3)$$

for all  $n \in \mathbb{N}$  and  $f \in H^{2,2}(M)$ . Assume further that  $\lambda_i < \lambda_{i+1}$  for some  $i \in \mathbb{N}$ . Then

$$\langle b_j, \psi_k \rangle = 0$$

for all  $1 \leq j \leq i < k$ .

*Proof.* Let  $k > i$  be fixed. Let  $\ell$  be the largest integer  $\ell \leq k-1$  such that  $\lambda_\ell < \lambda_{\ell+1}$ . Then we have  $i \leq \ell$  and  $\lambda_{\ell+1} = \lambda_{\ell+2} = \dots = \lambda_k$ .

Let  $f = c_1 \psi_1 + \dots + c_\ell \psi_\ell + c \psi_k$  such that  $\langle f, b_j \rangle = 0$  for all  $j \in \{1, \dots, \ell\}$  and  $f \neq 0$ . Such a  $f$  exists as this is an underdetermined linear equation system. By scaling, we may assume that

$$c_1^2 + \dots + c_\ell^2 + c^2 = 1.$$

Using  $\langle f, b_j \rangle = 0$  for all  $j \leq \ell$  and using Equation 3.5.3 for  $n = \ell$ , we get

$$1 = \sum_{m=1}^{\ell} c_m^2 + c^2 = \|f\|^2 = \left\| f - \sum_{m=1}^{\ell} \langle f, b_m \rangle b_m \right\|^2 \leq \frac{1}{\lambda_{\ell+1}} \|\nabla f\|^2$$

As  $\|\nabla f\|^2 = \langle -\Delta f, f \rangle$  we have

$$\frac{1}{\lambda_{\ell+1}} \|\nabla f\|^2 = \frac{1}{\lambda_{\ell+1}} \left( \sum_{m=1}^{\ell} c_m^2 \lambda_m + c^2 \lambda_k \right).$$

We use  $\lambda_{\ell+1} = \lambda_k$  to obtain

$$-\lambda_{\ell+1}c^2 \leq \sum_{m=1}^{\ell} \lambda_m c_m^2.$$

Using  $c_1^2 + \dots + c_\ell^2 + c^2 = 1$ , this is equivalent to

$$\lambda_{\ell+1} \sum_{m=1}^{\ell} c_m^2 \leq \sum_{m=1}^{\ell} \lambda_m c_m^2$$

which is again equivalent to

$$\sum_{m=1}^{\ell} (\lambda_{\ell+1} - \lambda_m) c_m^2 \leq 0.$$

As  $\lambda_{\ell+1} > \lambda_m \geq 0$  for all  $m \leq \ell$  it follows  $c_m = 0$  for all  $m \leq \ell$ .

Therefore,  $f = \pm\psi_k$  and by choice of  $f$

$$\langle \psi_k, b_j \rangle = \pm \langle f, b_j \rangle = 0$$

for all  $j \in \{1, \dots, l\}$ . As  $i \leq \ell$ , this proves the claim. □

Now we use the lemma to prove Equation 3.5.2 from Theorem 3.5.1. Assume again

$$\left\| f - \sum_{i=1}^n \langle f, b_i \rangle b_i \right\| \leq \frac{\|\nabla f\|}{\sqrt{\lambda_{n+1}}}$$

for all  $n \in \mathbb{N}$  and  $f \in H^{2,2}(M)$ .

Let  $i_1 \geq 1$  be the smallest integer such that  $\lambda_{i_1} < \lambda_{i_1+1}$ . From the lemma we get

$$\langle b_j, \psi_k \rangle = 0$$

for all  $1 \leq j \leq i_1 < k$ . Therefore,  $b_1, \dots, b_{i_1} \in \text{span}\{\psi_1, \dots, \psi_{i_1}\}$  which implies that each  $b_1, \dots, b_{i_1}$  is an eigenfunction of  $-\Delta$  with corresponding eigenvalue  $\lambda_1 = \dots = \lambda_{i_1}$ . Due to dimensions, the functions  $b_1, \dots, b_{i_1}$  form an orthonormal basis of

$$\text{span}\{\psi_1, \dots, \psi_{i_1}\} = \text{span}\{b_1, \dots, b_{i_1}\}.$$

Let  $i_2 \geq i_1 + 1$  be the next smallest integer such that  $\lambda_{i_2} < \lambda_{i_2+1}$ . From the lemma we get as above  $b_{i_1+1}, \dots, b_{i_2} \in \text{span}\{\psi_1, \dots, \psi_{i_2}\}$ . Using  $\text{span}\{\psi_1, \dots, \psi_{i_1}\} = \text{span}\{b_1, \dots, b_{i_1}\}$ , this

implies by orthogonality of the  $b_j$  and due to dimensions

$$\text{span}\{\psi_{i_1+1}, \dots, \psi_{i_2}\} = \text{span}\{b_{i_1+1}, \dots, b_{i_2}\}.$$

Analogously, we proceed for the next blocks. □

Theorem 3.5.1 implies that the eigenbasis for the Laplace-Beltrami operator is, with respect to the maximal  $L^2$ -error, optimal for the representation of all Sobolev functions  $f \in H^{2,2}(M)$  with a gradient bounded by a constant  $c > 0$ .

In Section 2.2, we saw that not every element of  $L^2(M)$  is a possible coordinate function of an embedding of the car part. Assuming, for instance, that the embeddings of the car part at the different timesteps of the simulations are smooth, isometric transformations of the reference embedding, the set  $C$  of possible coordinate functions is given by

$$C = \{g \in L^2(M) \mid g = f_x \text{ for a } C^\infty\text{-isometry } f : M \rightarrow f(M) \subset \mathbb{R}^3\}.$$

Under this assumption, the Euclidean norm of the gradient of the coordinate functions is at each point of the manifold bounded by  $\sqrt{2}$ . From this follows that the  $L^2$ -norms of the gradients of the coordinate functions are bounded by  $\int_M \sqrt{2} dA$ .

However, not every function  $f \in H^{2,2}(M)$  with  $\|\nabla f\| \leq \int_M \sqrt{2} dA$  is an element of  $C$ . Hence, it is not clear whether the eigenbasis of the Laplace-Beltrami operator is optimal for the representation of the functions in  $C$ . Nevertheless, the theorem might be a step in the right direction to explain the numerical observations.

Further, the theorem explains Iza-Teran's observations in [Iza17], that the eigenfunctions of the Laplace-Beltrami operator are also well suited to represent other simulation data like the stress or the temperature. Usually, those functions are as well smooth and have a bounded gradient.

Note, that we did not specify the metric used on the manifold  $M$ . The theorem can be applied to all three operators used in this thesis. Depending on the relation expected between the different embeddings of the simulated object, for instance isometric with respect to the Euclidean metric, to the equi-affine invariant metric or to the "covariance metric" from Section 3.1.3, the theorem would suggest to use the corresponding operator.

### 3.6 Summary

Let us summarize our results concerning the separation of effects, the decay of the spectral coefficients and the connection to the invariances of the used operators.

We saw that the observed transformations in the separation of effects are due to the form of the eigenfunctions of the used operator. However, we could not find a proper link between the form of the eigenfunctions and specific transformations. For the Laplace-Beltrami operator, for instance, we could not find a proper link between the eigenfunctions and isometric transformations.

We saw results from the representation of groups, linking the eigenspaces of the Laplace-Beltrami operator on the sphere to the representation of the group of rotations. We saw that such a link between the eigenspaces of the Laplace-Beltrami operator on a general submanifold and more general isometric transformations is not given. Especially, we saw that the isometric transformations we are interested in are of the form  $g : M \rightarrow g(M) \subset \mathbb{R}^3$  for a regular surface  $M \subset \mathbb{R}^3$  and do not form a group.

Further, we saw that the transformations upon variation of the spectral coefficients of the Laplace-Beltrami operator might seem to be isometric, but rarely are isometric.

We compared the transformations upon variation of the spectral coefficients of three operators with different invariances. However, for all operators, the transformations were similar.

Taken together, I do not see a reason to conjecture a link between the invariances of the used operator and the observed transformations.

The representation of the data in the spectral domain of an operator yields the opportunity to analyse separately the influence of parameter changes on different spectral coefficients. The idea in the separation of effects is that this enables us to investigate separately the influence of parameter changes on different basic transformations. However, the transformations corresponding to single spectral coefficients may at first sight seem to be reasonable physical transformations, but rarely are. There does not seem to be a link to the invariances of the operators and we saw that in general physically impossible crossings of the car part occur. Therefore, the benefit of a partitioning of the complex transformation between the embeddings into the transformations corresponding to variations of spectral coefficients of "invariant" operators is questionable. The eigenbases of those operators do, from a physical point of view, not seem to be better suited than any other basis of  $L^2(M)$  or, in the discrete case, other bases of  $\mathbb{R}^N$ .

Concerning the decay of the spectral coefficients and the reconstruction properties, our numerical observations indicates that the eigenbasis of the Laplace-Beltrami operator using the induced Euclidean metric is better suited for the low-dimensional representation of our embeddings than the eigenbases of the other operators.

We saw an optimality statement for the representation of smooth functions in the spectral domain of a Laplace-Beltrami operator and saw to what extent this can be used to justify the representation of simulation data in the spectral domain of a Laplace-Beltrami operator for compression purposes.

A numerical comparison to other state-of-the-art dimensionality reduction and compression approaches is needed.

Finally, in this thesis, we employed a Laplace-Beltrami operator using an equi-affine invariant metric. While the observations for the operator were similar as the observations for the other operators, especially the eigenfunctions seem to be noisier and their ordering differs from the expected multi-resolution nature of eigenfunctions of Laplace-Beltrami operators, see for instance [JN01]. This might be due to the many hyperbolic and parabolic points on the surfaces of car parts and the many boundaries at which a good numerical approximation of the continuous metric is difficult.

## 4 Taylor approach

In this chapter, we will see a different approach for the representation of the simulation data. The fact that the different embeddings of the car part are really similar and Iza-Teran's assumption that all embeddings are transformations of a reference embedding gave me the idea to focus directly on the transformations. Instead of looking for a different representation of the embeddings, I wanted to represent those transformations. To do so, we will consider their Taylor expansion.

In the first part of this chapter, I will shortly present the idea and the numerical realization of the approach. In Section 4.2, we will consider an exemplary application of the approach in the analysis of crash simulations. We will see that only few coefficients in the Taylor approach are needed to represent similar data and see a way to obtain an invariance under affine transformations.

### 4.1 Theoretical framework

The Taylor approach can be applied to many types of data. It can be similar curves in  $\mathbb{R}^2$  or  $\mathbb{R}^3$ , similar surfaces in  $\mathbb{R}^3$  or even structures in higher dimensions.

As motivated in Section 2.2, we assume that all embeddings are smooth, injective transformations of a reference embedding  $M$ , modelled as  $k$ -dimensional submanifold of  $\mathbb{R}^d$ , *i.e.* each embedding  $T$  is the image of an element  $f \in Emb(M, \mathbb{R}^d)$ .

A smooth function on a submanifold can locally be extended to an open neighbourhood of the submanifold. Consider the components  $f_1, \dots, f_d$  of  $f$ . Assume they can be extended to  $\mathbb{R}^d$  and that their extensions can globally be represented by their Taylor series, *i.e.*

$$f_i(x) = \sum_{|\alpha| \in \mathbb{N}_0^d} \frac{x^\alpha}{\alpha!} D^\alpha f_i(0) \text{ for all } x \in \mathbb{R}^d, i = 1, \dots, d. \quad (4.1.1)$$

Here,  $\alpha \in \mathbb{N}_0^d$  is a multi-index,  $|\alpha| = \sum_{i=1}^d \alpha_i$ ,  $x^\alpha = x_1^{\alpha_1} \dots x_d^{\alpha_d}$  and  $D^\alpha = \partial_{x_1}^{\alpha_1} \dots \partial_{x_d}^{\alpha_d}$ . We are interested in the coefficients  $D^\alpha f_i(0)$  which characterize the transformation  $f$ .

In the discrete setting, we are given  $N$  nodes  $x^1, \dots, x^N \in \mathbb{R}^d$  on the reference embedding  $M$  and the positions of the corresponding points on the transformed embedding  $T$ , *i.e.*  $f(x^1), \dots, f(x^N)$ .

From Equation 4.1.1, we obtain

$$\begin{pmatrix} f_i(x^1) \\ \vdots \\ f_i(x^N) \end{pmatrix} = \sum_{|\alpha| \in \mathbb{N}_0^d} \frac{D^\alpha f_i(0)}{\alpha!} \begin{pmatrix} (x^1)^\alpha \\ \vdots \\ (x^N)^\alpha \end{pmatrix}.$$

Neglecting summands for  $\alpha > M$  for some  $M \in \mathbb{N}_0$ , we consider the linear equation system

$$\begin{pmatrix} f_i(x^1) \\ \vdots \\ f_i(x^N) \end{pmatrix} = \sum_{|\alpha| \leq M} c_{i,\alpha} \begin{pmatrix} (x^1)^\alpha \\ \vdots \\ (x^N)^\alpha \end{pmatrix}. \quad (4.1.2)$$

We define

$$K = |\{\alpha \in \mathbb{N}_0^d \mid |\alpha| \leq M\}| = \binom{M+d}{d}.$$

Depending on  $N$  and  $K$  and on whether or not the vectors on the right are linearly independent, this linear equation system has zero, one or infinitely many solutions. Therefore, we do not look for a solution, but build an orthonormal basis of the space spanned by the vectors on the right and project on this basis. The projection coefficients are used to characterize the transformation  $f$ .

This procedure yields the best fit of the reference embedding, given as points  $x^1, \dots, x^N$ , to the transformed embedding, given as points  $f(x^1), \dots, f(x^N)$ , with a polynomial  $P : \mathbb{R}^d \rightarrow \mathbb{R}^d$  of degree  $\leq M$ .

To represent all affine transformations of the reference embedding, for example translations and rotations, it suffices to choose  $M = 1$ , yielding  $(d+1)d$  coefficients, which is exactly the number of degrees of freedom of an affine transformation from  $\mathbb{R}^d$  to  $\mathbb{R}^d$ .

Mathematically, we minimize for all  $i = 1, \dots, d$

$$\left\| \begin{pmatrix} f_i(x^1) - P_i(x^1) \\ \vdots \\ f_i(x^N) - P_i(x^N) \end{pmatrix} \right\|_{\mathbb{R}^N}$$

over all polynomials  $P : \mathbb{R}^d \rightarrow \mathbb{R}^d$  of degree  $\leq M$ .

Note, that the dimensionality of the space of functions of the form

$$\sum_{|\alpha| \leq M} c_{i,\alpha} \begin{pmatrix} (x^1)^\alpha \\ \vdots \\ (x^N)^\alpha \end{pmatrix},$$

respectively the dimensionality of the space

$$\{(P(x_1), \dots, P(x_N))^T | P : \mathbb{R}^d \rightarrow \mathbb{R}^d \text{ a polynomial of degree } \leq M\} \subset \mathbb{R}^{N \times d},$$

depends on the reference embedding. Given for example, that all points  $x^i$  of the reference embedding fulfil  $x_d^i = 0$ , then the vectors  $((x^1)^\alpha, \dots, (x^N)^\alpha)$  are for all  $\alpha = (0, \dots, 0, \alpha_d)$  linearly dependent.

Concerning the numerical orthonormalization of the vectors, we assume  $K \leq N$  and use the QR-decomposition using Householder reflections, see for example [Bin09]. This procedure is more stable than the Gram-Schmidt algorithm.

We write the matrix  $X \in \mathbb{R}^{N \times K}$  with columns  $((x^1)^\alpha, \dots, (x^N)^\alpha)^T$ ,  $\alpha \in \mathbb{N}_0^d$  with  $|\alpha| \leq M$ , as product  $X = QR$  for an orthogonal matrix  $Q \in \mathbb{R}^{N \times N}$  and an upper triangular matrix  $R \in \mathbb{R}^{N \times K}$ . As  $R$  is an upper triangular matrix, the span of the columns of  $X$  is contained in the span of the first  $K$  columns of  $Q$ .

The reduced QR-decomposition is given by  $X = Q_1 R_1$  where  $Q_1 \in \mathbb{R}^{N \times K}$  consists of the first  $K$  columns of  $Q$  and the upper triangular matrix  $R_1 \in \mathbb{R}^{K \times K}$  consists of the first  $K$  rows of  $R$ .

In the case that the columns of  $X$  are linearly independent, the span of the columns of  $X$  equals the span of the columns of  $Q_1$ . To obtain equality in the case that the columns of  $X$  are not linearly independent, we delete all columns of  $Q_1$  for which the corresponding row of  $R_1$  is the zero vector.

For the numerical computation, I use the function `qr` from the python library `numpy.linalg`, which is an interface of the LAPACK routines `dgeqrf` and `dorgqr`. It yields the reduced QR-decomposition  $X = Q_1 R_1$ . Next, I delete the columns of  $Q_1$  for which the corresponding rows are zero vectors and project the coordinate-functions of the embeddings on the remaining columns.

Let us consider the following simple example. Our data are the numerical solutions of the

following system of time dependent ordinary differential equations

$$\begin{aligned}\dot{x} &= x^3 + xy^2 - x - y \\ \dot{y} &= y^3 + x^2y - y + x\end{aligned}\tag{4.1.3}$$

in the interval  $t \in [0, 8]$  for different initial conditions. As initial conditions we take  $x_0 = 0.4 \cdot \cos(\theta)$ ,  $y_0 = 0.4 \cdot \sin(\theta)$  for eleven equidistant samples  $\theta \in [0, 2\pi]$ . For the discrete solution we choose the timestep  $\Delta t = 0.01$  yielding eleven vectors  $x^1, \dots, x^{11} \in \mathbb{R}^{2 \times 802}$ , see Figure 4.1.

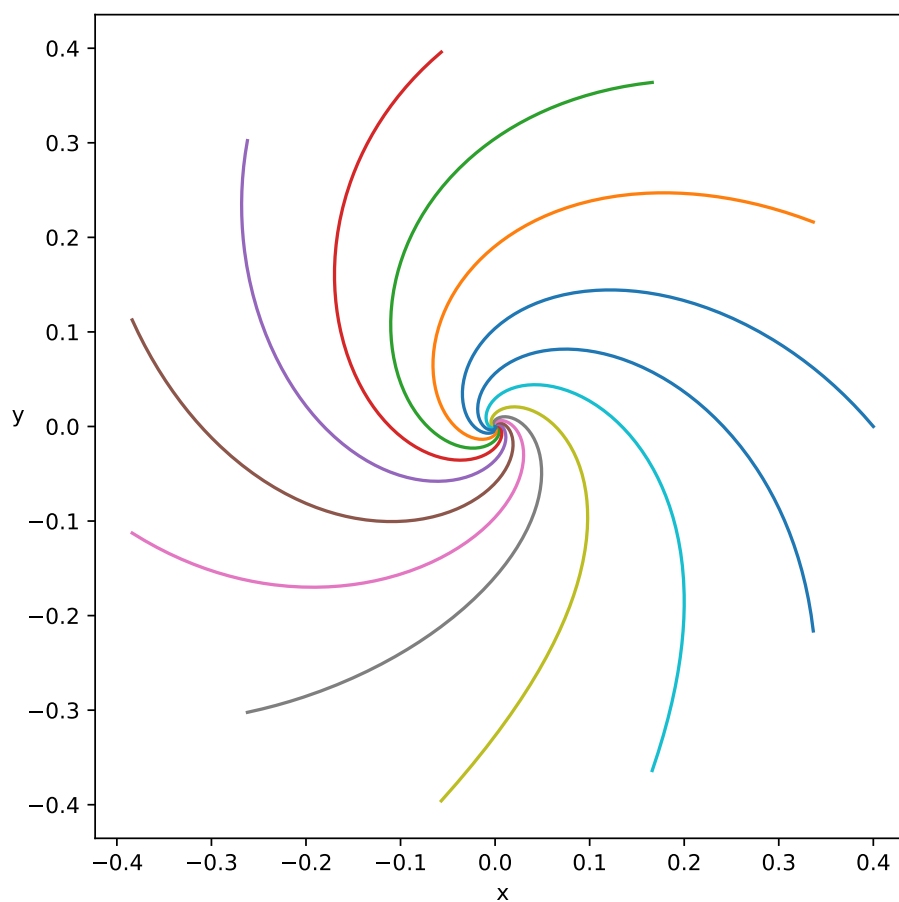


Figure 4.1: Eleven solutions of the system of time dependent ordinary differential equations 4.1.3 for different initial conditions.

For the numerical computation, I used the function `ode` in the python library `scipy.linalg`.

We see that the solution vectors  $x^i$  differ only by rotation. Consequently, choosing any vector  $x^i$  as reference embedding and following the Taylor approach for  $M = 1$ , we can represent all

vectors  $x^1, \dots, x^{11}$  with only six projection coefficients per vector, the number of degrees of freedom of a general affine transformation from  $\mathbb{R}^2$  to  $\mathbb{R}^2$ .

In Section 3.4, we saw that the invariant operator approach needs for an exact representation all 1604 projection coefficients. This is because the invariant operator approach builds a basis of  $L^2(M)$ , respectively  $\mathbb{R}^{802}$ , and can represent any element of those spaces. We saw that we obtain a good approximation of smooth functions in  $L^2(M)$  using only the first coefficients and especially all smooth deformations of  $M$  have smooth coordinate functions. However, the Taylor approach has in the case of simple transformations between the embeddings an advantage, as it only focusses on the representation of the transformations. On the other hand it is open, whether or not it yields in the limit of  $M = \infty$  a basis of  $L^2(M)$ .

## 4.2 Undoing transformations

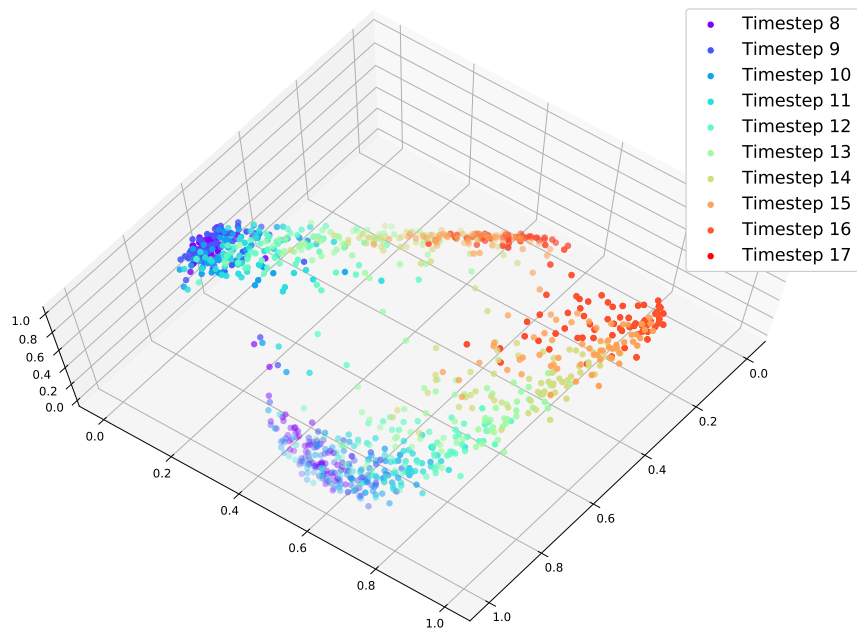
Given the projection coefficients as characterization of the transformations between the embeddings, we can for example use them as feature vectors in another dimensionality reduction method. We will demonstrate this with Diffusion maps, a nonlinear method for dimensionality reduction. See for example [CL06] for details or [Tes16] for a short introduction to the method.

We consider again the simulation bundle presented in Section 2.1, consisting of 116 crash simulations with 17 timesteps. We consider the embeddings of the car part at the timesteps 8 to 17.

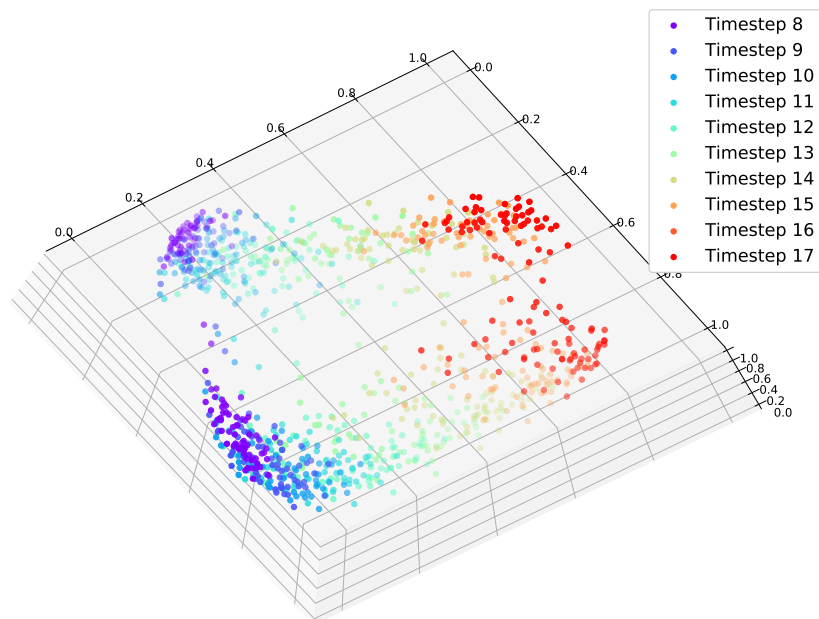
As reference embedding, we choose the car part at timestep 1 in an arbitrary simulation. Then, we calculate for each embedding of the car part the twelve projection coefficients for a maximal polynomial degree  $M = 1$  and apply Diffusion maps. The obtained embedding in the 3-dimensional space is similar to the embedding obtained applying Diffusion maps on the original data, where each embedding is described by a vector in  $\mathbb{R}^{3 \cdot 1714}$ , see Figure 4.2.

Hence, the first twelve projection coefficients contain the information that is used by Diffusion maps to embed the original data.

The first twelve projection coefficients of the Taylor approach are only able to represent affine transformations of the reference geometry, for example translations and rotations. However, this type of transformation might not be of high interest for the engineer who wants to focus on actual deformations of the part. The Taylor approach yields a simple possibility to remove the influence of such transformations. In the last section, we saw that the projection on the polynomials of degree  $\leq 1$  corresponds to finding the best affine fit of the reference embedding



(a) Embedding for the original data.



(b) Embedding for the projection coefficients.

Figure 4.2: Diffusion maps embedding for the original data given as vectors in  $\mathbb{R}^{5142}$  and for the first twelve projection coefficients from the Taylor approach with maximal polynomial degree one.

to the transformed embedding in the sense that we minimize for all  $i \in \{1, 2, 3\}$

$$\left\| \begin{pmatrix} f_i(x^1) - P_i(x^1) \\ \vdots \\ f_i(x^N) - P_i(x^N) \end{pmatrix} \right\|_{\mathbb{R}^N} \quad (4.2.1)$$

over all affine transformations  $P : \mathbb{R}^3 \rightarrow \mathbb{R}^3$ ,  $P(x) = Ax + b$ , where  $x^1, \dots, x^N \in \mathbb{R}^{3 \times 1714}$  is the reference embedding. Indeed, we can use the projection coefficients to obtain the minimizing transformation  $P$ . To see this, let

$$\begin{pmatrix} 1 & x_1^1 & x_2^1 & x_3^1 \\ \vdots & \vdots & \vdots & \vdots \\ 1 & x_1^N & x_2^N & x_3^N \end{pmatrix} = \begin{pmatrix} (q_1) & (q_2) & (q_3) & (q_4) \end{pmatrix} \cdot \begin{pmatrix} r_{11} & r_{12} & r_{13} & r_{14} \\ & r_{22} & r_{23} & r_{24} \\ & & r_{33} & r_{34} \\ & & & r_{44} \end{pmatrix}$$

be the reduced  $QR$ -decomposition of the matrix  $X$ . Assuming that the columns (1),  $(x_1)$ ,  $(x_2)$  and  $(x_3)$  of  $X$  are linearly independent, it holds  $r_{ii} \neq 0$ . We write

$$\begin{aligned} (1) = r_{11}(q_1) & \Rightarrow (q_1) = \frac{1}{r_{11}}(1) \\ (x_1) = r_{12}(q_1) + r_{22}(q_2) & \Rightarrow (q_2) = \frac{1}{r_{22}}(x_1) - \frac{r_{12}}{r_{11}r_{22}}(1) \\ (x_2) = r_{13}(q_1) + r_{23}(q_2) + r_{33}(q_3) & \Rightarrow (q_3) = \frac{1}{r_{33}}(x_2) - \frac{r_{23}}{r_{22}r_{33}}(x_1) + \left( \frac{r_{12}r_{23}}{r_{11}r_{22}r_{33}} - \frac{r_{13}}{r_{11}r_{33}} \right)(1) \end{aligned}$$

and

$$\begin{aligned} (x_3) &= r_{14}(q_1) + r_{24}(q_2) + r_{34}(q_3) + r_{44}(q_4) \\ \Rightarrow (q_4) &= \frac{1}{r_{44}}(x_3) - \frac{r_{34}}{r_{33}r_{44}}(x_2) + \left( \frac{r_{23}r_{34}}{r_{22}r_{33}r_{44}} - \frac{r_{24}}{r_{22}r_{44}} \right)(x_1) \\ &+ \left( \frac{r_{12}r_{24}}{r_{11}r_{22}r_{44}} + \frac{r_{13}r_{34}}{r_{11}r_{33}r_{44}} - \frac{r_{14}}{r_{11}r_{44}} - \frac{r_{12}r_{23}r_{34}}{r_{11}r_{22}r_{33}r_{44}} \right)(1). \end{aligned}$$

Let  $c_i^j$ ,  $i = 1, 2, 3$ ,  $j = 1, \dots, 4$ , be the projection coefficients of  $(f_i(x^1), \dots, f_i(x^N))^T$  on  $(q_j)$ . We have

$$(P_i(x^1), \dots, P_i(x^N))^T = c_i^1(q_1) + c_i^2(q_2) + c_i^3(q_3) + c_i^4(q_4)$$

for a minimizing  $P$  of Equation 4.2.1. Inserting the above equations for  $(q_j)$ , we get

$$\begin{aligned}
(P_i(x^1), \dots, P_i(x^N))^T = & \left( \frac{c_i^1}{r_{11}} - \frac{c_i^2 r_{12}}{r_{11} r_{22}} - \frac{c_i^3 r_{13}}{r_{11} r_{33}} + \frac{c_i^3 r_{12} r_{23}}{r_{11} r_{22} r_{33}} - \frac{c_i^4 r_{14}}{r_{11} r_{44}} \right. \\
& \left. + \frac{c_i^4 r_{12} r_{24}}{r_{11} r_{22} r_{44}} + \frac{c_i^4 r_{13} r_{34}}{r_{11} r_{33} r_{44}} - \frac{c_i^4 r_{12} r_{23} r_{34}}{r_{11} r_{22} r_{33} r_{44}} \right) (1) \\
& + \left( \frac{c_i^2}{r_{22}} - \frac{c_i^3 r_{23}}{r_{22} r_{33}} - \frac{c_i^4 r_{24}}{r_{22} r_{44}} + \frac{c_i^4 r_{23} r_{34}}{r_{22} r_{33} r_{44}} \right) (x_1) \\
& + \left( \frac{c_i^3}{r_{33}} - \frac{c_i^4 r_{34}}{r_{33} r_{44}} \right) (x_2) \\
& + \frac{c_i^4}{r_{44}} (x_3).
\end{aligned}$$

Defining the sum in front of (1) as  $b_i$  and the expressions in front of  $(x_1)$ ,  $(x_2)$  and  $(x_3)$  as  $a_{i1}$ ,  $a_{i2}$  and  $a_{i3}$ , we see that  $P$  is given as  $P(x) = Ax + b$ . To undo the affine transformation  $P$  from the transformed embedding  $(f(x^1), \dots, f(x^N))$ , we compute  $(A^{-1}(f(x^1) - b), \dots, A^{-1}(f(x^N) - b))$ .

Using the resulting vectors as feature vectors for Diffusion maps yields the embedding shown in Figure 4.3. The influence of the time on the embedding is mostly removed.

The timesteps 8 to 17 of each simulation differ mainly by small translations and rotations due to the bouncing of the car when it hits the wall. Those influences removed, the embedding depends now primarily on the bending of the beam. Figure 4.4 shows two embeddings of the left cluster, one of each cluster in the middle and two of the right cluster.

### 4.3 Summary

The Taylor approach is a new idea for the analysis of simulation bundles. It can be used for tasks as compression and reconstruction of simulation data, denoising - for example given an exact reference embedding before the crash and noisy embeddings during the crash - and the undoing of transformations.

Its performance in those task and whether or not an undoing of transformations is of interest depends however highly on the specific data. Consider, for example, once more Figure 4.1: Whichever reference embedding we choose, all other embeddings are linear transformations of it. Therefore, we get an exact reconstruction of the embeddings using only six projection coefficients.

The idea to characterize the transformations between a reference embedding and transformed

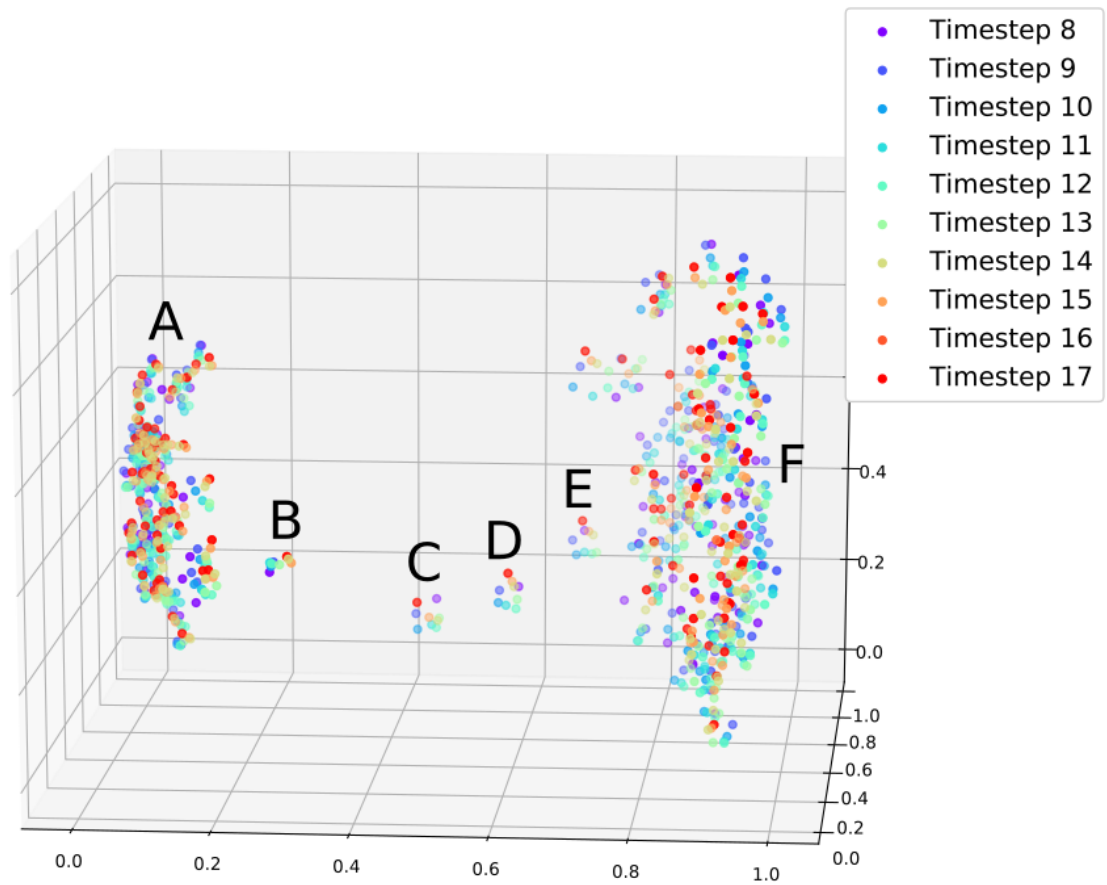
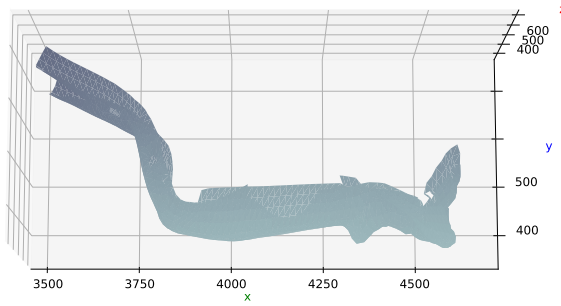


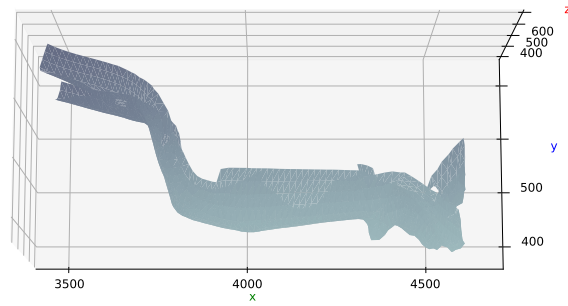
Figure 4.3: Diffusion maps embedding with clusters A to F for the crash data after undoing the best affine transformation of the reference embedding to the transformed embedding.

embeddings might yield further approaches for the analysis of simulation bundles, the Taylor expansion being only one possibility of a characterization.

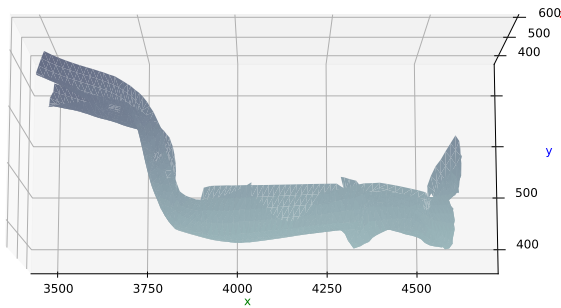
Especially, the Taylor approach uses polynomials and while a polynomial of degree zero corresponds to translations, polynomials of degree one correspond to affine transformations. Affine transformations like rotations are mostly physically reasonable transformations, but in general not all affine transformations of the reference embedding are physically reasonable and the same holds for quadratic and higher order transformations. An approach focussing on the characterization of the transformations between the reference embedding and the transformed embeddings but respecting physical constraints would be highly interesting.



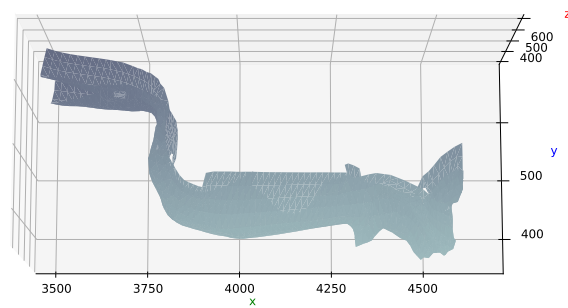
(a) Cluster A.



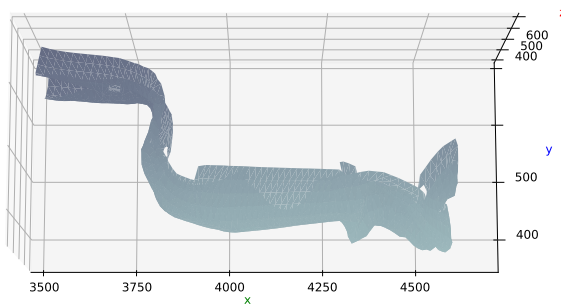
(b) Cluster A.



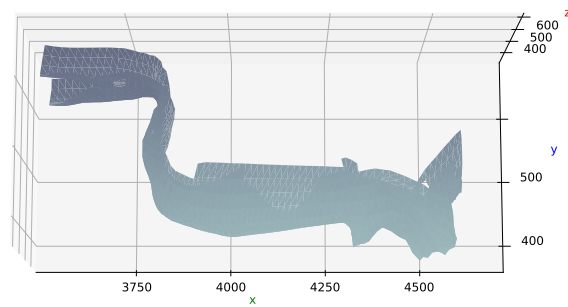
(c) Cluster B.



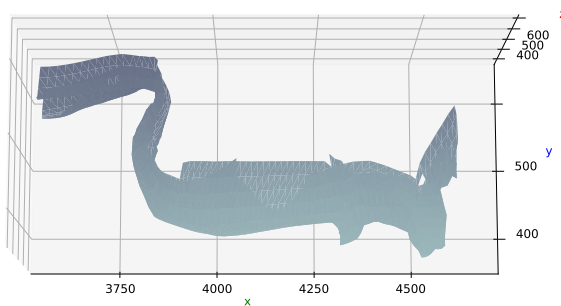
(d) Cluster C.



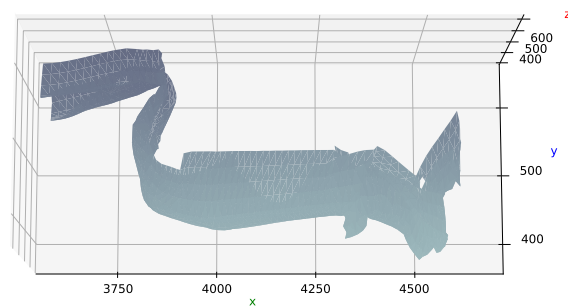
(e) Cluster D.



(f) Cluster E.



(g) Cluster F.



(h) Cluster F.

Figure 4.4: Embeddings of the beam corresponding to the different clusters in Figure 4.3.

## 5 Conclusion

In Chapter 3 of this thesis, we investigated the invariant operator approach. Concerning the decay of the spectral coefficients, the main result is an optimality estimate for the representation of smooth functions in the spectral domain of Laplace-Beltrami operators. Concerning the separation of effects, the main results are that the transformations upon variation of chosen spectral coefficients do not seem to be linked to the invariances of the employed operator and do not fulfil any physical constraints. Consequently, a partitioning of complex transformations in those "basic transformations" seems to be of no use for the analysis of simulation bundles.

In Chapter 4, I shortly presented the Taylor approach, a novel approach for the investigation of simulation bundles. The approach resulted from the idea to focus on the representation of the transformations between similar embeddings instead of representing the embeddings directly. We saw some first results and possible applications. However, there are still many gaps that I could not fill, focussing this thesis mainly on the investigation of the invariant operator approach.

Similarly to the invariant operator approach, the Taylor approach does not respect physical constraints for the transformations between the embeddings. Developing an approach that focusses on the characterization of the transformations between similar embeddings and respects suitable physical constraints is an interesting topic of research.

## References

- [Afl16] Y. Aflalo et al. “Best bases for signal spaces”. In: *Comptes Rendus Mathématique* 354.12 (2016), pp. 1155–1167.
- [AK13] Y. Aflalo and R. Kimmel. “Spectral multidimensional scaling”. In: *Proceedings of the National Academy of Sciences of the United States of America* 110.45 (2013), pp. 18052–18057.
- [Bär10] C. Bär. *Elementare Differentialgeometrie*. 2nd ed. De Gruyter, 2010.
- [BG17] H. Brezis and D. Gómez-Castro. “Rigidity of optimal bases for signal spaces”. In: *Comptes Rendus Mathématique* 355.7 (2017), pp. 780–785.
- [Bin09] D. Bindel. *Matrix Computations*. <https://www.cs.cornell.edu/~bindel/class/cs6210-f09/lec18.pdf> (2018). 2009.
- [Bla23] W. Blaschke. *Vorlesungen über Differentialgeometrie und geometrische Grundlagen von Einsteins Relativitätstheorie*. 1923.
- [Boa15] R. Boagey. “From physical to virtual: will technology see the end of the traditional crash test?” In: *Automotive Megatrends Magazine* (Q3 2015), pp. 12–16.
- [CL06] R. Coifman and F. Lafon. “Diffusion maps”. In: *Applied and computational harmonic analysis* 21.1 (2006), pp. 5–30.
- [Gal13] J. Gallier. *Notes on Spherical Harmonics and Linear Representations of Lie Groups*. <http://www.cis.upenn.edu/~cis610/sharmonics.pdf> (2018). 2013.
- [Gri09] D. Grieser. *Der Laplace-Operator auf einer Riemannschen Mannigfaltigkeit*. <http://www.staff.uni-oldenburg.de/daniel.grieser/wwwlehre/Schriebe/Laplace-Beltrami.pdf> (2018). 2009.
- [Hel10] B. Helffer. *Spectral theory and applications. An elementary introductory course*. <https://www.math.u-psud.fr/~helffer/m2bucarest2010.pdf> (2018). 2010.
- [IG17] R. Iza-Teran and J. Garcke. *A Geometrical Method for the Analysis of Simulation Bundles*. Tech. rep. Fraunhofer SCAI, Sankt Augustin, Institut für Numerische Simulation, Universität Bonn, 2017.
- [Iza17] R. Iza-Teran. “Geometrical Methods for the Analysis of Simulation Bundles”. PhD thesis. Institut für Numerische Simulation, Universität Bonn, 2017.
- [JN01] D. Jakobson and N. Nadirashvili. “Geometric Properties Of Eigenfunctions”. In: *Russian Mathematical Surveys* 56 (2001).

- [KG00] Z. Karni and C. Gotsman. “Spectral Compression of Mesh Geometry”. In: *Proceedings of the 27th Annual Conference on Computer Graphics and Interactive Techniques* (2000), pp. 279–286.
- [Mic08] P. Michor. *Topics in Differential Geometry*. American Mathematical Society, 2008.
- [MM06] P. W. Michor and D. Mumford. “Riemannian Geometries on Spaces of Plane Curves”. In: *Journal of the European Mathematical Society* 8.1 (2006), pp. 1–48.
- [Ra10] D. Raviv and M. Bronstein et al. “Affine-invariant diffusion geometry for the analysis of deformable 3D shapes”. In: *Proceedings / CVPR, IEEE Computer Society Conference on Computer Vision and Pattern Recognition*. (2010).
- [Ra14] D. Raviv and A. M. Bronstein et al. “Equi-affine Invariant Geometry for Shape Analysis”. In: *Journal of Mathematical Imaging and Vision* 50 (2014), pp. 144–163.
- [SC08] A. Singer and R.R. Coifman. “Non-linear independent component analysis with diffusion maps”. In: *Applied and Computational Harmonic Analysis* 25.2 (2008), pp. 226–239.
- [Sug90] M. Sugiura. *Unitary Representations and Harmonic Analysis: An Introduction*. Developments in Animal and Veterinary Sciences. North-Holland, 1990.
- [Tau95] G. Taubin. “A Signal Processing Approach to Fair Surface Design”. In: *Proceedings of the 22nd Annual Conference on Computer Graphics and Interactive Techniques* (1995), pp. 351–358.
- [TC14] R. Talmon and R. R. Coifman. “Intrinsic modeling of stochastic dynamical systems using empirical geometry”. In: *Applied and Computational Harmonic Analysis* 39.1 (2014), pp. 138–160.
- [Tes16] T. Tesch. “Betrachtung der Scatter-Transformation zur Analyse von Winddaten”. Bachelor’s Thesis. Institut für Numerische Simulation, Universität Bonn, 2016.